

**STRUCTURAL MONITORING OF A 10M FIBRE REINFORCED
POLYMER BRIDGE SUBJECTED TO SEVERE DAMAGE**

**SURVEILLANCE DE L'ETAT DE LA STRUCTURE D'UN PONT EN
POLYMERE RENFORCE DE FIBRES DE 10 M LOURDEMENT
ENDOMMAGE**

A Thesis Submitted

to the Faculty of Engineering of the Royal Military College of Canada

by

Richard A. Lim

In Partial Fulfilment of the Requirements for the Degree of

Master of Applied Science in Civil Engineering

April 2016

**© This thesis may be used within the Department of National Defence, but copyright
for open publication remains the property of the author**

ABSTRACT

Structural Health Monitoring (SHM) is a field of growing importance in Civil Engineering and its use has grown significantly during the past decade. The ability to monitor structures and assess their structural integrity has become increasingly important as many North American structures approach the end of their design lives. Actively monitoring structures such as bridges can have great benefits not only in civilian but also in military applications. When deployed on military operations, troops are often faced with the need to use bridges that are damaged, poorly constructed or designed for smaller loads than required by the operation. The ability to monitor these bridges and review real-time response of the structure under load can save time, energy, money and reduce the risk of injury to deployed troops and damage to the infrastructure.

The 10 m Fibre Reinforced Polymer (FRP) box beam bridge used for this investigation was developed and constructed at the Royal Military College of Canada for research on temporary deployable bridges. During this study, the quasi-static and dynamic behaviour of the bridge was investigated under laboratory conditions to determine if damage could be detected with a simple wireless monitoring system through shifts in the bridge's frequency. Incremental damage was done to the bridge as both quasi-static and dynamic testing was completed at each damage stage. Using instrumentation such as strain gauges and accelerometers, the data was collected and processed so it could be analyzed in both time and frequency-domains.

From dynamic testing and the use of wired and wireless accelerometers and strain gauges, it was determined, using time and frequency-domain analyses that damage to supportive structural members caused significant shifts in the frequency of the structure. The use of the Fast Fourier Transform (FFT) on the experimental data allowed for a frequency reduction of 21% to be easily observed over 18 damage stages which included both major and minor structural components that caused a reduction up to 45% in the bridge stiffness under static loads.

Using commercial Finite Element Analysis (FEA) software, SAP2000 and ANSYS, the bridge was modelled to represent different levels of damage and the response of the model to both static and dynamic loading was observed. It was determined that both modeling programs produced results that appropriately represented the experimental behaviour. It was shown that the bridge response to different severe damage stages could be adequately predicted using commercially available FEA software.

RÉSUMÉ

La surveillance de l'état des structures (SES) est un domaine en plein essor qui prend de plus en plus d'importance depuis une décennie en génie civil. La capacité de surveiller des structures et d'évaluer leur intégrité structurale revêt effectivement une importance croissante en Amérique du Nord, où beaucoup de structures approchent la fin de leur durée de vie utile. La surveillance active de structures telles que les ponts offre des avantages considérables pour des applications civiles et militaires. Lorsqu'ils participent à des opérations militaires en déploiement, les militaires sont souvent appelés à emprunter des ponts endommagés, mal construits ou conçus pour supporter des charges plus faibles que ce qu'exige l'opération en cours. La capacité de surveiller ces ponts et d'étudier en temps réel le comportement sous chargement permet de gagner du temps et d'économiser de l'énergie et de l'argent, en plus de réduire les risques de blessure pour les troupes déployées et d'éviter d'endommager l'infrastructure.

Un pont à poutres-caisson en polymère renforcé de fibres (PRF) de 10 m utilisé pour la présente étude a été conçu et érigé au Collège militaire royal du Canada dans le cadre de la recherche sur les ponts temporaires. Au cours de cette étude, le comportement quasi statique et dynamique du pont en conditions de laboratoire a été étudié afin de déterminer s'il était possible de détecter des dommages au moyen d'un simple système de surveillance sans fil sensible aux altérations de la fréquence du pont. Des dommages ont été infligés au pont successivement, chaque étape étant suivie d'essais quasi statiques et dynamiques. À l'aide d'instruments tels que des extensomètres et des accéléromètres, les données recueillies ont été traitées afin d'effectuer une analyse dans le temps et fréquentielle.

Les essais dynamiques ont permis de déterminer, au moyen d'analyses dans le temps et fréquentielles, que les dommages infligés aux éléments structuraux de soutien provoquaient d'importantes altérations de la fréquence de la structure. Le traitement des données expérimentales par transformation de Fourier rapide (TFR) a permis d'observer aisément une réduction de la fréquence de 21 % au fil des 18 étapes d'endommagement qui touchaient des éléments structuraux majeurs et mineurs et qui ont

entraîné une réduction atteignant jusqu'à 45 % de la rigidité du pont sous chargement statique.

À l'aide de logiciels commerciaux d'analyse par éléments finis (AEF), SAP2000 et ANSYS, le pont a été modélisé à différents niveaux d'endommagement afin d'observer la réaction du modèle sous chargement statiques et dynamiques. Les deux logiciels de modélisation ont produit des résultats qui représentaient fidèlement le comportement observé expérimentalement. Il a ainsi été démontré que le comportement du pont aux diverses étapes d'endommagement grave pouvait être prédite de façon adéquate au moyen de logiciels d'AEF disponible dans l'industrie.

ACKNOWLEDGMENTS

I would like to express my most sincere thanks to my supervisor Dr. Gordon Wight for his guidance, patience, encouragement and support throughout this research project. It was Dr. Wight who encouraged me to challenge myself and offered me the opportunity to further my post-secondary education.

I would also like to thank Mr. Dexter Gaskin for his helpful experience and guidance within the laboratory. It was because of his hours of hard work within the laboratory that testing was able to progress smoothly. I must also acknowledge 2Lt J.C. Ouellet who contributed his time to help with the set-up of the testing apparatus in the laboratory.

I would also like to thank my Mom, Dad, Brother and Dan MacGregor for all their support and encouragement not only during my Master's program but also throughout my undergraduate studies.

TABLE OF CONTENTS

ABSTRACT	i
RÉSUMÉ	iii
ACKNOWLEDGMENTS	v
TABLE OF CONTENTS	vi
LIST OF FIGURES	ix
LIST OF TABLES	xiii
ACRONYMS	xiv
TERMS	xv
CHAPTER 1 : INTRODUCTION	1
1.1 Background	1
1.2 RESEARCH OBJECTIVES	5
1.3 SCOPE	5
1.4 CONTENTS	6
CHAPTER 2 : SHM BACKGROUND	8
2.1 STRUCTURAL HEALTH MONITORING	8
2.2 BRIDGE MONITORING	10
2.3 INSTRUMENTATION	12
2.4 SUMMARY	20
CHAPTER 3 : LITERATURE REVIEW	21
3.1 GENERAL	21

3.2	VIBRATION BASED DAMAGE DETECTION.....	21
3.3	SIGNAL PROCESSING.....	26
3.4	FRP BRIDGE MONITORING	31
3.5	EXPERIMENTAL BRIDGE	32
3.6	SUMMARY.....	35
CHAPTER 4 : EXPERIMENTAL PROCEDURES.....		37
4.1	GENERAL.....	37
4.2	BRIDGE DESCRIPTION.....	38
4.3	SET-UP.....	40
4.4	DATA ACQUISITION.....	45
4.5	INSTRUMENTATION.....	47
4.6	EXPERIMENTAL PROGRAM	54
4.7	LOADING	63
4.8	SUMMARY.....	64
CHAPTER 5 : EXPERIMENTAL RESULTS.....		65
5.1	GENERAL.....	65
5.2	QUASI-STATIC TEST RESULTS	65
5.3	DYNAMIC TEST RESULTS.....	71
5.4	SUMMARY.....	88
CHAPTER 6 : MODELING.....		89
6.1	GENERAL.....	89
6.2	ANSYS MODELS	89
6.3	SAP2000 MODELS	95
6.4	FAILURE PREDICTION	104

6.5	SUMMARY.....	105
CHAPTER 7 : CONCLUSION.....		106
7.1	GENERAL.....	106
7.2	CONCLUSIONS.....	106
7.3	RECOMMENDATIONS FOR FUTURE WORK.....	108
REFERENCES.....		109
APPENDIX A:.....		114
	<i>Calculation of Single Point load for MLC 30 design Bridge</i>	<i>114</i>
APPENDIX B:.....		116
	<i>WIRED RAW DATA (EXAMPLE).....</i>	<i>116</i>
APPENDIX C:.....		117
	<i>WIRELESS RAW DATA (EXAMPLE)</i>	<i>117</i>
APPENDIX D:.....		118
	<i>MATLAB CODE.....</i>	<i>118</i>

LIST OF FIGURES

Figure 1-1: War damaged and temporarily repaired bridge in Komar, Bosnia (Maj Stevens. MWF).....	3
Figure 2-1: Flow of Data into information into decisions adapted from Houston (2011).....	9
Figure 2-2: Strain Gauge averaging effect (ISIS Canada, 2001)	16
Figure 2-3: A typical cross-section of a LVDT coil assembly (Macro Sensors, 2003)	17
Figure 2-4: Wireless network possible orientations: a) star; b) peer-to-peer; c) two-tier (Lynch & Loh, 2006).....	19
Figure 3-1: Deck and box girder damage on the Kumar II bridge (Honorio, Wight, Erki, & Heffernan, 2003)	26
Figure 3-2: Deficiencies spotted in the frequency domain (Ramirez, 1985).....	27
Figure 3-3: Experimental 10m GFRP bridge	32
Figure 3-4: Bison Vehicle used by Landherr (2008).....	35
Figure 4-1: Bridge Loading Concept	37
Figure 4-2: Components of half of the bridge (Xie, 2007)	39
Figure 4-3: Release mechanism (before modifying chain mechanism).....	41
Figure 4-4: Top of Harness	42
Figure 4-5: Bottom of Harness.....	42
Figure 4-6: West End Support Pedestal	43
Figure 4-7: Actuator mounted in place on the support frame	44
Figure 4-8: Narada Wireless DAQ Node	46

Figure 4-9: Narada Base Station	46
Figure 4-10: Strain Gauge Locations (North Side of Bridge)	50
Figure 4-11: Strain Gauge location (Bottom of Bridge)	50
Figure 4-12: Accelerometer Locations (Bottom of Bridge).....	51
Figure 4-13: Dytran 3055B2 Accelerometer.....	51
Figure 4-14: MEMSIC CXL04GP1 Accelerometer.....	52
Figure 4-15: LVDT locations in elevation view and plan view	53
Figure 4-16: Bridge Damage created using a reciprocating saw	57
Figure 4-17: Damage Stage 1 (South Side).....	59
Figure 4-18: Damage Stage 4.....	59
Figure 4-19: Damage Stage 6.....	59
Figure 4-20: Damage Stage 7 West Side	59
Figure 4-21: Damage Stage 8.....	60
Figure 4-22: Damage Stage 10.....	60
Figure 4-23: Damage Stage 12.....	60
Figure 4-24: Damage Stage 15.....	60
Figure 4-25: Damage Stage 16.....	61
Figure 4-26: Damage Stage 17.....	61
Figure 4-27: Damage Stage 19.....	61
Figure 4-28: 3D model of bridge at Damage Stage 18	62
Figure 4-29: Actuator loading on dispersion block.....	63
Figure 5-1: Load-Deflection of Damage Stage 1 and 18	66
Figure 5-2: Load-Deflection repeatability for Damage Stage 1	67

Figure 5-3: Load-Deflection repeatability for Damage Stage 18.....	67
Figure 5-4: Load-Strain comparison for Damage Stage 1 Test 2	69
Figure 5-5: Bridge displacement under 150 kN load at different damage stages	70
Figure 5-6: Bridge stiffness under 150kN load at different damage stages .	70
Figure 5-7: Comparison of wired and wireless time-domain strain response of Damage Stage 7	74
Figure 5-8: Comparison of wired and wireless time-domain strain response Damage Stage 15.....	74
Figure 5-9: Comparison of frequency response from initial state to Damage Stage 18 of SG_U3.....	75
Figure 5-10: Dynamic response in frequency-domain for initial state stage. (A) ACC_3, (B) ACC_2-0, (C) SG_U3 and (D) SG_2-2	77
Figure 5-11: SG_2-2 frequency (A) Damage Stage 2, (B) Damage Stage 5, (C) Damage Stage 8, (D) Damage Stage 13, (E) Damage Stage 16, (F) Damage Stage 17.....	79
Figure 5-12: Bridge frequency for damage stages	82
Figure 5-13: Frequency change of Bridge during change in stiffness	82
Figure 5-14: The 2nd frequency of bridge for damage stages	83
Figure 5-15: 100 kN load dynamic test FFT figures for Damage Stage 15-19	85
Figure 5-16: Standard height test compared to 100 kN load test for Damage Stage 15	86
Figure 5-17: Frequency changes for both dynamic tests over incremental damage stages.....	86
Figure 5-18: 2nd Frequency r for standard height tests and 100 kN load tests	87

Figure 6-1: Vertical displacement result of quasi-static Damage Stage 1 ANSYS model (mm).....	92
Figure 6-2: Bridge profile of Damage Stage 1 with 150 kN load	93
Figure 6-3: Vertical displacement result of quasi-static Damage Stage 18 ANSYS model.....	94
Figure 6-4: Bridge profile of Damage Stage 18 with 150 kN load	94
Figure 6-5: SAP2000 Model at Damage Stage 18	96
Figure 6-6: SAP2000 vertical displacement envelope of Damage Stage 1..	97
Figure 6-7: Time-domain Damage Stage 1 displacement response	98
Figure 6-8: Time-domain Damage Stage 1 acceleration response.....	99
Figure 6-9: Time-domain Damage Stage 18 displacement response	100
Figure 6-10: Time-domain Damage Stage 18 acceleration response.....	101
Figure 6-11: SAP2000 Damage Stage 18 model FFT.....	102
Figure 6-12: Experimental Damage stage 18 FFT	102
Figure 6-13: Frequency of SAP models and instruments	103
Figure A-1: Bending Moments of Wheeled Vehicles as per STANAG 2021. The selected span and MLC has been noted.	114

LIST OF TABLES

Table 2-1: SHM Instrumentation	13
Table 4-1: Bridge components (Xie, 2007).....	39
Table 4-2: Location Descriptions of Wireless Instrumentation	48
Table 4-3: Location Descriptions of Wired Instrumentation	49
Table 4-4: Test Matrix.....	55
Table 4-5: Damage Scheme	58
Table 5-1: Damping Ratios of Damage Stages	72
Table 5-2: Calculated frequency shifts from time-domain ACC_2 and SG_U3	75
Table 6-1: Material Properties (Xie, 2007)	91

ACRONYMS

ACC	Accelerometer
ASCE	American Society of Civil Engineers
CP	Command Post
DFT	Discrete Fourier Transform
FEA	Finite Element Analysis
FEM	Finite Element Method
FFT	Fast Fourier Transform
FOS	Fibre Optic Sensors
FRP	Fibre Reinforced Polymer
GFRP	Glass Fibre Reinforced Polymer
IED	Improvised Explosive Device
ISIS	Innovative Sensing for Intelligent Structures
LVDT	Linear Variable Differential Transformer
MEMS	Micro Electromechanical System
MERG	Military Engineering Research Group
PIV	Particle Image Velocimetry
SG	Strain gauge
SHM	Structural Health Monitoring
SME	Subject Matter Expert
VBDD	Vibration Based Damage Detection

TERMS

$T =$	Period of wave
$\omega_o =$	Is taken from the period of $x(t)$ and equal to $2\pi/T$
$N =$	number of samples being considered
$n =$	The time sample index. Its values are $n = 0, 1, 2, \dots, N-1$
$k =$	The index for the computed set of discrete frequency components. Its values are $k = 0, 1, 2, \dots, N-1$
$F_N =$	Nyquist frequency
$F_S =$	The sampling rate
$\Delta t =$	Sample interval
$x_1 =$	amplitude of the first oscillation
$x_2 =$	amplitude of the oscillation that occurs 'm' cycles later
$m =$	number of cycles
$\delta =$	damping ratio

CHAPTER 1: INTRODUCTION

1.1 Background

Codes and design methodologies have been implemented to ensure that society can safely use structures like bridges and buildings without hesitation. Despite best design and construction practices, structures are often subjected to harsh loading scenarios and severe environmental conditions not anticipated during design which will result in long term deterioration (Lynch & Loh, 2006) and occasionally overloading. Structural Health Monitoring (SHM) is a tool for engineers that can be used to detect damage and changes in structural behaviour at the earliest stages. When damage is detected early, steps can be taken to mitigate the extent and effect of damage on a structure or at least ensure that the structure is being safely operated.

Structural monitoring is a very important practice in locations such as Canada where structures are exposed to a wide range of adverse climates and heavy loads. In 2001, over 40% of Canadian bridges were 30 years old and many of these were in need of rehabilitation or replacement (ISIS Canada, 2001). While that data may be considered dated, the American Society of Civil Engineers (ASCE) found in its 2013 infrastructure report card that the average age of the 607,380 bridges in the USA is 42 years old and over two hundred million trips are taken daily over deficient bridges in the nation's 102 largest metropolitan regions (ASCE, 2013). Along with these staggering statistics, the deterioration and collapse of bridges such as La Concorde Bridge in Montreal (Commission of Inquiry, 2006-2007), have emphasized the need to monitor bridges to detect damage and deterioration early, before damage, injuries or loss of access result.

The first typical step of current bridge monitoring practice is an on-site inspection. These inspections can be long and difficult depending on the size, location, condition of the bridge and the experience of the inspector. Monitoring systems with sensors can be an additional tool for inspectors to gather data regarding bridge behaviour that is not readily visible to the naked eye. Early generation monitoring systems involved instruments wired to a central data system where the data was stored on site and must

still be collected, sorted and processed in person. Externally powered and networked, wired systems have been more recently employed. The development of wireless systems to monitor structures significantly reduces the number of man-hours and costs to both install and maintain the monitoring infrastructure. The ability to quickly and efficiently monitor the behaviour of structures is not only of great benefit to the civilian population but it can be utilized as a great tool by organizations that are dependent on bridge infrastructure for their success, such as deployed military forces.

A common issue with military deployments is the mobility of ground forces, as well as the integrity of supply and convoy routes. In many of the locations that our military troops are deployed, there are not effectively-enforced, comprehensive reference codes similar to the ones that are used and relied on in Canada for the construction of infrastructure. Many bridges and highways are not built to Canadian standards. In many cases, maintenance is poor and these structures may be subjected to loads that exceed their design loads. These structures, specifically bridges, are typically not only under-designed according to our Bridge Code, S6-14 (Canadian Standards Association, 2014) but the loading or environment may have caused significant damage to components of the structures. Furthermore when these structures are located in a conflict zone, the bridges may be subjected to battle damage as seen in Figure 1-1. This damage can result in an internal redistribution of forces creating local overloading effects when the bridge is trafficked. Military traffic can be much heavier in both volume and loads than normal day-to-day traffic in many of these places around the world, once again potentially overloading portions of the bridge structure. Because of this, select monitoring of bridges must be done to ensure that they are able to withstand the traffic that will allow operations to be sustained.



Figure 1-1: War damaged and temporarily repaired bridge in Komar, Bosnia (Maj Stevens. MWF)

The concept of being able to attach wireless sensing networks to the bridges so that they can be continuously monitored from an off-site location is a great asset for a military engineering organization. From these networks, an engineer who is not on site can monitor multiple assets (bridges) at one time and may be able to almost instantaneously recognize any major deterioration or damage, whether from overuse and regular traffic or a traumatic event such as an Improvised Explosive Device (IED) attack or air strike.

With the risk-taking environment of military operations and the need for rapid decision making, an SHM system that can be rapidly deployed while still offering accurate relevant information is a great asset. For example, a Command Post (CP) would be able to monitor several different bridges on a supply route. Being able to see how the different bridges are responding to vehicle traffic can influence command decisions regarding the use of routes. If a sudden irregular response is detected, then possibly a bridge that has been damaged from a traffic or non-traffic source, such as an IED can be avoided, traffic rerouted and military engineers can be immediately dispatched to assess the structure. Furthermore if it becomes necessary to conduct a risk crossing (NATO, 2011) of a damaged bridge structure by a

heavy military vehicle, an in-place SHM system monitored by knowledgeable military engineers would dramatically decrease the level of the risk that would normally be associated with this crossing. An SHM system would be a valuable tool to monitor route bridges, detect extreme events, and reduce the risk of failures. It would facilitate appropriate decision-making for sustaining the mobility of military forces.

To design for such an ideal situation, the SHM system must meet certain criteria. Firstly, the proper sensors must be used to monitor relevant structural responses. Secondly, the system must be deployable and capable of being installed quickly and with relative ease by someone who is not necessarily a subject matter expert (SME). Using accelerometers, strain gauges, transducers and video cameras, the bridge's deflection and deformations can be obtained and monitored for any irregularities or changes and the stresses applied to the structural components can be estimated. Not only will information be gained on the behaviour and state of the bridge structures but intelligence information on the volume and nature of traffic can also be recorded.

Although many of these bridges on deployed operations will be traditional civilian pattern bridges, where bridges have been destroyed or where crossings have been improvised, light-weight deployable bridges may also be used. Structural health monitoring may also be used to assess the behaviour of these structures, particularly in the severe loading and environmental conditions where these structures may be deployed.

While SHM is a field of practice that is being considered as a monitoring option to assess the state and behaviour of bridges, the change of signal that can be detected from heavy and stiff North American structures that have been subjected to deterioration, may be much less significant than the changes that could be detected in similar bridges subjected to extremely heavy loadings and potentially severe battle damage that may occur during operations. When lightweight deployable bridges are employed in operations, it is anticipated that changes in behaviour observed in these types of structure will also be very significant and detectable.

For this project, in an effort to investigate the application of SHM that could be used to monitor the behaviour of bridge structures on deployed operations, commercially available sensors and wireless and wired data acquisition systems were used to monitor the structural behaviour of a 10m

light GFRP box beam structure that was subjected to increasingly severe structural damage.

1.2 RESEARCH OBJECTIVES

The intent of the research contained in this thesis project was to investigate using SHM technologies to assess the behaviour of a 10 m span GFRP bridge when subjected to severe damage. The primary objectives of this project were to experimentally determine the detectable changes in static and dynamic behaviour of the bridge as it was subjected to increasing severe damage and to predict these behaviours using commercially available Finite Elements Analysis (FEA) software. In particular, the following behaviours were monitored and predicted:

- Under quasi-static loading, both the load-deflection and load-strain response of the bridge was monitored, predicted and analysed.
- The change in dynamic response of the bridge including the change of accelerations and strains both in the time and frequency-domain were analyzed to determine if shifts or changes in these responses could act as damage indicators for the bridge using both experimental and predictive modeling data.
- In addition to monitoring and predicting the changing response of the GFRP bridge, a further objective of the project was to investigate the feasibility of using commercially available wireless sensing technology to monitor the bridge behaviour during military operations.

1.3 SCOPE

The purpose of this project was to determine if damage to bridge structures during deployed military operations could be adequately monitored using a simple, commercially available wireless health monitoring system. In order to pursue this intent, this particular experiment was limited to a single bridge structure that was a 10m span and constructed entirely of GFRP. The bridge was assembled as a simple beam with pin and roller end conditions. The experimentation included both quasi-static and dynamic testing with results being monitored and recorded by both wired and commercially

available wireless systems. For safety reasons, repeatability and convenience, the bridge was not exposed to vehicle loading but instead, the loading for the quasi-static testing was produced by a 250 kN actuator. Excitation for the dynamic test was produced by deflecting the structure to a predetermined deflection and rapidly releasing it.

With the main application being one of military deployment, it was necessary for the system to be easily put in place and for the results to be easily understood. For this particular study, an SHM system using accelerometers supplemented by strain gauges was applied. It is expected that changes in frequency, caused by damage, will provide a rapid method to determine the overall bridge response to increasing levels of damage. The system used during this study was one that could be put in place quickly and inexpensively, so it could be rapidly used and subsequently abandoned if necessary. For these reasons, the type of sensors and data acquisition (DA) system considered had to be commercially available, relatively inexpensive and be able to function with a small number of sensors. A limited number of sensors and one wireless DA system was used during this investigation, supplemented by additional sensors connected to a wired DA system to confirm structural behaviour.

Modeling the experimental program is a valuable tool to confirm results as well as predict responses of bridges to different damage levels. The finite element modeling done for this experiment was relatively simple, to mimic what could be done by military structural engineering specialists in deployable operations. The bridge structure itself is represented in moderate detail and linear-elastic finite element modeling was completed.

Although the scope of this investigation has been limited to a single, lightweight, short-span bridge structure, it is believed that the results of this project may be more widely applied to remotely monitor a variety of heavily damaged bridges that may be encountered during operations.

1.4 CONTENTS

Chapter 1 provides a general background to the subject of SHM when employed for military operations, the objectives, and the scope of the research and the organization of this document. Chapter 2 is a more in-depth review of SHM and how it is specifically applied to bridges. Also in this chapter, the types of instrumentation used in this experimentation are

discussed. Chapter 3 offers a review of literature of previous vibration-based damage detection studies, an introduction to the monitoring of damaged FRP bridges and finally, previous work on the experimental bridge used during this study is summarized.

Chapter 4 explains the experimental procedure including the set-up, details of the instrumentation that was used, the loading and the experimental program. The 5th chapter summarizes the experimental results, including both quasi-static and dynamic findings.

Chapter 6 presents the FEA model and the results of the FEA. These results are compared to those obtained experimentally. The final chapter, Chapter 7, includes conclusions based on the experimental and predicted results and recommendations for future work.

CHAPTER 2: SHM BACKGROUND

2.1 STRUCTURAL HEALTH MONITORING

Structural Health Monitoring (SHM) is about assessing the in-service performance of structures using a variety of measurement techniques (ISIS Canada, 2011). It is the process of monitoring a structure, acquiring data, processing data and inferring future behaviours of the structure. The goal of structural monitoring is to gain knowledge of the integrity of in-service structures on a continuous real-time basis (Gastineau, Johnson, & Schultz, 2009).

An often-used analogy of SHM is to that of a doctor checking the health of their patients (ISIS Canada, 2001). A doctor uses specialized tools to check a patient's health just as an engineer utilizes specialized equipment to check the integrity of a structure. If a person's blood pressure is too high, a doctor prescribes corrective medicine or procedures. SHM acts in a similar way, if the data from sensors indicates excessive stress on a structure; the engineer can take measures to rectify the situation as the flow diagram from Huston (2011) shows in Figure 2-1. Decisions can be taken to repair or strengthen the structure or to limit the size of traffic on the bridge. SHM allows potential problems to be resolved before they become catastrophic failures.

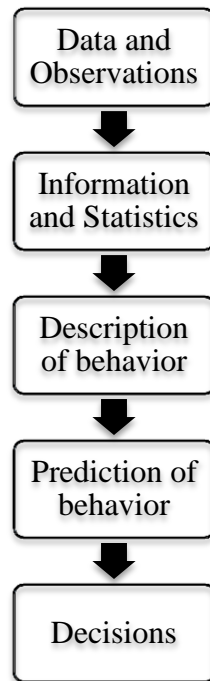


Figure 2-1: Flow of Data into information into decisions adapted from Houston (2011)

Early SHM combined manual observations and experience-based assumptions with mathematical models for predicted behaviours. With the understanding of structural behaviour, SHM systems can combine measurements of loads and structural responses to estimate the current state of a structure and to provide a prognosis for the future (Houston, 2011). Structural health monitoring provides tools and information for engineers who look to improve sustainability of structures, which is becoming ever more important in today's societies.

Structural Health Monitoring can help owners, builders and designers of structures in rational decision making. It allows managers to optimize maintenance activities, while possibly increasing structure safety and creating better designs for future projects (Houston, 2011). The ability for early damage detection correlates with less down time for inspection and repair of structures and also helps with the efficiency of resource allocations

which all aid in financial savings. SHM can also reduce risks for organizations such as military forces deployed on operations. Understanding the integrity of structures within an AOR (Area of Responsibility) allows commanders to make informed decisions and to minimize safety risks to their troops. The poor state of many existing structures and the benefits of SHM has greatly increased the profile of infrastructure monitoring, specifically bridges. Many bridges are now being constructed with monitoring systems employed as an integral part of the construction process and it is because of these advances that organizations such as military forces have begun researching and employing bridge monitoring techniques.

2.2 BRIDGE MONITORING

In addition to the increasing age of Canadian bridges, the United States reports that of the 570,000 existing highway bridges in that country, about 187,000 bridges were classified as deficient in 1997, and an estimated 5,000 additional bridges were becoming deficient each year (Chase & Washer, 1997). Bridges in Ontario must be inspected every two years as dictated by the Ministry of transportation, which is similar for all provinces in Canada. These inspections can vary and be inconsistent due to the different inspectors and the vagueness of the code that enforces visual inspections. In the Ontario Structure Inspection Manual (OSIM) (MTO, 2008) it is stated that ‘A detailed visual inspection is an element-by-element “close-up” visual assessment of material defects, performance deficiencies and maintenance needs of a structure.’ The manual goes on to define “Close-up” as ‘a distance close enough to determine the condition of the element.’ The use of an ambiguous term in the definition allows the wide interpretation of how close and detailed an inspector must be on their inspections. It is also noted in the OSIM that although bridges must be inspected every two years, more detailed investigations and non-destructive testing techniques will be required on many bridges (Ministry of Transportation (Ontario), 2008). The visual inspections are highly subjective and rely heavily on the inspector’s experience and knowledge, which makes the method unreliable if no other methods are used in combination with the required visual inspection (FHWA, 2001).

In addition to gradual damage due to environmental and typical vehicle loading, sudden damage leading to bridge collapses can occur from

collisions. As stated by Doebling et al. (1996), more than 13% of identified failures of US bridges since 1950 are attributed to collisions.

The importance of bridges is easily understandable and that is why the personnel responsible for bridge behaviour must be aware of the condition of the bridges with 'real time' updates. Naturally an SHM system can provide information on the integrity of the bridge; however, the typical SHM system that is employed in North America may not be as effective in deployable situations. The first major difference is the time period that the structure will be monitored. On a deployment, the monitoring of a bridge would be for a relatively short term period; weeks, months, a few years, but almost never for an entire lifespan of the structure, which is what an SHM system may be designed to monitor when used in urban civilian settings. The structural integrity of bridges being monitored will also likely be lower than structures typically monitored in North America. Lastly, the loading and possible damages to bridge structures used by military operations can be drastically different than envisioned during the design process of the bridge structure.

While monitoring the integrity of bridges is just as, if not more important to deployed military forces than their civilian counterparts, they ensure the bridges condition and integrity using inspections rather than monitoring. Detailed guidelines for these bridge inspections are set out in the B-GL-361-014FP-001 Manual for Military Nonstandard Fixed Bridges (DND, 2002). As is outlined in the manual, the extent and thoroughness of an inspection depends on the combat situation and the future plans for the bridge. If the bridge is intended to be used beyond the immediate tactical needs, such that it will be used in future supply routes, the inspection should be detailed enough to ensure prolonged service of the bridge structure. If there are plans to abandon or demolish the bridge structure then a hasty inspection will likely suffice (DND, 2002). It is also expected that bridges are inspected monthly and sometimes daily (DND, 2002). It is apparent that many man-hours are dedicated to bridge inspections for deployed forces. It can be understood how an SHM network could be used to minimize the man hours necessary to ensure the structural integrity of the bridge structures in theatre.

Understanding the operational characteristics of the bridge, including the load-carrying mechanism and the possible damaged regions of the bridge is one of the most important steps in creating and developing a reliable SHM

for a bridge (Mosavi, Vibration-based Damage Detection and Health Monitoring of Bridges, 2010). For example, in a simply-supported reinforced concrete bridge structure, the point of the greatest deflection and highest moments will be at mid-span. Understanding that mid-span will represent the largest deflections can help determine where to position instrumentation for a monitoring system as well as which type of instrument to use for assessing bridge response.

2.3 INSTRUMENTATION

There are many different types of sensors and instruments that can be used and combined to create a simple or complex monitoring system. Some of the most commonly used instruments include accelerometers (piezoelectric and MEMS), LVDT's, foil strain gauges and Fibre Optic Sensors (FOS) that can measure strain, displacement and even temperature. Video-monitoring and Particle Image Velocimetry (PIV) has also made recent strides to become a very valid option in not only measuring displacement but also strain. Table 2-1 describes the different instrumentation available for an SHM system and possible selection criteria for use within a military setting.

The instrumentation devices presented in this section were selected for a military application SHM network because of their simplicity, ease of use, relatively low cost and the quickness with which a system of these instruments could be erected. Further discussion of accelerometers, strain gauges and LVDTs are provided in the following sections. Because of their higher initial cost and the limited scope of this particular project, FOS and video monitoring were not employed on this particular project and are not discussed further.

Table 2-1: SHM Instrumentation

Sensors	Installation	Cost	Application	Remarks
Accelerometers	Simple to apply	Moderate	Monitors overall behaviour of bridge vibrations and dynamic response	<ul style="list-style-type: none"> -Easy to monitor -Knowledge of structure is required -Significant damage may be required to register effects -Affected by the mass of traffic on a structure
Strain Gauge	Simple to apply	Inexpensive	Monitors strain of critical damaged components	<ul style="list-style-type: none"> -Easy to monitor -Knowledge of structure is required -Only provides information on components -placement location may be critical

LVDT	Can be difficult to find a stationary reference location to attach to	Moderate	Monitors deflection of overall bridge as well as critical components.	-Easy to monitor -Knowledge of structure is required -Sensitive to small movements of reference base of instrument
Fibre Optic Sensors	Application required over a long length	Sensor cost low to moderate but required DA is expensive	Monitor strain of the overall bridge or at critical components	-Knowledge of structure is required - single FOS can provide specific deformation information at several locations along its length
Video	Can be difficult to find a stationary reference location	Expensive for dynamic monitoring	Monitor strain and deflection of overall bridge	-Need advanced knowledge of software -Need large data storage space

2.3.1 ACCELEROMETERS

Accelerometers measure acceleration forces, which can be quasi-static such as gravity, or more commonly for engineering purposes, dynamic which is caused by moving or vibrating the accelerometer (Anderjasic, 2008). Accelerometers commonly used in civil engineering are piezoelectric accelerometers and micro electromechanical system (MEMS) accelerometers.

Piezoelectric accelerometers are made of a piezoelectric crystal and an attached mass that is coupled to a supporting base. When the base undergoes a movement, the mass exerts an inertia force on the crystal element. The force produces a proportional electric charge within the crystal (ISIS Canada, 2001).

In contrast, the MEMS accelerometer is essentially a damped oscillator. The accelerometer includes a movable proof mass with plates that are attached through a suspension system to a reference frame. The movable plates and fixed outer plates act as capacitors. The deflection of the proof mass is measured using the capacitance difference (Anderjasic, 2008). Essentially the acceleration from a MEMS accelerometer is determined by the distance of the proof mass from the fixed plates, or the change in capacitor distance.

Typically piezoelectric accelerometers are light and small and operate over wide acceleration and frequency ranges. While MEMS accelerometers tend to be bulkier they are very sensitive to small accelerations and provide better resolution (ISIS Canada, 2001).

2.3.2 STRAIN GAUGES

Foil strain gauges are attached to structural elements and wired to data reading units (ISIS Canada, 2001) that are used to measure strain in the element which can later be used to estimate stress in the material. When attaching the strain gauge to the element, specialized strain gauge adhesive is usually used to bond the gauge to the element, so that it will be affected by tension and compression forces the same way the element would. Strain gauges come in many different sizes and shapes, but in the simplest forms they are nothing more than a system of electrical current resistors. The strain experienced by the specimen is transferred directly to the strain gauge, which responds with a linear change in electrical resistance (National

Instruments, 2013). Foil strain gauges are relatively cheap and easy to use, however, they can be damaged easily and take time and effort to attach and wire for usage.

The main component in determining which strain gauge is appropriate is the strain sensitive alloy used in the foil grid. Common alloys include constantan, nickel-chromium and isoelastic alloys (ISIS Canada, 2001). Constantan is the oldest and most widely used alloy because it has the best overall combination of properties needed for many strain gauge applications. These properties include adequately high strain sensitivity, or gauge factor, that is relatively insensitive to strain level and temperature, and it is characterized by good fatigue life and relatively high elongation capacity (ISIS Canada, 2001).

In addition to the alloy of a strain gauge, the gauge length must be considered. Strain gauges tend to average strain over the area covered by its grid as demonstrated in Figure 2-2

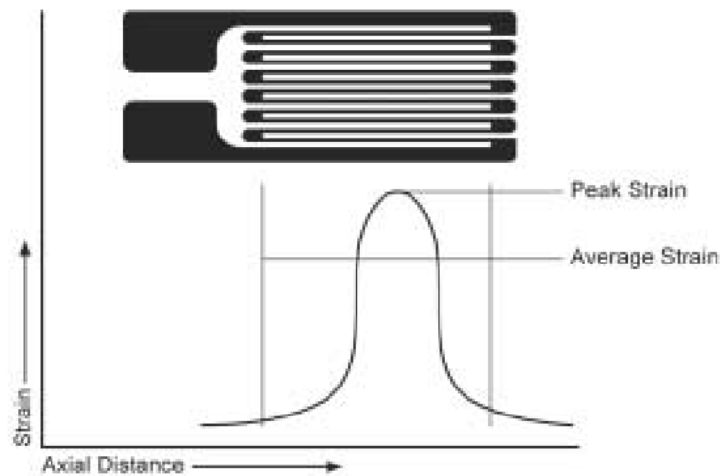


Figure 2-2: Strain Gauge averaging effect (ISIS Canada, 2001)

A smaller gauge length is required for highly localized strain; however, when the average strain is sought over a length, the gauge must be long enough to ensure that the average strain can be obtained over the length

required (ISIS Canada, 2001). The longer gauges also provide improved heat dissipation, to minimize thermal effects of the gauge and to increase performance and accuracy. When choosing a foil strain gauge for a project, the environment, desired area of strain readings and wiring requirements must all be considered.

2.3.3 LINEAR VARIABLE DIFFERENTIAL TRANSDUCER

Linear variable differential transducers (LVDTs) are used for displacement measurements. An LVDT is made of a primary winding between a pair of identically wound secondary windings as the stationary element and the magnetically conductive core as the moving element (Macro Sensors, 2003) (Figure 2-3).

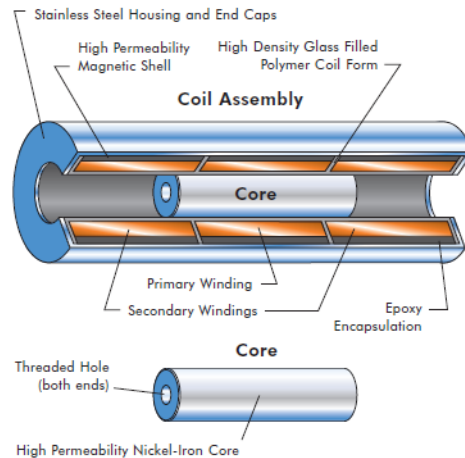


Figure 2-3: A typical cross-section of a LVDT coil assembly (Macro Sensors, 2003)

When an AC excitation is applied to the primary winding, it generates an inductance current in the secondary wirings. When the magnetically conductive core is equidistant between the secondary wirings there is no voltage at the secondary outputs. When the core moves, a differential voltage is induced at the secondary output, the magnitude of which changes linearly with the magnitude of the core's distance from center (ISIS Canada, 2001).

LVDTs come in different sizes with different sensitivities. They can measure movements of small fractions of a millimeter or centimeters of movement. Before selecting the appropriate LVDT for a project, the total displacement to be measured must be estimated to ensure the entire displacement can be measured.

2.3.4 DATA ACQUISITION

Data acquisition is the process of measuring an electrical or physical phenomenon such as voltage, current, temperature, pressure or sound with a computer (National Instruments, 2013). Data acquisition hardware acts as an interface between a computer and the signals from sensors. It primarily functions as a device that digitizes incoming analog signals so that a computer can interpret them (National Instruments, 2013). The main components of a DAQ device are the signal conditioning, the analog to digital converter and the computer bus. The signal conditioner manipulates a signal into a form that is suitable for the analog to digital converter by manipulating the signal by doing such things as cleaning signal noise, amplifying, filtering or isolating the signal (National Instruments, 2013). The analog to digital converter takes periodic samples of the analog signal at a predefined rate, as analog signals continuously vary over time. The final component, the computer bus, serves as the communication interface between the DAQ and the computer and is commonly offered as USB, PCI and Ethernet (National Instruments, 2013).

While components may consist of various hardware and operate different software within an SHM network, the process is typically similar to the one described above. In a wired system, the sensors are typically all wired individually to the data acquisition components. In a wireless system there are many different ways to arrange the system. Systems can include wireless sensors that transmit their data wirelessly to one collection point or can have sensors that are wired to nodes that gather the data from the sensors and transmit the collected data to the receiver; which could be a storage device or a real-time device such as a computer. Three examples of wireless networks are shown in Figure 2-4. The star orientation has multiple instruments all transferring data to a central node before it is processed. In the peer to peer arrangement, sensors are able to transmit data to other nodes as needed and eventually to the computer or data storage unit. The final illustration is of a two tier arrangement where smaller ‘star’ arrangements are used within a peer to peer arrangement of larger nodes.

The advantage of using a wireless network is the small amount of wiring necessary to have a network fully functional. Compared to a wired network, where each node must be carefully wired, labeled and connected to the proper terminal at the data acquisition, the wireless network may be considered a “plug and play” system. The current downfall with wireless systems is the available bandwidth. Wired systems can transfer data quickly and in large sums, only limited by how quickly the acquisition system can handle and process the raw data. In the case of the wireless systems the data acquisition system and nodes must have enough bandwidth to wirelessly transmit and receive data; typically this can cause data gathering speed and size to be slower and smaller than wired systems.

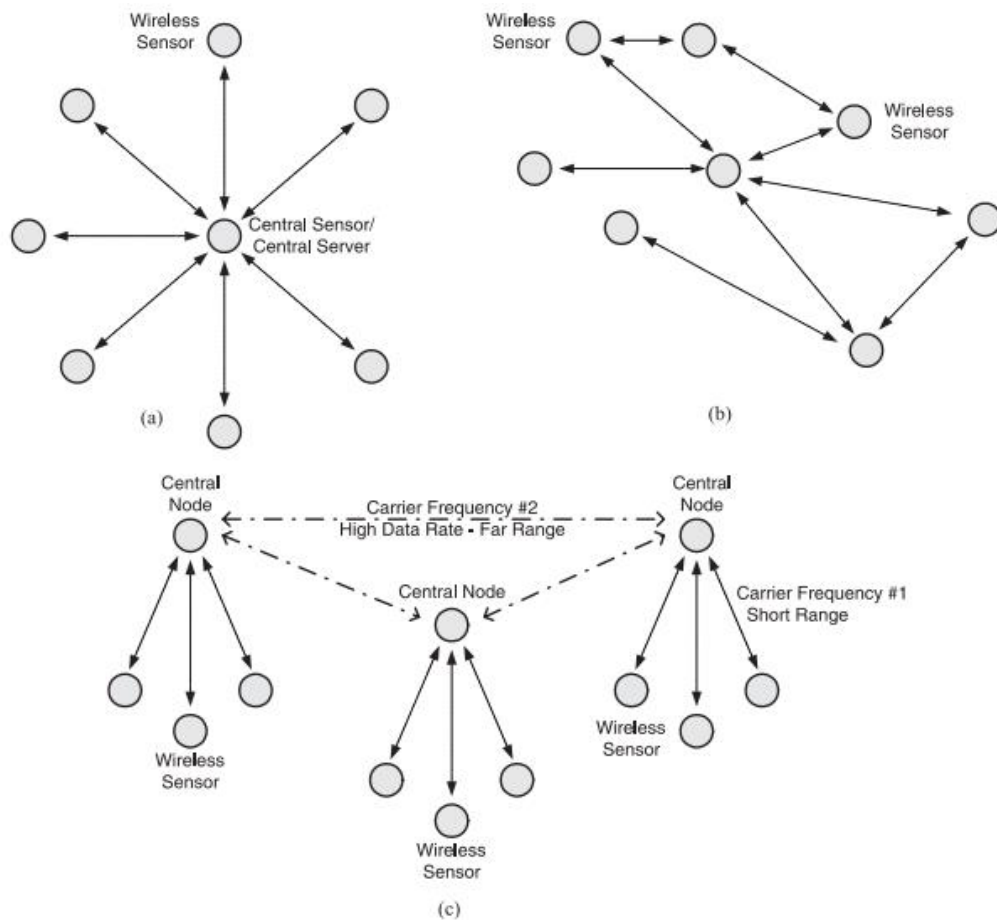


Figure 2-4: Wireless network possible orientations: a) star; b) peer-to-peer; c) two-tier (Lynch & Loh, 2006)

2.4 SUMMARY

Structural Health Monitoring as a concept has been reviewed. SHM and its importance as it pertains to bridge structures has become increasingly important in today's society and was discussed. The basic instrumentation employed in SHM systems that were used in this experiment has been described and their functions have been defined. The simplicity of the chosen instrumentation reinforces the selection of these sensors as appropriate for use in deployed military operations. The general practice of SHM has been reviewed as background to literature reviews in Chapter 3 of vibration damage detection, the data processing related to SHM and previous testing done on the GFRP Bridge used in the experimental laboratory testing.

CHAPTER 3: LITERATURE REVIEW

3.1 GENERAL

SHM in bridges has become a topic of growing interest due to the accelerating deterioration and occasionally compromised integrity of civilian structures. This deteriorated infrastructure is very apparent in large bridges in Canadian cities such as Montreal and the severity of consequences can be seen in the La Concord bridge collapse in 2006 (Commission of Inquiry, 2006-2007). While bridges in these urban centres and Canadian highways come under scrutiny, Canadian Forces are sent abroad and expected to use bridges that are often more severely damaged. Typical SHM systems for civil applications involve several sensors that are in place for the structure's entire life span. However, for situations that are relatively short-term and inhibit the installation of large SHM networks, as may be potentially required on military deployments, a different approach may be considered. One such method used in several engineering fields is vibration-based damage detection. This method offers a technique that is thorough enough for bridge monitoring but can also offer results that an engineer; without an extensive background in bridge responses, can understand and interpret.

Along with the evolving health monitoring systems, there have been great strides in the development of FRP products for use in bridge structures. The high strength to weight ratios of FRP components have made FRP bridges a subject of interest for deployable, short-term bridges that are suitable for use by deployed military forces.

3.2 VIBRATION BASED DAMAGE DETECTION

Vibration-based SHM in its infancy was used primarily in the aerospace and mechanical engineering fields while its use for monitoring civil engineering structures is more recent. The general purpose of vibration based damage detection (VBDD) is to determine if there is damage to a structure, based on the changes to its dynamic properties, such as frequency, mode shape and damping ratios (ISIS Canada, 2001). The application of VBDD methods to civil engineering structures such as bridges has been complicated by a

combination of factors, including the relatively large size of these structures, the inherently greater uncertainties in material properties, support conditions, connectivity of components, variability in loading and environmental conditions (Zhou, 2006). As reported in Mosavi (2010), in early uses of frequency change for damage detection, offshore oil industries found that natural frequencies changed considerably for some damage cases while they did not change for others. They concluded that whenever damage occurred in a structural member with high structural redundancy, the natural frequencies were not a good indicator of damage. When it can be detected, natural frequency change is an attractive method for determining damage because it is relatively simple to measure from just a few accessible points on the structure (Mosavi, *Vibration-based Damage Detection and Health Monitoring of Bridges*, 2010). Since the effective stiffness and mass are global properties, the resonant frequencies tend to be sensitive to global changes to the mechanical properties and less sensitive to local changes in stiffness and mass (Huston, 2011) which may mask the effects of minor damage.

Salawu and Williams noted that during full-scale ambient vibration testing, Creed was able to measure natural frequencies of a six-span concrete motorway bridge repeatedly within 2.5% (Salawu & Williams, 1995). This would imply that a natural frequency change outside the 2.5% would indicate a change in the motorway structure and potentially the onset of damage. Determining frequency changes of a bridge structure is a simple way to determine if damage is present, but much research has been done to determine the variability of frequencies due to ambient affects. Farrar et al. (1997) conducted vibration measurements on a concrete composite bridge in New Mexico that showed frequency variations due to different factors. The first of these factors was due to temperature changes. They found that the first mode frequency varied approximately 5% during a 24 hr period which correlated to deck temperatures. The other notable change in resonant frequencies was found by exciting the bridge with vehicles on the bridge, increasing the mass added to the bridge which translated into a 19% change in frequency. Mosavi et al. (2012) also conducted vibration measurements on a steel-concrete composite bridge to determine frequency change due to temperature. Their research found an average first mode frequency change of 1-2% from morning temperatures to temperatures at noon. While temperature changes can result in frequency response changes, damage to the bridge has been shown to cause frequency changes exceeding those associated with temperature changes.

Research has been conducted to determine if changes in natural frequencies is a reliable damage detection method. Many researchers come to the same conclusion that the change in natural frequency is able to detect extensive damage but it is not able to accurately determine where the damage is. Tests done by Mosavi (2010) on damaged I-beams found a decrease in natural frequencies is the direct result of the decrease in the stiffness of the beam by introducing damage. It was also determined that the amount of decrease in the natural frequencies increased as the extent of the induced damage increased. As Wang (2011), determined; with testing on a multi-girder composite concrete bridge superstructure, the natural frequencies of the system steadily decreased as damage states were introduced incrementally to various structural elements (Wang, 2011). While the changes were small and not outside the changes expected due to environmental affects, the damage induced on the bridge was small and local.

Roeck et al (2000) completed vibration testing on a Swiss bridge, the Z24. While the authors noted that ambient temperature changes from 0° to 30° degrees Celsius caused a 3% shift in the first natural frequency of the bridge, they determined that damage could still be detected from frequency shifts and the shift due to temperature could be filtered out of the damage detection data (De Roeck, Peeters, & Maeck, 2000). Applied damage to the Z24 bridge for the testing included damage such as; chipping of concrete at the underside, due to vehicle over height and corrosion, settlement of foundation, failure of tendon wires, failure of tendon anchors and failure of concrete hinges. It was determined that from the applied damage scenarios that the frequency shifted up to 7%. In addition, it was found that only damage scenarios that produce stiffness reductions could be identified; for instance a loss of prestress will only result in measurable change in frequencies if it is accompanied by cracking (De Roeck, Peeters, & Maeck, 2000).

Kato and Shimada (1986) studied a 5 year old bridge in a local district that was taken out of use to make way for a new highway interchange. This bridge was used to study bridge vibrations during the bridge's failure process. The bridge was a prestressed concrete voided slab bridge, which seemed to have carried less than its design weight and had no visible cracks (Kato & Shimada, 1986). The bridge underwent six static tests and three vibration tests. Ambient vibrations were used to excite the bridge after the final three static tests. Cracks were detected during static tests and were

considered to be the damage to the bridge. The data was digitalised and processed using a Fast Fourier Transform (FFT). From there it was determined that the natural frequency of the first vertical motion decreased as loading cycles [damage] increased. The three different damage stages caused the first vertical motion natural frequency to decrease by 17% (Kato & Shimada, 1986). While cracks formed and caused a small decrease in frequency, it was not until the prestressing wires reached the elastic limit that large changes were observed. This field study again exemplified that flexural support damage can be detected by frequency shift, and that larger damage will have larger effects on the frequency response.

Hsieh, Halling and Barr (2006), wrote an overview of three bridges that underwent testing to determine the change in frequency. The first bridge was the I-80 flyover bridge in Salt Lake City that underwent forced and ambient vibration tests over a four year period. It was found that over four years, a 4.4% change in frequency was detected (Hsieh, Halling, & Barr, 2006). Testing done on the South Temple Bridge, also in Salt Lake City, was conducted by forced vibration with damaging and repairing different bents on the bridge. Testing concluded that measurable frequencies were reduced due to damages and increased due to repairs. The final bridge tests summarized were of the I-215 Curved Girder Overpass in Salt Lake City. For the testing, forced vibration was applied to the bridge with changing boundary conditions (support conditions). The support conditions were reduced, which could represent damage to said support conditions. It was determined that as support conditions were reduced so were the frequencies of the bridge. During the first phase of testing which included a complete severance of the bridge abutments and integral approach aprons from the bridge deck and parapets, a 28% reduction in frequency was found. A further attempt to reduce as much restraint as possible resulted in a further 25% reduction in frequency (Hsieh, Halling, & Barr, 2006). From all three bridges it can be seen that damage and degradation could be detected by the frequency change in the bridge.

Mazurek and DeWolf (1990) completed laboratory tests on a model of a full scale bridge that also confirmed the usefulness of frequency change as a damage indicator. The model was built of two I-section girders securely joined together by ties on the top and bottom. This made the girders unable to act independently and caused the model essentially to be a box girder. Degradation tests were completed using ambient vibrations. The deterioration considered was support failure and crack propagation. By

removing a support at mid-span to simulate support failure, only a small frequency shift in the second mode was detectable. However, with the introduction of a crack on one of the girders, a frequency shift became quite apparent. The first crack length only slightly changed the frequency but as the crack length increased, the rate of frequency change also increased. The crack became large enough to reduce the overall bridge vertical flexural moment of inertia to 67% of the original cross-section. Associated with the damage and reduction in stiffness, the percent change in the 1st bending frequency was approximately 11% (Mazurek & DeWolf, 1990).

As illustrated in this section, determining if damage is present on a large civilian bridge structure can be difficult when only using frequency shifts. However, the damages inflicted on these bridges are representative of gradual degradation or small acute damage that is consistent with well-maintained civilian bridges in thriving societies. In most literature about frequency shift damage detection, it is noted that the process would work better with large damage that causes frequency shifts much larger than those obtained through temperature changes. In the case of deployable military operations, where there is a higher acceptable tolerance of risk, it is only the large incidences of damage that may cause bridge failure that are of most concern. Forces on deployed operations are exposed to many situations where there is severe bridge damage. As seen in Figure 3-1, a bridge had a girder as well as the bridge deck heavily damaged by artillery or air ordnance. Damage such as this can be a common sight for military units in theatres of operations and cannot be avoided, whether for military operations or for public safety. With severe damage such as this, it appears reasonable that indications of this damage and subsequent degradations can be determined from VBDD.



Figure 3-1: Deck and box girder damage on the Kumar II bridge (Honorio, Wight, Erki, & Heffernan, 2003)

3.3 SIGNAL PROCESSING

Transducers typically record data in the time domain as a continuous signal. While most people are comfortable reading data in the time domain, it is necessary to process the data into the frequency domain for structural analysis. By studying the data in the frequency domain, small changes in the dynamic response of a damaged component are made apparent by visible frequency changes as demonstrated by Ramirez (1985) in Figure 3-2.

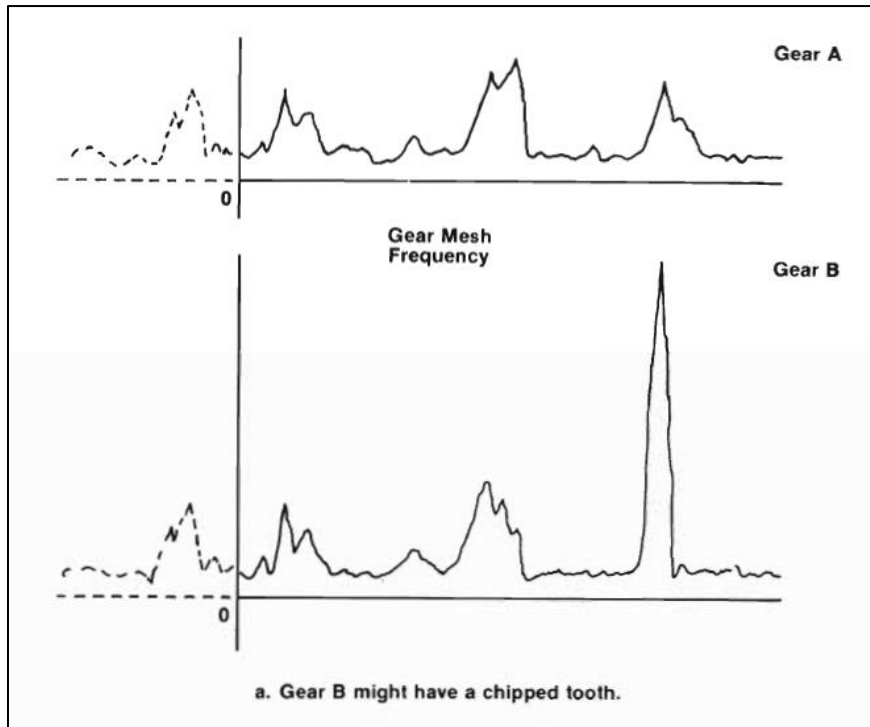


Figure 3-2: Deficiencies spotted in the frequency domain (Ramirez, 1985)

The Fourier series was founded to show how a mathematical series of sine and cosine terms can be developed to analyze heat conduction in solid bodies (Ramirez, 1985). The Fourier series today is defined as (Ramirez, 1985):

$$x(t) = a_0 + \sum_{n=1}^{\infty} (a_n \cos n\omega_0 t + b_n \sin n\omega_0 t) \quad (3-1)$$

$$a_0 = \frac{1}{T} \int_0^T x(t) dt \quad (3-2)$$

The remaining coefficients, a_n and b_n are evaluated for $n=1,2,3,\dots$ by

$$a_n = \frac{2}{T} \int_0^T x(t) \cos n\omega_0 t dt \quad (3-3)$$

and

$$b_n = \frac{2}{T} \int_0^T x(t) \sin n\omega_0 t dt \quad (3-4)$$

The Fourier series is intended for use with periodic waveforms while the Fourier integral, shown in Equation (3-5), is to be used for non-periodic waveforms. The major difference between the series and integral is that, the Fourier series transforms time-domain functions to frequency-domain magnitudes and phases at specific, discrete frequencies. The Fourier integral, on the other hand, evaluates to a continuous function of frequency.

$$X(f) = \int_{-\infty}^{\infty} x(t)e^{-j2\pi ft} dt \quad (3-5)$$

Both the Fourier series and Fourier integral are constrained to waveforms that are mathematically describable; in other words they can't be used unless an equation can be written for it. The mathematics for both is very long and tedious. While tables and charts exist for common waveforms, the mental investment required to transform a non-common waveform usually proves to be too great. It is for these reasons that waveform digitizing and digital signal processing is used. This is where the Discrete Fourier Transform (DFT) and the Fast Fourier transform (FFT) become applicable in transforming waveforms from the time-domain to the frequency-domain. The DFT and FFT operate on finite sequences; sets of data with each point discretely and evenly spaced in time, however, real-life waveforms are analog in nature. These waveforms are continuous and they must be sampled at discrete points and be digitalized before the DFT or the FFT algorithm can be applied (Ramirez, 1985).

The DFT is used with digitized signals, and like the family of Fourier analysis, it is based on decomposing signals in sinusoids (Smith, 1997). The first of three common ways that the DFT is used is to calculate a signals frequency spectrum; a direct examination of information encoded in the frequency, phase and amplitude of the component sinusoids. The second use is to find a system's frequency response from the system's impulse response and vice versa, allowing systems to be analyzed in the frequency domain. Finally the DFT is used as an intermediate step in more elaborate signal processing techniques such as the FFT (Smith, 1997). The DFT can be used to represent every output signal as a group of cosine waves, each with a specified amplitude and phase shift. This means that any linear system can be completely described by how it changes the amplitude and

phase of cosine waves passing through it, this information is called the frequency response (Smith, 1997). Using both the Fourier series and Fourier integral the DFT can be determined as:

$$X_d(k) = \sum_{n=0}^{N-1} x(n)e^{\frac{-j2\pi kn}{N}} \quad (3-6)$$

Where

- N = number of samples being considered
- n = the time sample index. Its values are $n = 0, 1, 2, \dots, N-1$
- k = the index for the computed set of discrete frequency components.
Its values are $k = 0, 1, 2, \dots, N-1$

The greatest problem for the Fourier transforms in early years was the amount of time and effort to do the computation. It wasn't until the 1960's that a breakthrough was made to speed up the computing of larger sample sizes, when James W. Tukey and J.W. Cooley came together to form the Cooley-Tukey algorithm, which, for the most part, is simply referred to as the FFT (Ramirez, 1985).

The FFT is an efficient implementation of the DFT which maps a sequence $x(n)$ into the frequency domain; and is the most widely used in digital signal processing (Rao, Kim, & Hwang, 2010). The FFT takes advantage of the fact that the calculation of the coefficients of the DFT can be carried out iteratively, which results in a considerable savings of computation time (Cochran, et al., 1967). The FFT is able to process the signal much quicker than the DFT for a couple of reasons, first is that the FFT will typically only compute the Fourier coefficients for the positive frequency domain, since the negative frequency domain is just a duplicate for the positive half for real functions of time (Ramirez, 1985). The larger reason for the time saving is the use of a log function for the amount of operations that must be completed, which requires significantly less computational effort (Cochran, et al., 1967).

One of the most important considerations when using the FFT is ensuring the sample size is large enough. Due to the Nyquist frequency, F_N , sample rates must be greater than twice the highest frequency. The Nyquist frequency determines the highest frequency component of a waveform that

can be defined by sampling. It is determined by the sampling rate and is given by:

$$F_N = \frac{F_S}{2} = \frac{1}{2} \Delta t \quad (3-7)$$

Where F_s is the sampling rate and is equal to the reciprocal of the sample interval, Δt . This means that a component at the Nyquist frequency is sampled twice over its period, a component less than the Nyquist frequency is sampled more than twice on each cycle, and one greater is sampled less than twice per cycle (Ramirez, 1985). This is important because it takes at least two points per cycle to uniquely define a sinusoid of given amplitude and frequency. Therefore, components below the Nyquist frequency are correctly defined, while a component above the Nyquist frequency has less than 2 samples per cycle and is redefined as a low-frequency alias. The alias will fall below the Nyquist frequency by the amount the original component exceeds the Nyquist component (Ramirez, 1985). If an appropriate sample size is not used, aliasing could cause an incorrect analysis of results. A frequency response may be apparent in a data set due to aliasing and not component response. This could lead to conclusions that a component is damaged when in fact it is good working order. It is for this reason that a general understanding of the frequency response is required when doing data analysis in the frequency domain.

3.3.1 MATLAB

As discussed in this chapter, it is necessary to use a computer to quickly and efficiently complete a Fourier transform using the FFT. One such software package that can be used to implement the FFT is MATLAB. MATLAB is a high-level language and interactive environment for numerical computation, visualization and programming (MathWorks, 2012). One of the applications of MATLAB is signal processing, in which the software uses the Fast Fourier Transform. The built in FFT function returns the discrete Fourier transform of a vectored or matricide input. One benefit of using a program such as MATLAB is that recorded data from the SHM system can be brought in to be used directly in Excel format.

3.4 FRP BRIDGE MONITORING

While FRP has started to become a more widely-accepted material in structural design and construction, there are still very few instances of entire FRP bridges. Research and dynamic response data for full-scale bridges constructed entirely of FRP is relatively new and limited. Research on the response of severely damaged bridges is almost non-existent at this time. While research and publications of damaged FRP bridges are scarce, there have been projects to monitor the integrity of a few FRP bridges in service.

One such project is captured by Zhang et al. (2006) who gives an overview of the dynamic performance of an FRP bridge in service in Kansas. The bridge is 7.08 m in length, 8.45 m wide and 0.57 m thick. It is composed of three sandwich panels laid side-by-side and connected by interlocking longitudinal joints. A finite element model was created for the bridge and a concrete slab bridge with similar dimensions and static properties. The models were exposed to moving vehicle loads to capture the differences in dynamic responses between a concrete and FRP bridge. From the different vehicle models used on the bridges, it was determined that for this case, the FRP bridge had significantly lower dynamic impact factors when compared to the concrete bridge. Therefore, the researchers suggested dynamic impact factors specified in the AASHTO for conventional bridges can also be safely applied to the strength design of FRP bridges (Zhang, Cai, Shi, & Wang, 2006). The other significant result from the project was that accelerations and the natural frequency from the FRP bridge were found to be significantly higher than the accelerations found in the concrete bridge (Zhang, Cai, Shi, & Wang, 2006).

At the Royal Military College of Canada a full-scale Pratt truss bridge was constructed of standard pultruded GFRP sections with a span of 6 m and a width of 3 m. While the bridge included steel bolts and timber and steel decking, the other major components were entirely comprised of GFRP (Yantha, 1995). Both static and dynamic laboratory tests were conducted on the bridge, which was simply supported for both sets of testing. The static tests were conducted using both a 250 kN and 500 kN actuator to load the bridge. For dynamic testing, an impact hammer was used to excite the bridge structure. From the static testing, it was determined that the bridge remained linear-elastic under 150 kN loads, that there was no difference in structure stiffness when using steel bolts or GFRP threaded rod as connections and the maximum vertical displacements up to failure were

within the limits prescribed by the code at that time (Yantha, 1995). Dynamic results showed that the addition of pretensioned cables caused higher first natural frequencies, the GFRP connection resulted in lower natural frequencies and the addition of the truss braces and steel edge plates improved dynamic performance.

3.5 EXPERIMENTAL BRIDGE

The experimental GFRP Bridge used in testing was designed by structural engineering members of the “Military Engineering Research Group (MERG)” at the Royal Military College. The bridge was developed to be deployable in operations to restore access and mobility to damaged bridges on supply and traffic routes. The 10-m span full-scale box-beam shown in Figure 3-3 was designed and built using commercially available GFRP pultruded sections purchased from Creative Pultrusions Inc. (Xie, 2007).



Figure 3-3: Experimental 10m GFRP bridge

The bridge was designed with practical use in mind. The most noticeable design feature of the bridge is the two different slopes of the bridge which has many benefits. By designing a double slope approach of the bridge, the geometry is closer to the parabolic shape of the bending moment curve than what it would have been using a single slope (Xie, 2007). The change in slope is a more economical use of materials, as it reduced the mid-span height without compromising the span of the box beam (Landherr, 2008). Finally, the two slopes reduce the change in angle at the apex, thereby reducing the impact force caused by a vehicle going over the apex and increasing driver comfort (Landherr, 2008). Aside from the double sloped approach, the bridge was also designed in two halves with a metal hinge attaching the halves. The ability of the bridge to be folded in two 5m halves, allows the bridge to be transported much easier in deployable situations. Finally the ribbed deck of the bridge not only offers obvious traction to vehicles, but it also disperses vehicle loads across the entire width of the bridge to lessen the possibility of puncture damage.

Xie (2007) and Landherr (2008) both conducted quasi-static and dynamic tests on the GFRP Bridge used for experimentation. Xie's (2007) quasi-static testing included loading with and without the ribbed deck to determine the added stiffness of the ribbed deck, as well as different patch loading positions to simulate vehicle wheels. Single patch testing conducted by Xie (2007) used loads of 50 kN and 65 kN while double patch loading was done with loads of 57 + 57 kN and 55 + 55 kN. Under a 50 kN load, Xie (2007) determined that the ribbed deck's stiffness contribution was about 1.9 times of the ramp plates without the ribbed decking. Using patch loading to simulate vehicle wheel locations of an MLC 30 vehicle, a displacement of 25.4 mm and 30.8 mm was measured for loading on mid-plane and loading 305 mm off-centre respectively. It was also determined from the patch loading, off of centerline, that the bridge had sufficient torsional rigidity.

Similarly to Xie (2007), Landherr (2008) conducted quasi-static testing in the laboratory, using a 1000 kN capacity actuator in a similar loading frame used by Xie (2007). The quasi-static testing included two tests of a 100 kN load and a single test of a 150 kN load, in which both strain and displacement were measured. The maximum deflection observed at 150 kN was 32.5mm at mid-span, while a deflection of just over 20mm was recorded for a load of 100 kN.

Strains at mid-span were recorded as the highest magnitude of strain at 1154 and -1109 microstrain. A strain gauge on an GFRP tube close to mid-span experienced the highest strain value for an GFRP member during the 150 kN loading of 707 microstrain which corresponded to a stress value of 20.2 MPa. All the strain data observed were within the ultimate material strengths on the bridge, ensuring the safety of future field and dynamic testing.

Dynamic testing conducted by Xie (2007), was done using an impact hammer. The 20 kg hammer head was dropped from a maximum height of 1.5 m which loaded the bridge with a maximum load of 42 kN. From the dynamic testing, the first natural frequency was found to be 12.1 Hz and a damping of 3.3%. Landherr (2008) also conducted dynamic testing of the bridge structure; however, it was done using moving vehicles. Landherr's dynamic testing was done in the field using a Bison vehicle, an MLC 16 vehicle shown in Figure 3-4. As the bridge is only one track of a two track bridge, a gravel ramp was constructed parallel and to a similar profile as the bridge to act as the second track. To acquire dynamic responses of the bridge, the Bison was driven across the bridge at speeds varying from 10 km/h to 25 km/h. To induce additional dynamic impact, tests were conducted with a wood beam placed across the bridge and with the bison braking on the bridge. From the vehicle loading during field testing it was determined that frequency response of the bridge was very similar to the dynamic testing performed by Xie (2007) with a first natural frequency found to be 11 Hz. These results confirm that laboratory dynamic testing can be done to infer field-testing results.

The last testing performed on the bridge before this experimentation was dynamic response of the bridge after damage; mostly minor. The damage included debonding of the top plate, crushing of the ribbed decking and buckling of the webs. It was determined that the natural frequency of the bridge structure changed less than 1 Hz which would not likely be enough of a change to conclude that debonding has occurred and not some other influence (Landherr, Wight, Green, & Erki, 2009). Similar results were found with the ribbed deck crushing and the buckling of the web. This data showed that small damage had little effect on the natural frequency of the bridge structure.



Figure 3-4: Bison Vehicle used by Landherr (2008)

3.6 SUMMARY

The concepts of Vibration Based Damage Detection, some of its shortcomings and case studies using VBDD have been reviewed. The Fourier transfer and its necessity within VBDD was outlined. Previous testing completed on the GFRP Bridge used in this experimentation was examined for comparison in later chapters.

While there has been a substantial amount of SHM and VBDD testing on bridge structures, there remains a dearth of research in two areas that are addressed in the experimental and modelling work outlined in this project. The first is the reliability of using wireless SHM systems on full scale heavily damaged bridge structures and the second is determining the static and dynamic response of a GFRP Bridge that is subjected to increasingly severe damage. Accelerometers and strain gauges were used as the main sensors in the monitoring system because of their ease of application to a large bridge structure and the relative low cost of the sensors. Static single

point load and dynamic hold and release were used to excite the bridge. Both loading mechanisms were used because they were easily applied and repeatable in the laboratory setting. They both cause bridge responses that would be simpler than the more complicated vehicle loading cases. This is a necessity at this stage to determine if damage is detectable in the simplest loading patterns before moving to more complex loading cases.

CHAPTER 4: EXPERIMENTAL PROCEDURES

4.1 GENERAL

The experiment involved the testing of the bridge, starting from a lightly damaged state, incurred during previous testing (Xie (2007, Landherr (2008) and Landherr et al., 2009); referred to as the initial state, and at varying damaged states using a push down and release test. The bridge was first tested in its initial state, followed by the damaged stages where the bridge was deliberately damaged in different areas. The bridge was tested as simply supported as depicted in Figure 4-1 with a load applied at mid-span and a hold/release mechanism at mid-span. This mechanism held the bridge at the deflection imposed by the actuator and upon release the bridge was free to respond dynamically.

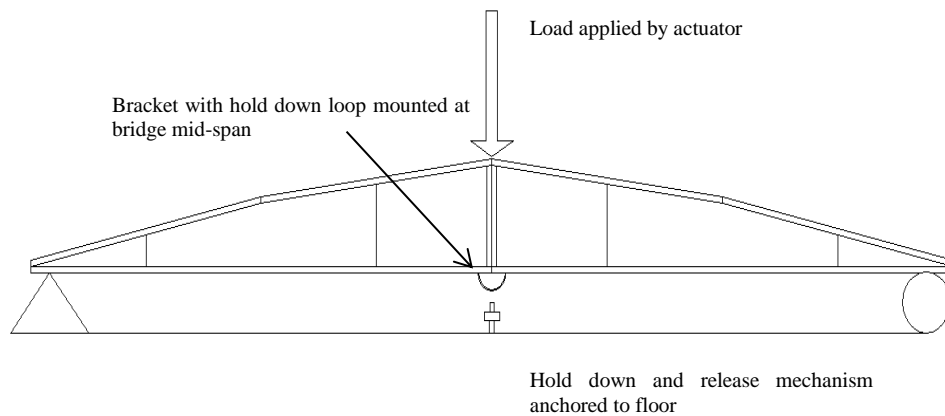


Figure 4-1: Bridge Loading Concept

A monitoring system of accelerometers, strain gauges and LVDTs were used to monitor the change in bridge response to dynamic and quasi-static loading. Sensor placement was selected to attempt to capture overall bridge response.

4.2 BRIDGE DESCRIPTION

The bridge was designed and built by the MERG group at RMC in 2005. As presented by Xie (2007) and Landherr (2008), three types of GFRP products were purchased from Creative Pultrusions Inc. for the construction of the box beam bridge: 1625 series (thermoset vinyl ester class 1 FRP) rectangular tube, 1625 polyester series flat sheet, and Flowgrip solid flooring panel. The sections of GFRP used were a 50.8 x 50.8 x 6.4 mm tube, a 6.4 mm thick plate and a 40mm thick ribbed deck. One half of the symmetrical bridge is shown in Figure 4-2 with its components as it was first displayed by Xie (2007) in Table 4-1.

The bridge has a mid-span height of 0.90 m plus 0.04 m for a ribbed GFRP panel intended as the wearing surface. The width of the bridge is 1.22 m. The GFRP sections were bonded together throughout the bridge to minimize non-GFRP parts, to keep the bridge as light and strong as possible and to minimize stress concentration points. The bridge represents a single track of a double track bridge that was designed for a Military Load Class (MLC) 30, which in accordance with NATO specifications represents two standardized vehicles, a tracked vehicle of 27.22 Tonnes and a wheeled vehicle of 30.84 Tonnes (Wight, Erki, Shyu, Tanovic, & Xie, 2006)

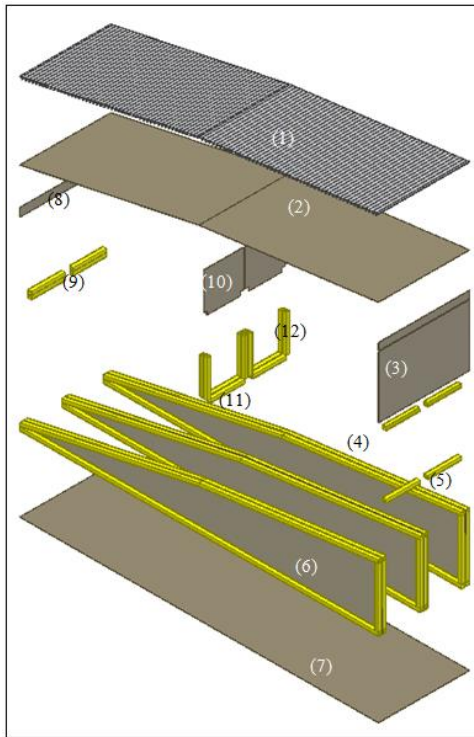


Figure 4-2: Components of half of the bridge (Xie, 2007)

Table 4-1: Bridge components (Xie, 2007)

Number	Name of the components
1	ramp ribbed decking
2	ramp plate (top plate)
3	mid-span diaphragm
4	mid-span diaphragm transversal tube (upper)
5	mid-span diaphragm transversal tube (lower)
6	beams
7	base plate
8	end cover plate
9	end transversal tube
10	quarter-span diaphragm
11	quarter-span diaphragm transversal tube
12	quarter-span diaphragm vertical tube

4.3 SET-UP

The major parts of the laboratory set-up were the hold down and release mechanism, the bridge harness and the support connections. It was assumed, based on a review of results from Landherr (2008) that were conducted using an actual vehicle, that the experiment would be based on an initial displacement of 32.5 mm at a load of approximately 150 kN. Previous testing was used as a reference point to determine at what heights both the bridge and the quick release mechanism would have to be adjusted to. The bridge supports were placed on 610 mm high pedestals to ensure that there was sufficient room underneath the bridge for the release mechanism, the bridge displacement, and access space under the bridge to place the bridge hook into the release mechanism.

4.3.1 Release Mechanism

The release mechanism consisted of a large quick release hook on a threaded rod, securely screwed into the structural floor. The cable from the quick release was hooked into a turnbuckle that was connected to a smaller quick release attached to the support column (Figure 4-3). The use of two quick releases was to ensure that the release mechanism would not interfere with any of the data acquisition equipment set up on the south side of the bridge. Once the bridge was in a depressed position, the clamp suspended from the bridge, was manually moved into the quick release; the turnbuckle was attached and tightened between both quick releases to remove as much slack as possible from the system.



Figure 4-3: Release mechanism (before modifying chain mechanism)

Once the bridge was held by the release mechanism and all sensor systems were ready for testing, the quick release was pulled allowing the bridge structure to vibrate freely.

4.3.2 Bridge Harness

The bridge harness at mid-span was the second part of the hold down mechanism. The harness was comprised of two (2) C-channels, four (4) high strength threaded rods, two (2) 19 mm steel blocks, a reinforced 102 mm HSS and a 35M bar bent into a hook. On the bridge deck, the C-channels acted as the top of the harness as seen in Figure 4-4. Trimmed 51 x 102 mm beams were placed under the C-channels to help with the force distribution, ensuring that the edges of the C-channels didn't damage the deck of the bridge while subjected to the loading force. Under the bridge, as depicted in Figure 4-5, the HSS was reinforced with two (2) 9.5 mm steel plates along the sidewalls to ensure the beam wouldn't bend under high loads. The HSS was placed with either end on the steel plates and with trimmed 51 x 102 mm beams on top to keep it square when tightened up against the steel bridge hinge. At the middle of the HSS, a high strength bolt passed through the hook and the HSS, which allowed the hook to swing so it would not hit the release mechanism as the bridge was being deflected.



Figure 4-4: Top of Harness

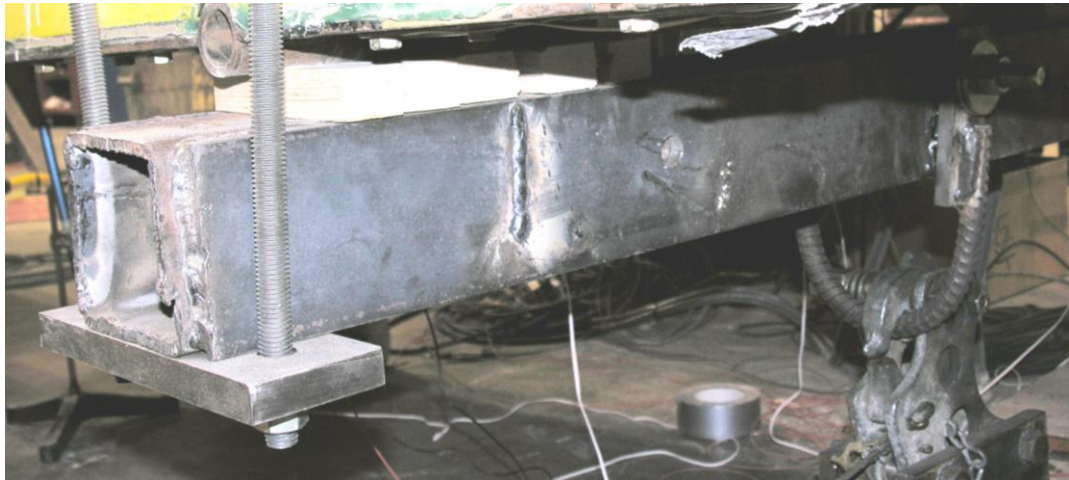


Figure 4-5: Bottom of Harness

After the first few preliminary tests, the initial slack from the system was minimized by adjustment and tightening of the system. Slack still remained in the C-channel and the hook underneath. The C-channel on top of the deck was connected at its ends which created a bending effect in the middle of the channel, it was determined that this slack and its effect on the bridge deflection was similar and repeatable during each test.

4.3.3 Support Connections

The Bridge was supported by 610 mm high pedestals with the bridge supports located at 200 mm from either end of the bridge. Each pedestal had 25.4 mm solid steel pipe welded on top to act as pin supports shown in Figure 4-6, an image of the West end support pedestal.



Figure 4-6: West End Support Pedestal

It was apparent after the first preliminary dynamic test that the bridge was lifting off the pedestals causing excessive vibration. To minimize the problem, two (2) large adjustable clamps were used to hold the bridge to the pedestals at each end. In addition, to ensure the pedestals remained on the floor, HSS members were laid over the bottom flanges of the pedestals and bolted to the floor. An LVDT was placed at either end to verify that the bridge was not lifting from the pedestals during loading and release.

4.3.4 Actuator

A 250 kN MTS hydraulic actuator was used for the laboratory experiment. The actuator was mounted in a support frame and held in place by a cross-member to ensure the actuator did not sway during or between testing as photographed in Figure 4-7. The actuator was positioned to provide at least 100 mm of clearance above the bridge for dynamic testing, yet was able to impose the necessary deflection on the bridge.



Figure 4-7: Actuator mounted in place on the support frame

4.4 DATA ACQUISITION

All wired instrumentation data was collected using a Hottinger Baldwin Messtechnik (HBM) MGCplus data acquisition unit. The software used in conjunction with the MGCplus unit was CATMAN Professional, an HBM product; this software was able to save all the data into Microsoft Excel spreadsheets or in .txt format to later be converted to Excel format. This data acquisition unit was very simple to set up for the different sensors used in the monitoring system. The MGCplus also synchronised the measurement of all channels while using its auto calibration to eliminate temperature influence on the amplifier (HBM, 2013).

Sampling rates for the experiment were conducted at two different rates. The accelerometers were recorded a sampling rate of 1200Hz while the strain gauges and LVDTs recorded at a rate of 600Hz. The use of a 600Hz sample size was necessary due to storage limitations of the DAQ. A 1200Hz sampling rate was used for the accelerometers to ensure that no frequencies were aliased above the Nyquist frequency of the 600Hz sampling rate. These sampling rates were sufficiently high to monitor potential electrical interference that may be noted at approximately 50-60Hz.

The 'wireless' sensors were wired to the two Narada Wireless Data Acquisition nodes and the data was collected by the Narada Base Station that was plugged into a laptop. The wireless data was collected on a laptop with Narada software installed on it. The Narada software operates in MS-DOS and saves the data as a text file, which was later imported into an Excel spreadsheet.

The wireless DAQ nodes that were encased in plastic boxes for protection contained three (3) channels for this experiment (Figure 4-8), two (2) for strain gauges and one (1) for an accelerometer. The wireless DAQ nodes can be customized for different experimentation and different cards can be put in for different sensors. The Narada base station, shown in Figure 4-9, was connected to a notebook computer using a mini-USB cable.

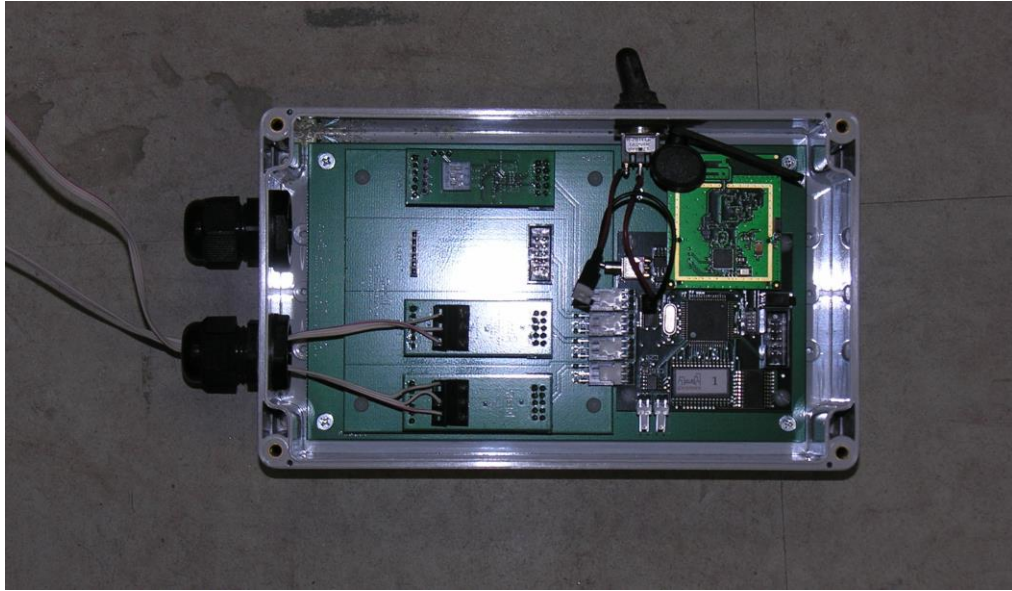


Figure 4-8: Narada Wireless DAQ Node

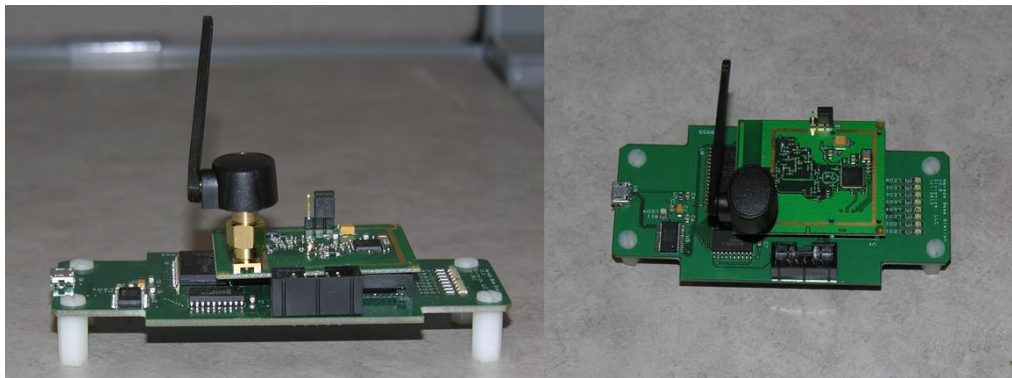


Figure 4-9: Narada Base Station

4.5 INSTRUMENTATION

The Piezo and MEMS accelerometers, strain gauges and LVDTs used during the experiment were all calibrated before being installed onto the bridge. The description and location of the different wireless and wired instrumentation used is listed in Table 4-2 and Table 4-3 respectively. The location of the instrumentation is also outlined in Figures 4-10, 4-11, and 4-12. The wireless instruments are labelled for the type of instrument, the wireless node they are attached to and the channel in that node that the instrument occupies. The wired instruments are labelled for the type of instrument, then are numerically ordered from the north side to south side and East to West, and noted with a B or T for bottom or top respectively.

In order to have an overall representation of the bridges' behaviour in its evolving damaged state, a large number of sensors were placed at various positions on the structure. The wired monitoring system was used to monitor up to 48 independent sensors. A limited number of channels of wireless data acquisition were available in the system. Therefore wireless sensors were only placed at critical locations, to determine the systems feasibility. The sensors on the bottom of the deck at mid-span were deemed the critical sensors as all loading was placed at mid-span and it was predicted the maximum strains and deflections would occur there. Both wired and wireless sensors were positioned at these critical locations. Other wired sensor locations were selected for their ability to predict local maximums as well as suitable locations that may provide indications of changes in global response.

Table 4-2: Location Descriptions of Wireless Instrumentation

Wireless		
Instrument	Description	Location
ACC_1-0	East - Mid plane on bottom plate	4450 mm (mid-span)
ACC_2-0	West - Mid plane on bottom plate	44750 mm (mid-span)
SG_1-2	East - Mid plane on bottom plate	2400 mm (1/4 span)
SG_1-3	East - Mid plane on bottom plate	4450 mm (mid-span)
SG_2-2	West - Mid plane on bottom plate	44750 mm (mid-span)
SG_2-3	West - Mid plane on bottom plate	2400 mm (1/4 span)

ACC = Accelerometer

SG = Strain gauge

Table 4-3: Location Descriptions of Wired Instrumentation

Wired			
Instrument	Description	Location (dist from respective end)	Notes
ACC_1	East - Mid plane on bottom plate	2400 mm (1/4 span)	removed with dam 17
ACC_2	East - Mid plane on bottom plate	4450 mm (mid-span)	
ACC_3	West - Mid plane on bottom plate	44750 mm (mid-span)	
ACC_4	West - Mid plane on bottom plate	2400 mm (1/4 span)	
LVDT_1	East - Mid plane on bottom plate	2400 mm (1/4 span)	removed with dam 17
LVDT_2	East - North outside tube	4600 mm (mid-span)	
LVDT_3	West - South outside tube	4600 mm (mid-span)	
LVDT_4	West - Mid plane on bottom plate	2400 mm (1/4 span)	
LVDT_East	East - Mid plane on ribbed deck	200 mm	moved after dam 16
LVDT_West	West - Mid plane on ribbed deck	200 mm	
LVDT_Dam17 SE	East - South outside tube	3000 mm	began dam 17
LVDT_Dam17 NE	East - North outside tube	3000 mm	began dam 17
SG_B2	East - North top of bottom tube	2400 mm (1/4 span)	
SG_B3	East - North top of bottom tube	3600 mm (3/8 span)	
SG_B4	East - North top of bottom tube	4600 mm (mid-span)	
SG_B5	West - North top of bottom tube	4600 mm (mid-span)	
SG_B6	West - North top of bottom tube	3600 mm (3/8 span)	
SG_B7	West - North top of bottom tube	2400 mm (1/4 span)	
SG_B9	East - South top of bottom tube	2400 mm (1/4 span)	
SG_B10	East - South top of bottom tube	3600 mm (3/8 span)	
SG_B11	East - South top of bottom tube	4600 mm (mid-span)	
SG_B12	West - South top of bottom tube	4600 mm (mid-span)	
SG_B13	West - South top of bottom tube	3600 mm (3/8 span)	
SG_B14	West - South top of bottom tube	2400 mm (1/4 span)	
SG_T2	East - North bottom of top tube	2400 mm (1/4 span)	
SG_T3	East - North bottom of top tube	3600 mm (3/8 span)	
SG_T4	East - North bottom of top tube	4600 mm (mid-span)	
SG_T5	West - North bottom of top tube	4600 mm (mid-span)	
SG_T6	West - North bottom of top tube	3600 mm (3/8 span)	
SG_T7	West - North bottom of top tube	2400 mm (1/4 span)	
SG_T9	East - South bottom of top tube	2400 mm (1/4 span)	
SG_T10	East - South bottom of top tube	3600 mm (3/8 span)	
SG_T11	East - South bottom of top tube	4600 mm (mid-span)	
SG_T12	West - South bottom of top tube	4600 mm (mid-span)	
SG_T13	West - South bottom of top tube	3600 mm (3/8 span)	
SG_T14	West - South bottom of top tube	2400 mm (1/4 span)	
SG_U1	East - Mid plane on bottom plate	2400 mm (1/4 span)	removed with dam 17
SG_U2	East - Mid plane on bottom plate	4450 mm (mid-span)	
SG_U3	West - Mid plane on bottom plate	4750 mm (mid-span)	
SG_U4	West - Mid plane on bottom plate	2400 mm (1/4 span)	
SG_East_Deck E/W	East - Mid plane on top plate (East to West)	2200mm	used beginning dam 4
SG_Eas_Deck N/S	East - Mid plane on top plate (North to South)	2200mm	used beginning dam 4
SG_West_Deck E/W	West - Mid plane on ribbed deck (East to West)	2200mm	used in dam 4-9
SG_West_Deck N/s	West - Mid plane on ribbed deck (North to South)	2200mm	used in dam 4-9
SG_T_Nwdam	West - North bottom of top inside tube	3000mm	used dam 10-16
SG_B_Nwdam	West - North top of bottom inside tube	3000mm	used beginning dam 10
SG_B@Dam17 NE	East - North top of bottom tube	3000mm	used beginning dam 17
SG_B@Dam17 SE	East - South top of bottom tube	3000mm	used beginning dam 17

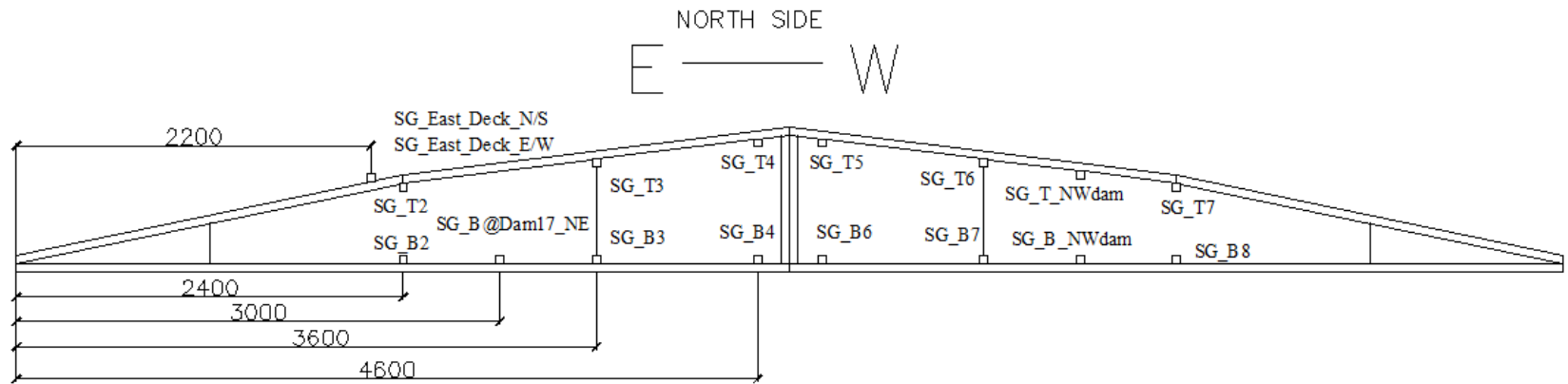


Figure 4-10: Strain Gauge Locations (North Side of Bridge)

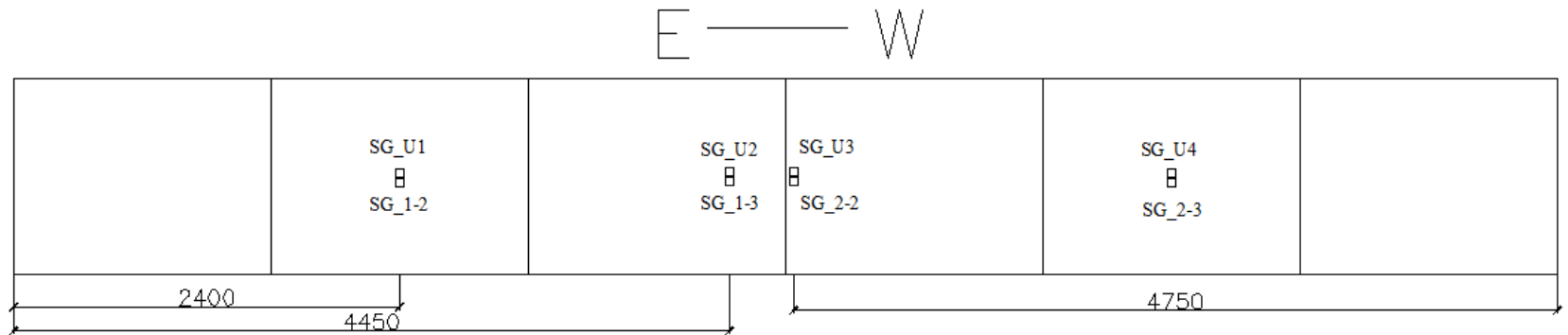


Figure 4-11: Strain Gauge location (Bottom of Bridge)

4.5.1 Accelerometers

Six accelerometers were placed on the underside of the bridge on its centerline as illustrated in Figure 4-12. Four of the accelerometers were wired and two were wireless. The wireless accelerometers were placed beside wired accelerometers for redundancy.

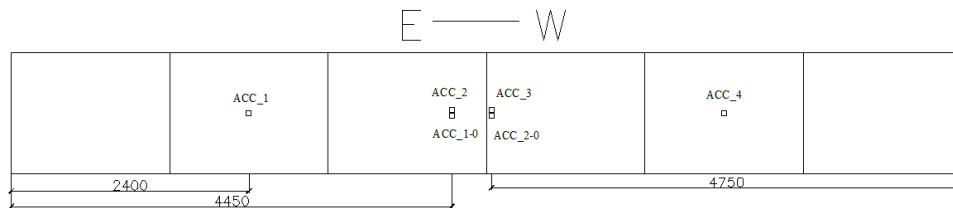


Figure 4-12: Accelerometer Locations (Bottom of Bridge)

4.5.1.1 Wired

Four Dytran 3055B2 Piezo-accelerometers (Figure 4-13) were positioned on the underside of the bridge. Two of the accelerometers were 50g range and two were 100g range instruments. The accelerometers were placed down the centerline of the bridge to pick up bridge accelerations in the longitudinal direction. All 4 of the accelerometers collected data at 1200 Hz and all were operational during the initial 16 stages of damage. However, Damage Stage 17 did cause accelerometer ACC_1 to be removed, leaving three working wired accelerometers for the final testing stages.



Figure 4-13: Dytran 3055B2 Accelerometer

4.5.1.2 Wireless

Two MEMSIC MEMS accelerometers (Figure 4-14) were used with the Narada instrumentation wireless nodes. Both accelerometers, ACC_1-0 and ACC_2-0, were placed beside wired accelerometers ACC_2 and ACC_3 for redundancy. Accelerations of the bridge measured larger than the 4g range of the accelerometers so the peaks of the accelerations were not fully captured by these instruments. Because of the redundancy of the wired accelerometers at the same locations, the frequency response of the two different accelerometers was compared and the bridge response could still be fully determined.



Figure 4-14: MEMSIC CXL04GP1 Accelerometer

4.5.2 STRAIN GAUGES

Thirty-two strain gauges were attached to the bridge throughout the experimentation; Figure 4-10 and Figure 4-11 show strain gauges on the north side and bottom of the bridge respectively. Twenty-four gauges were attached on the exterior tubes, twelve on the bottom tubes and twelve on the top tubes. Four gauges were attached to the centerline of the underside of the bridge. Four strain gauges were placed on the top plate on the East side of the bridge and on the ribbed deck on the west side of the deck beginning at Damage Stage 4. The strain gauges on the ribbed deck were moved after Damage Stage 9 to the North-West inside tubes at the damage area. At Damage Stage 17, SG_U1 and SG_T_NWdam renamed SG_B@Dam17NE and SG_B@Dam17SE and were respectively moved to the bottom outside tubes at the damage site on the east side. The types of strain gauges used were 10mm 120 ohm Kyowa electrical foil gauges.

4.5.3 LVDTs

Six (6) LVDTs were used along the bridge as shown in **Error! Reference source not found.**. Two were placed at mid-span, two at $\frac{1}{4}$ span and then two were used at the supports to determine if the bridge was lifting off the supports. At the later damage stages, LVDTs were relocated so the effects of differential damage between the North and South sides of the damaged area could be assessed. Table 4-3 describes the movement of the LVDT's at different damage stages. The LVDTs were renamed according to their new position.

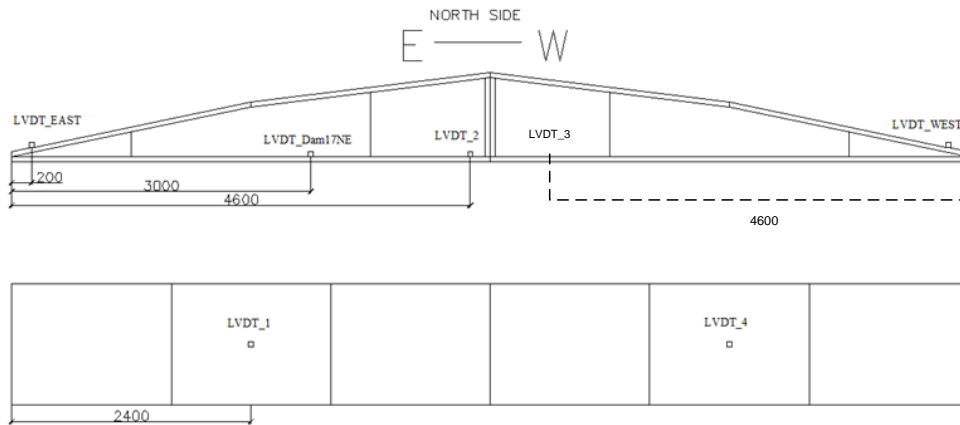




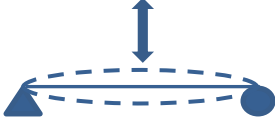


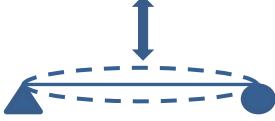


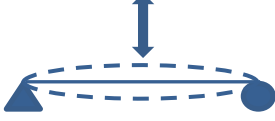
Figure 4-15: LVDT locations in elevation view and plan view

4.6 EXPERIMENTAL PROGRAM

To accomplish the research objectives, the bridge was tested under various different damage stages with both quasi-static and dynamic load cases. It was first tested in its initial state, and also at nineteen (19) increasingly severe damage stages, which ended after the bridge failed and could no longer support any sizable loads. For the damage stages from initial state to Damage Stage 17, the testing procedure was unchanged. Three tests were conducted at each damage stage for repeatability. Between the three tests a visual check was conducted on the data results to ensure that similar results were recorded and that there was no erroneous data that would indicate sensor error or test mechanism error. In the first and third tests, the bridge was loaded until it deflected to approximately 10 mm, so that it could be hooked and held with the release mechanism. It was then released for a dynamic response test. During the second test, the bridge was consistently loaded to 150 kN for quasi-static testing data before it was unloaded to an appropriate height to be hooked into the release mechanism whereupon it was released for a dynamic test. It was determined that for repeatability, the release mechanism would be left at a constant height and the bridge would be loaded until it could be hooked into the mechanism. Due to the changing strength of the bridge and tolerances in the harness and quick release mechanisms, the slack in the system made it extremely difficult to hook on and release the bridge from the same displacement for all the different damage stages.

In Damage Stages 17 to 19, the previous tests were conducted as well as additional tests holding and releasing the bridge as close as possible to the deflection that was created from a 100 kN load. This additional testing method provided results for similar loads at different damage stages, which was done to represent the effects of similar vehicle loads on a bridge at different damage stages. A test matrix representing the experimental program is shown in Table 4-4.

Table 4-4: Test Matrix

Damage Area	Quasi Static Tests	Dynamic Tests
<p>Web Damage</p>  <p>3 Damage Stages</p>	<p>1 Test per damage stage</p>  <p>3 Tests</p>	<p>3 Tests per damage stage</p>  <p>9 Tests</p>
<p>Deck Damage</p>  <p>6 Damage Stages</p>	<p>1 Test per damage stage</p>  <p>6 Tests</p>	<p>3 Tests per damage stage</p>  <p>18 Tests</p>
<p>Structural Tube Damage</p>  <p>10 Damage Stages</p>	<p>1 Test per damage stage</p>  <p>10 Tests</p>	<p>3 Tests per damage stage and an additional test for stages 17-19.</p>  <p>33 Tests</p>
<p>19 Total Damage Stages</p>	<p>19 Total Quasi Static Tests</p>	<p>60 Total Dynamic Tests</p>

4.6.1 DAMAGE SCHEME

To determine if damage to a bridge structure can be detected using VBDD in its simplest form, the experimental bridge was gradually damaged, until it failed under loading. It was decided to first damage the vertical walls of the structure and to leave intact all GFRP tubes in the structure which provided most of the flexural strength. It was also decided that the bridge would be damaged symmetrically at the earlier, smaller damage stages, to limit the likelihood that complex modes of vibration would develop from one side of the structure being relatively stiff when compared to the other side. While this is a less likely mode of damage in a battle-damage situation, this damage could be representative of gradual stiffness deterioration that may occur because of environmental or time-dependent effects. For later stages of the experiment, the damage was not applied symmetrically.

Due to previous testing on the bridge, the initial state of the bridge was with minor damage with a portion of both the North-East and South-East webs removed, creating 1000 x 450 mm holes. This initial damage stage allows for the feasibility of a field application where the only baseline available is the current state of the bridge. A damage scheme was created to simulate severe damage that could be caused by blast or collisions. All damage stages were created using an electric reciprocating saw to cut holes and remove members of the bridge demonstrated in Figure 4-16. The damage scheme description is presented in Table 4-5 and select damage stages are photographed in Figure 4-17 to Figure 4-27. Damage began by removing vertical wall sections on both the East and West ends of the bridge. The following damage stages included removing sections of the ribbed decking and cutting out sections of the bottom plate near the preexisting damage. Lastly, damage was created on the flexural support tubes to reduce the flexural stiffness of the bridge. A 3-D representation of the bridge showing its damaged state near the end of the experimental program (Stage 18) is shown in Figure 4-28. The stages at which significant visible damage occurred are indicated in the figure.

The damage was initially done symmetrically to both the East and West ends of the bridge. It was decided to begin this way in order to effect symmetric changes in the bridge stiffness, and to ensure that weakening of one side of the bridge did not cause an early failure of the entire bridge structure. The final six damage stages were only conducted on the East end of the bridge. By only damaging one side of the bridge, results can show

the effects of sudden damage; such as an IED explosion, projectile damage or vehicle collision damage, to one portion of the bridge.



Figure 4-16: Bridge Damage created using a reciprocating saw

Table 4-5: Damage Scheme

Stage	Description	Affected Area
Initial Condition	East - outer walls cut out (1000mm x 450mm hole)	2500mm - 3500mm from East end
Damage 1	West - outer walls cut out to be symmetrical (1000mm x 450mm hole)	2500mm - 3500mm from West end
Damage 2	East - middle wall cut out (1000mm x 450mm hole)	2500mm - 3500mm from East end
Damage 3	West - middle wall cut out (1000mm x 450mm hole)	2500mm - 3500mm from West end
Damage 4	East - ribbed deck removed (one section 600mm x 1220mm)	1900mm - 2500mm from East end
Damage 5	East - bottom plate cut out (2 x 1000mm x 550mm holes)	2500mm - 3500mm from East end
Damage 6	West - bottom plate cut out (2 x 1000mm x 550mm holes)	2500mm - 3500mm from West end
Damage 7	East & West - ribbed deck removed above damage areas (one section)	2500mm -3100mm from respective ends
Damage 8	East - top deck cut out (2 x 550mm x 450mm holes)	2500mm - 3050mm from East end
Damage 9	West - top deck cut out (2 x 550mm x 450mm holes)	2500mm - 3050mm from West end
Damage 10	East South - middle tubes cut through	2500mm - 3050mm from East end
Damage 11	West South - middle tubes cut through	2500mm - 3050mm from West end
Damage 12	East North - middle tube cut through (removing both middle tubes)	2500mm - 3050mm from East end
Damage 13	West North - middle tube cut through (removing both middle tubes)	2500mm - 3050mm from West end
END OF SYMMETRICAL DAMAGE		
Damage 14	East - bottom plate and middle tubes removed (550mm x 1220mm hole)	1750mm - 2300mm from East end
Damage 15	East - bottom plate and middle tubes removed (500mm x 1220mm hole)	3800mm - 4300mm from East end
Damage 16	East - removal of bottom plate, middle tubes and middle wall	3050mm - 4300mm from East end
Damage 17	East - remove inner-exterior NE tube	2500mm - 3500mm from East end
Damage 18	East - remove inner-exterior SE tube	2500mm - 3500mm from East end
Damage 19	East - cut in half way of both North and South outer tubes at 3050 (post failure)	3500mm from East end



Figure 4-17: Damage Stage 1 (South Side)

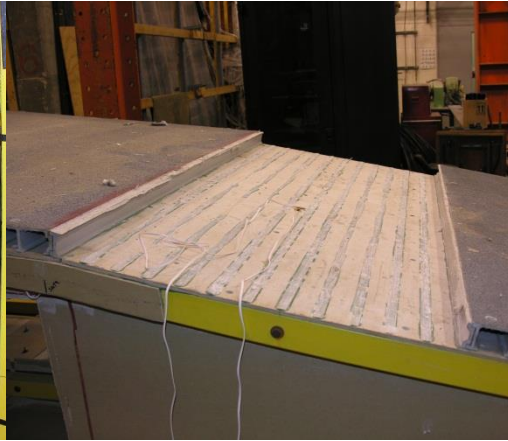


Figure 4-18: Damage Stage 4



Figure 4-19: Damage Stage 6



Figure 4-20: Damage Stage 7 West Side



Figure 4-21: Damage Stage 8

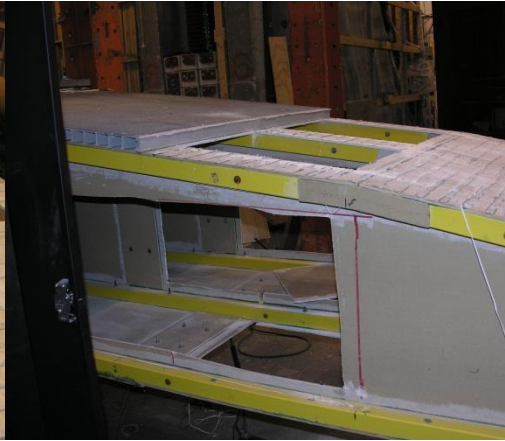


Figure 4-22: Damage Stage 10



Figure 4-23: Damage Stage 12



Figure 4-24: Damage Stage 15



Figure 4-25: Damage Stage 16



Figure 4-26: Damage Stage 17

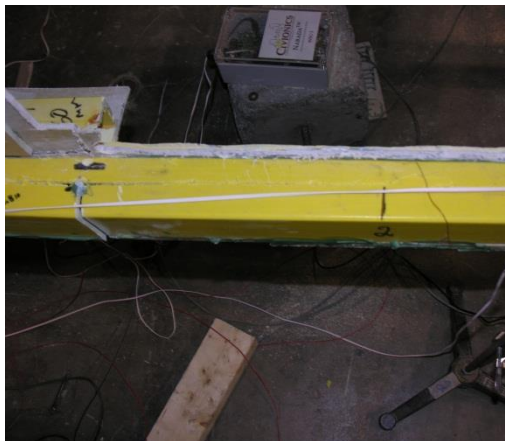


Figure 4-27: Damage Stage 19

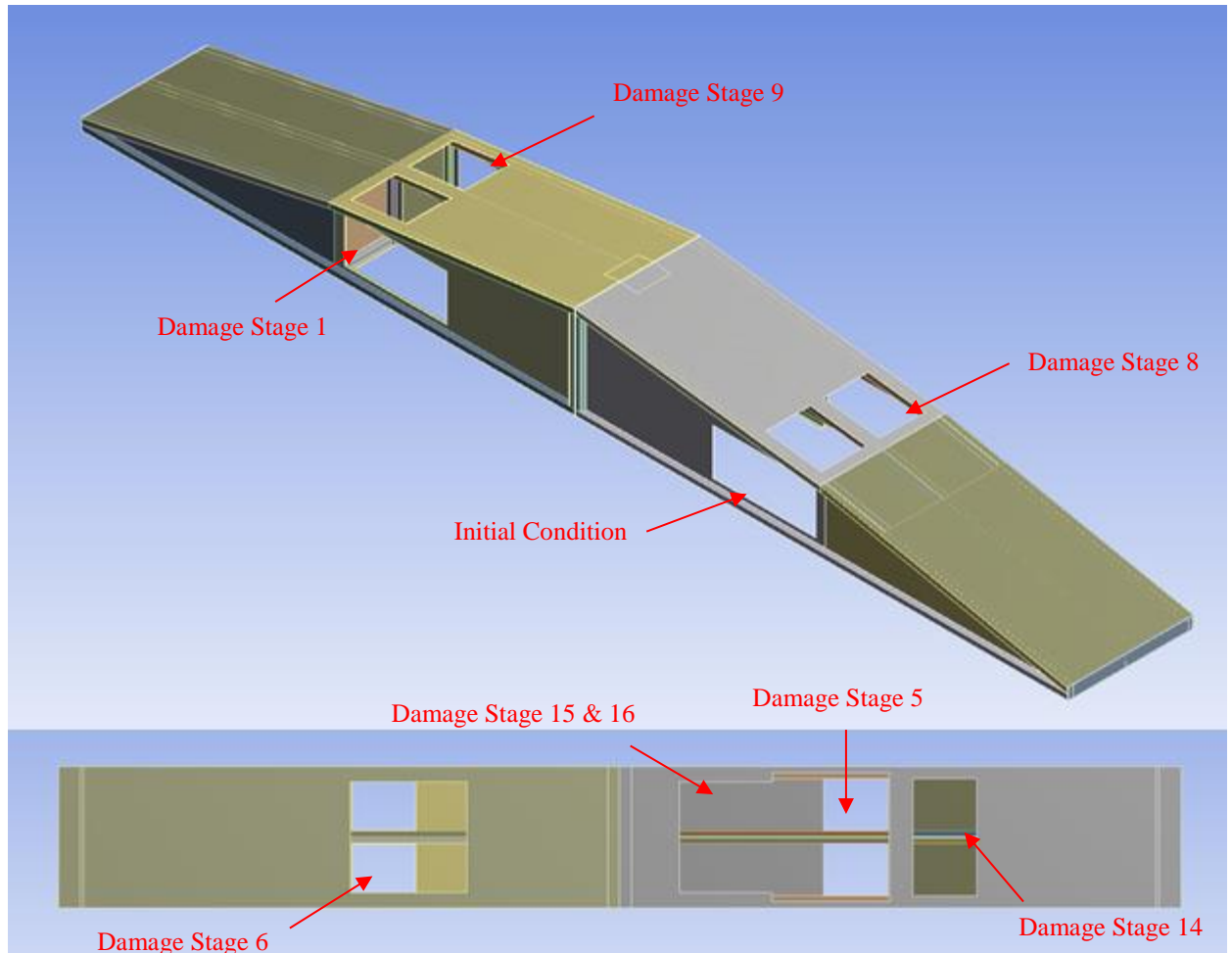


Figure 4-28: 3D model of bridge at Damage Stage 18

4.7 LOADING

Due to the nature of the setup and procedure for the dynamic testing of the bridge, quasi-static testing was conducted concurrently with the dynamic testing arrangement of the setup. After the bridge was in place and all instrumentation was installed, testing began using a hydraulic driven 250 kN capacity actuator. Using a custom-made wooden dispersion block (Figure 4-29) the actuator was used to load the Bridge for both the quasi-static and dynamic testing at mid-span.



Figure 4-29: Actuator loading on dispersion block

4.7.1 Quasi-Static Loading

Quasi-static testing was conducted during loading of the bridge for dynamic release testing. The bridge was designed for MLC 30 vehicles so it was determined that quasi-static loading would be done to approximately represent that load. As the bridge is only representative of one track or axle line for a two track system, a quasi-static load of 150 kN was applied to the bridge. Appendix A describes the derivation of the 150 kN point load which would generate a moment similar to MLC 30 wheeled vehicle as defined by STANAG 2021 (NATO, 2011). During the second test of the three performed at each damage stage, the quasi-static loading was conducted where the data from instrumentation was recorded and then the bridge was unloaded to the necessary displacement to continue with the

dynamic testing. While it was only test 2 that was considered the quasi-static test with the 150 kN load, the other two tests loading data was used as quasi static tests to compare for repeatability.

4.7.2 Dynamic Loading

Releasing the bridge structure from a consistent deflected position produced the free vibration needed for the dynamic testing. The release mechanism remained at a constant height for the experimentation. However, the stiffness of the bridge changed as damage increased. By requiring less force to depress the bridge, less elongation and apparent slack was observed in the harness and release mechanism.

Once the bridge was loaded sufficiently for the hook and release mechanism to be engaged, the bridge was held in place by the release mechanism. Once the hook was in place, the actuator was lifted off the bridge to allow sufficient clearance for bridge vibration. To begin the dynamic test, a rope was pulled which released the system of two quick releases. This process was repeated three times at each damage stage. In later damage stages (Damage Stages 15 to 19), the bridge was also held at a displacement approximately equivalent to a load of 100 kN (representing the service load of a MLC 30 wheeled vehicle.) and was then released to simulate the loading and response associated with consistent-weight vehicle traffic but the increased deflection that the bridge would be exposed to because of the damage.

4.8 SUMMARY

This section outlined the components necessary to set up the bridge in the test apparatus, which included the actuator, support connections, the bridge harness and the release mechanism. It also included a description of the specific instrumentation used to collect data during testing and the location of these instruments. Finally the experimental program was described including the damage scheme and the manner in which the bridge was loaded for the quasi-static and dynamic testing. The results of the laboratory experiment outlined in this chapter are provided in Chapter 5.

CHAPTER 5: EXPERIMENTAL RESULTS

5.1 GENERAL

The results from both the quasi-static and dynamic laboratory testing of the GFRP Bridge are presented in this chapter. Section 5.2 presents the results of the quasi-static test and Section 5.3 contains details of the dynamic testing results.

5.2 QUASI-STATIC TEST RESULTS

Quasi-static tests were used to evaluate the change in deflections and component strains as damage to the bridge progressed. Deflections provided an overall representation of the effects of damage on the bridge and strains, monitored at locations throughout the bridge, provided an indication of local effects of the damage.

As expected, the difference in deflection across the width of the bridge at mid-span from the North and South side of the bridge only differed by 1.3 mm. The 1.3 mm difference can be attributed to the straightening of an initial twist of the bridge. During set-up, it was discovered that the bridge was not perfectly flat along the bottom, and was actually contorted so it sat slightly uneven on the supports and this is likely the source of the 1.3 mm deflection across the bridge width. Even as the bridge lost transverse support through damage, the torsional rigidity remained and at Damage Stage 18, the North side of the bridge had a deflection of 41.0 mm while the South side of the bridge deflected 41.1 mm for a difference of 0.1 mm.

It was determined from the quasi-static loading that the bridge load-deflection response was not exactly linear; due to the seating issues discussed above, but was sufficiently close to be considered linear and remained linear despite the damage created in the bridge. Representative linear load-deflection curves of the bridge at mid-span are shown for Damage Stages 1 and 18 in Figure 5-1. The load-deflection response also indicated that the testing was repeatable because the loading from all three loading stages for the quasi-static and dynamic testing were similar, as shown in Figure 5-2 for Damage Stage 1. The slopes (stiffness) of the three

tests shown in Figure 5-2 were 7.05 kN/mm, 6.78 kN/mm and 7.02 kN/mm for Tests 1, 2 and 3 respectively. The testing remained repeatable throughout all the damage stages as demonstrated in Figure 5-3 for Damage Stage 18. As with Damage Stage 1, the slopes of the three tests are similar to each other. The slopes of the load-deflection tests for Damage Stage 18 were 3.58 kN/mm, 3.46 kN/mm and 3.62 kN/mm respectively for Tests 1, 2 and 3.

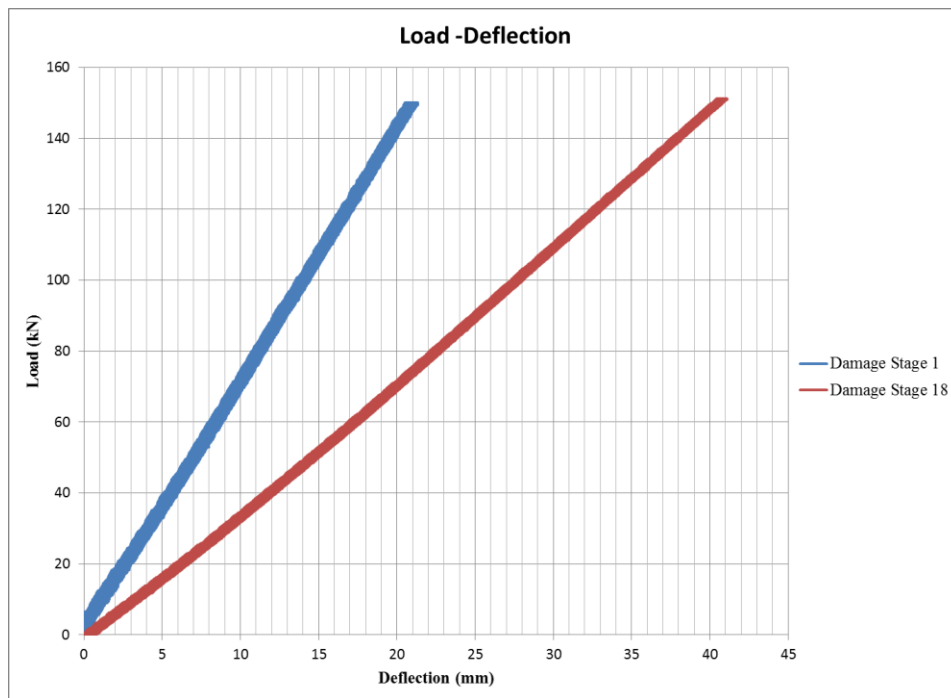


Figure 5-1: Load-Deflection of Damage Stage 1 and 18

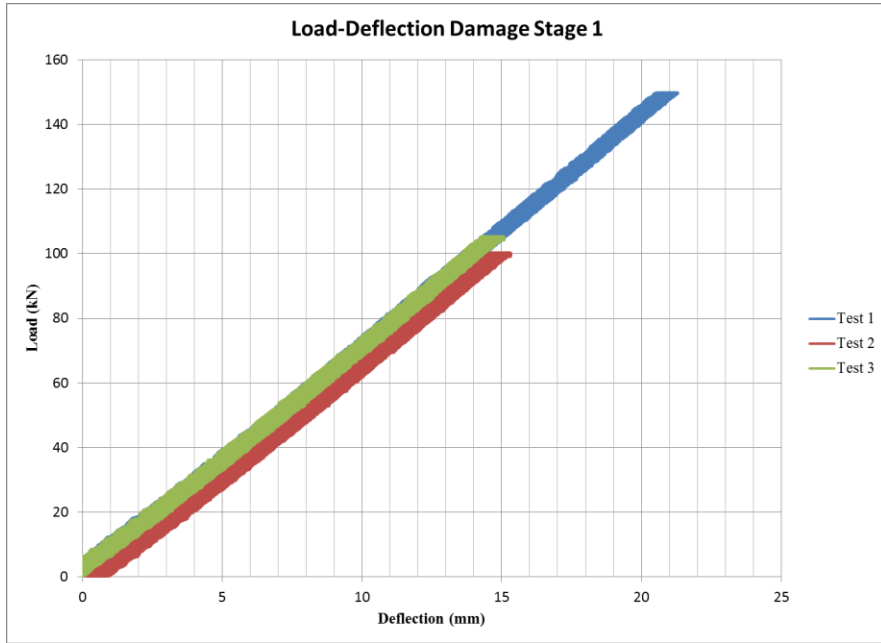


Figure 5-2: Load-Deflection repeatability for Damage Stage 1



Figure 5-3: Load-Deflection repeatability for Damage Stage 18

In addition to load-deflection response, the load-strain response was recorded and Damage Stage 1 load-strain results of Test 2 at mid-span are shown in Figure 5-4 for SG_U2 and SG_U3. The maximum strain at mid-span on the GFRP bottom was recorded at Damage Stage 1 with a strain of 1260 microstrain. The strain corresponded to a stress of 21 MPa, well under the ultimate material strength of 241 MPa for the GFRP plate (Xie, 2007). The largest strain for the supportive GFRP tubes was found to be in bottom outer tubes of the east side at $\frac{1}{4}$ spans, which was mid-length for that single tube. The tubes reached a maximum strain of 3374 microstrain at Damage Stage 18 which corresponded to a stress of 96.4 MPa which only 37% of the material's ultimate strength of 258 MPa.

Even at high levels of damage, when subjected to the design load, the stresses at critical locations of the structure were relatively low. It was apparent that the bridge was over-designed. This is partially attributable to the requirement to limit deflections when the structure is loaded. GFRP bridge structure design may be governed by Serviceability Limit States (SLS), such as deformation rather than Ultimate Limit States (ULS), such as material strength. Furthermore, because this bridge was intended to be suitable for military operations significant robustness and redundancy was intended in the design.

The strain in all the members was recovered upon the conclusion of the dynamic tests and no deformation or cracking was seen between tests at a damage stage. It was not until the induced failure of the bridge at Damage Stage 19 that the bridge had permanent deformation and large cracks.

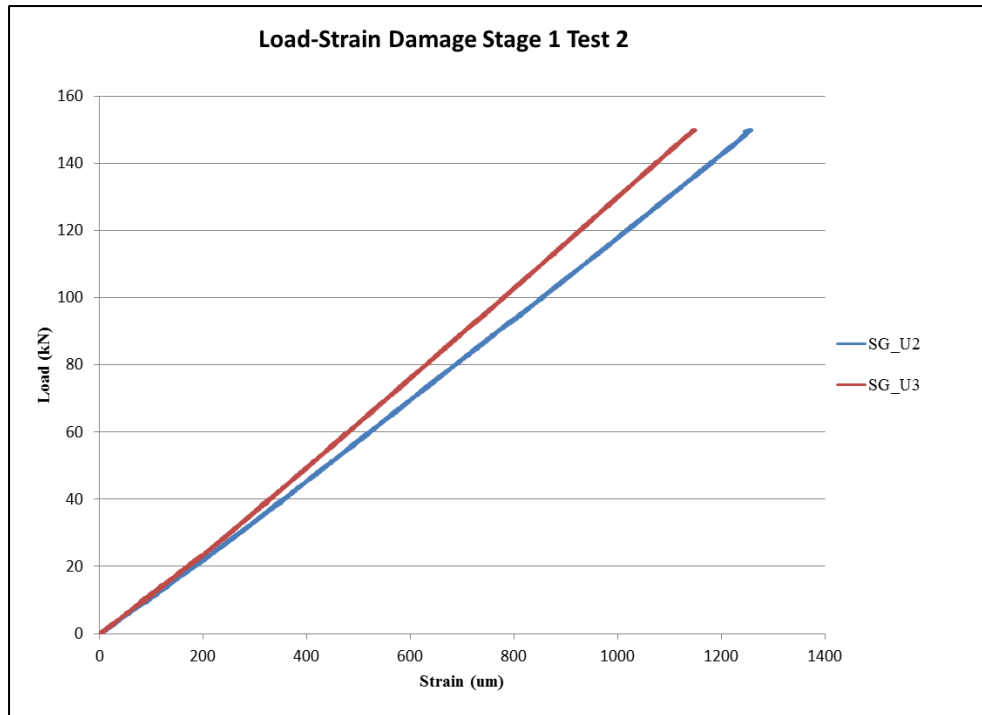


Figure 5-4: Load-Strain comparison for Damage Stage 1 Test 2

It was observed, as damage increased, that the displacement of the bridge increased under quasi-static loading, with maximum displacement occurring at mid-span. Figure 5-5 shows the increase in displacement as the damage stages increase, while Figure 5-6 shows the change in stiffness when compared to the changing damage stages. The stiffness was calculated using the simple beam equation for deflection with a single point load at mid-span to estimate a representative value for EI. As damage increased so did the displacement of the bridge but the displacement reached a maximum where the bridge failed and no additional controlled deflection was possible. From the graphs it can be seen that an increase in stiffness and decrease in displacement occurs from initial damage state to damage stage 1. This can be explained from the un-twisting and settling of the bridge.

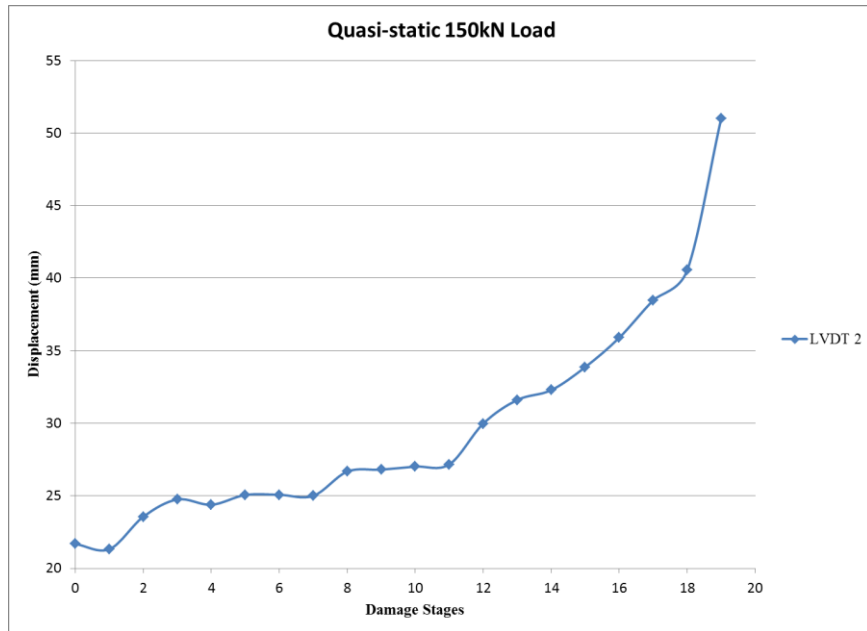


Figure 5-5: Bridge displacement under 150 kN load at different damage stages

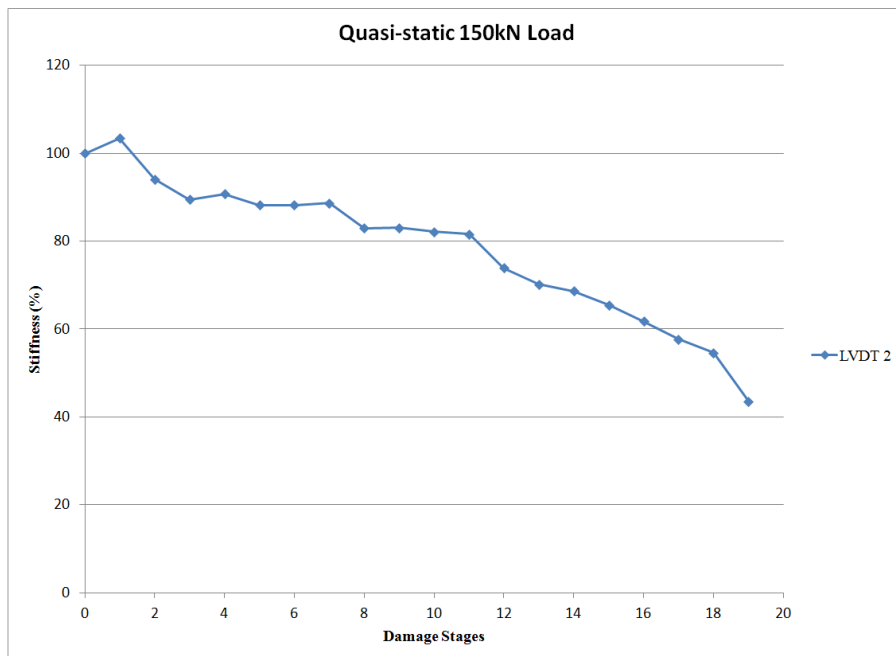


Figure 5-6: Bridge stiffness under 150kN load at different damage stages

5.3 DYNAMIC TEST RESULTS

The dynamic testing done on the bridge was monitored by a system that included wired LVDTs, strain gauges and accelerometers and wireless strain gauges and accelerometers. The wireless instrumentation was placed next to the wired instrumentation to explore and confirm the viability of exclusively using a wireless system for the dynamic monitoring of bridge structures during military operations.

5.3.1 TIME DOMAIN RESULTS

The data from all instrumentation was recorded in the time domain. The two data acquisition systems were manually initiated and not automatically triggered. Therefore, before any data could be compared, it had to be synchronized so all testing data began at the same time interval. Once synchronized, the data for each damage stage was compared in the time domain to quickly ensure that the tests were repeatable and that no major errors occurred during the tests.

Once all tests were completed, the frequency shifts and damping ratio of each damage stage was calculated. From the synchronized data set, the maximum and minimum data points were recorded with their discrete time intervals. The frequency for each oscillation; for both maxima and minima points, was calculated for a one second interval. The frequencies obtained using both the peak positive and negative values were averaged to determine a single average frequency of the damage stage, which for example for ACC_2 for the Damage Stage 1 and 2 was 11.5 Hz and 11.3 Hz respectively.

The damping ratio was calculated using (MIT OCW, 2010):

$$\ln\left(\frac{x_1}{x_2}\right) = \frac{2\pi \zeta m}{\sqrt{1 - \zeta^2}} \quad (5-1)$$

Where:

- x_1 = amplitude of the first oscillation
- x_2 = amplitude of the oscillation that occurs 'm' cycles later
- m = number of cycles
- ζ = damping ratio

To calculate the damping ratio, the number of oscillations occurring within one second was used with equation (5-1). By using all oscillations occurring within one second, the number of oscillations decreased as damage on the bridge progressed, therefore changing the value of ‘*m*’ for the different damage stages.

A first frequency of 11.37 Hz with a damping ratio of 0.042 was calculated for the bridge in the initial state using data from ACC_2. Using SG_U3 a frequency of 11.30 Hz was calculated and a damping ratio of 0.042. While the frequencies are slightly different, it is only the change of frequency due to damage in the system that is most significant. The damping ratios of the bridge do not change significantly as damage occurs on the bridge as Table 5-1 shows, and would not be as great an indicator as frequency shift for damage detection.

Table 5-1: Damping Ratios of Damage Stages

Damage Stage	Damping Ratio		Damage Stage	Damping Ratio
Initial	0.042		Damage 10	0.040
Damage 1	0.039		Damage 11	0.039
Damage 2	0.038		Damage 12	0.040
Damage 3	0.037		Damage 13	0.037
Damage 4	0.044		Damage 14	0.041
Damage 5	0.035		Damage 15	0.042
Damage 6	0.037		Damage 16	0.040
Damage 7	0.034		Damage 17	0.036
Damage 8	0.035		Damage 18	0.037
Damage 9	0.032		Damage 19	0.060

For the dynamic testing, a wireless network was used in conjunction with the wired network to prove the feasibility of using wireless equipment in a scenario representative of military engineering on deployed operations. The results obtained from the wireless network were very similar to those of the wired network. It was found that strains varied by less than 10% between the wireless and wired system throughout all 18 damage stages of testing. For brevity, only a single test from two damage stages are shown; Figure

5-7 and Figure 5-8 shows the comparison of the wired and wireless time-domain strain response for data from Damage Stage 7 test 3 and Damage Stage 15 test 3 respectively on the bottom side of the bridge at mid-span.

Damage to non-flexural components was detected by frequency shifts in both strain and acceleration data. However, these small shifts typically fell in the range of 0.05 to 0.175 Hz of a downward shift in frequency. It was not until damage was introduced into flexural components that larger changes in frequency; 0.19 to 0.70 Hz, were seen. In Table 5-2 the frequencies are calculated for all 19 damage stages for ACC_2 and SG_U3. From these tables, it can be seen that while damage to non-flexural components does not contribute largely to frequency shift, that once flexural components are damaged, as in Damage Stage 13, a larger frequency shift is observed. In Figure 5-9, the time-domain signal is shown to have significantly shifted from the initial state to Damage Stage 18 which was the final damage stage before failure. Damage Stage 18 showed a frequency of 9.06 Hz compared to the initial state stage of 11.37 Hz, a shift of approximately 21%.

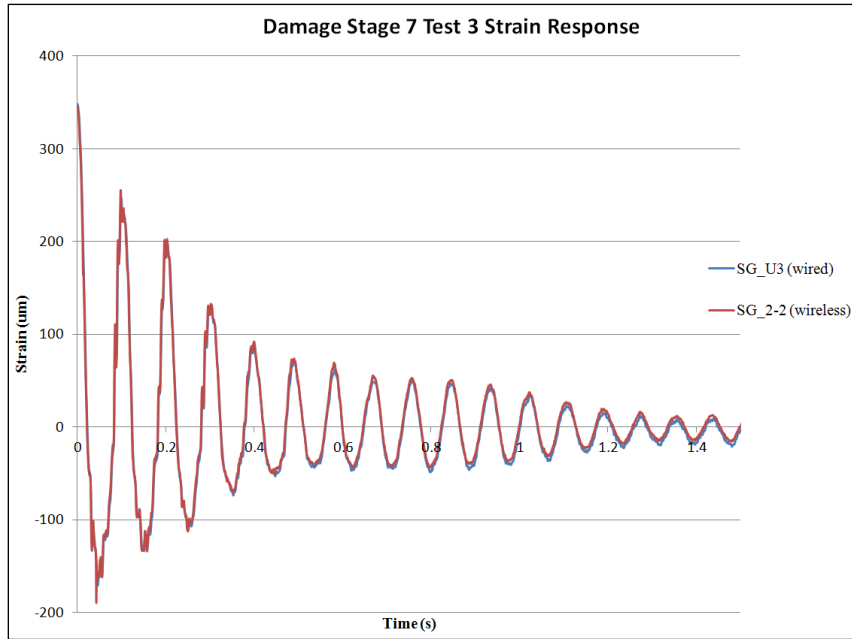


Figure 5-7: Comparison of wired and wireless time-domain strain response of Damage Stage 7

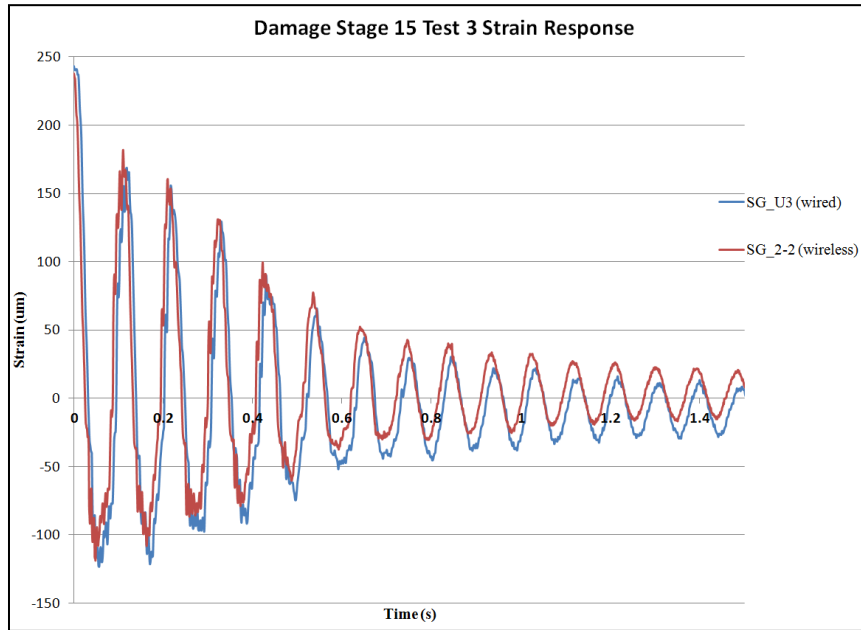


Figure 5-8: Comparison of wired and wireless time-domain strain response Damage Stage 15

Table 5-2: Calculated frequency shifts from time-domain ACC_2 and SG_U3

Damage Stage	ACC Frequency (Hz)	Strain Frequency (Hz)		Damage Stage	ACC Frequency (Hz)	Strain Frequency (Hz)
Initial	11.37	11.30		Damage 10	10.87	10.87
Damage 1	11.51	11.44		Damage 11	10.80	10.74
Damage 2	11.33	11.31		Damage 12	10.60	10.55
Damage 3	11.24	11.08		Damage 13	9.92	9.92
Damage 4	11.13	10.95		Damage 14	9.95	9.90
Damage 5	10.97	10.84		Damage 15	9.78	9.69
Damage 6	10.93	10.83		Damage 16	9.76	9.62
Damage 7	10.86	10.75		Damage 17	9.18	9.08
Damage 8	10.76	10.69		Damage 18	9.06	8.87
Damage 9	10.62	10.56		Damage 19	8.71	8.05

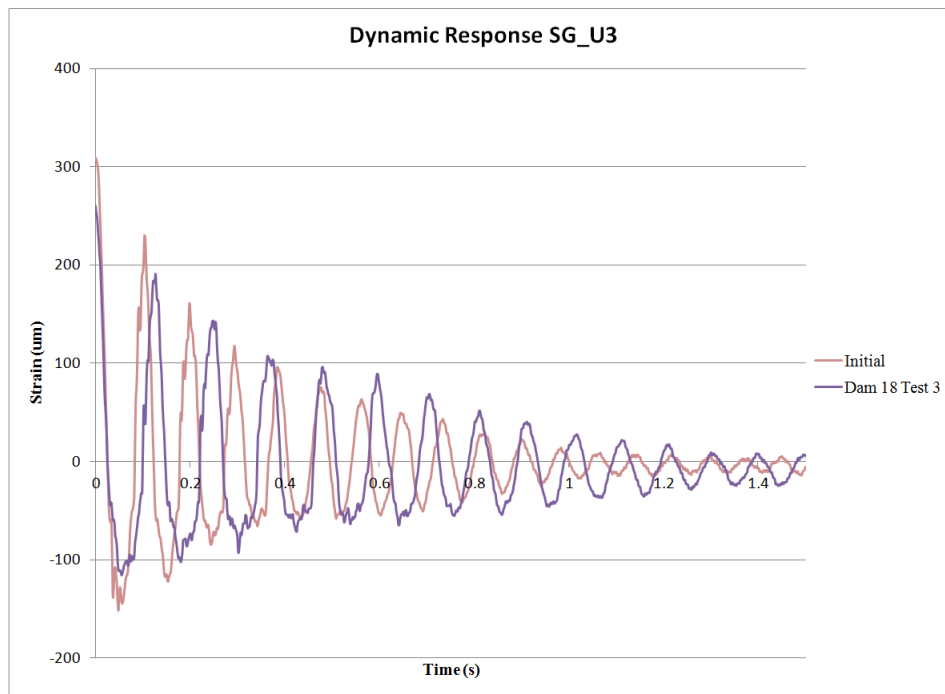


Figure 5-9: Comparison of frequency response from initial state to Damage Stage 18 of SG_U3

A gradual shift of this magnitude should be alarming enough to ensure that the structure was inspected before it reached failure. Within the 21% shift, there were also large shifts between damage stages that would be indicators that significant damage has occurred, such as between Damage Stage 12 and Damage Stage 13 where a 7% shift occurred when principal flexural components were removed. While all of this data was processed in the time domain, it was very tedious and time consuming, with the potential for significant human errors in detecting higher order vibrational response. It is for this reason that the data was processed into the frequency-domain for easier and more comprehensive analysis.

5.3.2 Frequency Domain Results

When the data is in the frequency domain, subtle shifts in frequency are easily detected. Using a Discrete Fast Fourier Transform aided by an algorithm in the program Matlab, the data for each damage stage was converted to the frequency domain. Once the data was processed to the frequency-domain, the dynamic response of the bridge became visually easy to characterize. The frequency was the Maximum of the graph, the amplitude in the graphs is the energy at each frequency.

The initial damage stage frequency-domain data is shown in Figure 5-10 for the accelerometers ACC_2, ACC_1-0 and the strain gauges SG_U3 and SG_2-2 which were all instruments on the underside of the bridge at mid-span. From these figures, the frequency of the bridge at its initial condition can be determined to be 11.2 Hz, determined from the maximum point on the graph. The figures show that a very similar frequency response was measured through the four different sensors, and therefore it can be assumed that all four sensors provide accurate frequency shift data. While both the wireless and wired strain gauges provide almost identical results in the frequency domain, the wireless and wired accelerometers show only similar results. This can be attributed to the use of different accelerometers and the fact that the wireless accelerometer was not able to pick up maximum and minimum accelerations. The frequency-domain results are not only comparable from sensor to sensor, but the results are very similar to the calculated time-domain results. The calculated time-domain frequencies of

11.37 Hz, 11.29 Hz for ACC_2 and SG_U3 respectively and 11.30 Hz and 11.23 Hz for ACC_1-0 and SG_2-2 respectively are very similar to the 11.2 Hz from the frequency domain; however the calculated time-domain frequencies are calculated using human selection of data points and an average over a one second time period, providing ample opportunity for errors.

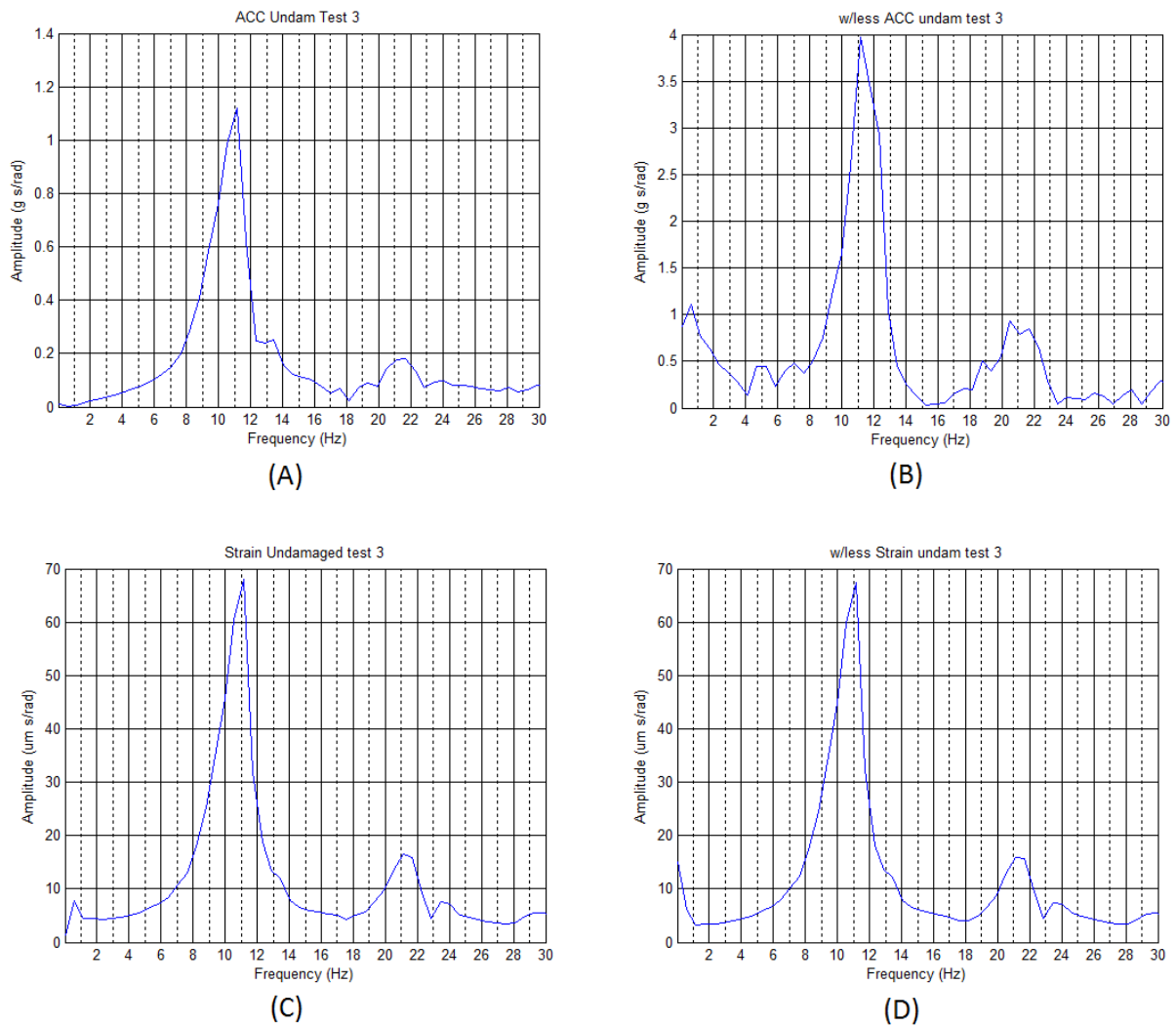


Figure 5-10: Dynamic response in frequency-domain for initial state stage. (A) ACC_3, (B) ACC_2-0, (C) SG_U3 and (D) SG_2-2

The frequency-domain figures provide a method to observe changes to the frequency response that are caused by damage to structural components. For brevity, the frequency-domain data of wireless SG_2-2 will be described. Much like the time-domain data, the frequency shift can be seen throughout the different damage stages in the frequency-domain.

Figure 5-11 (A) through (F) show the frequency domain of various damage stages, the frequency shift is visible through the damage progression.

Figure 5-11 (A) showing Damage Stage 2 is similar to the initial stage with a first frequency of approximately 11 Hz. It can also be noticed that there is second frequency response, with a frequency of approximately 21 Hz. Monitoring a change in either of these frequencies indicate that there is damage or a change to the bridge structure.

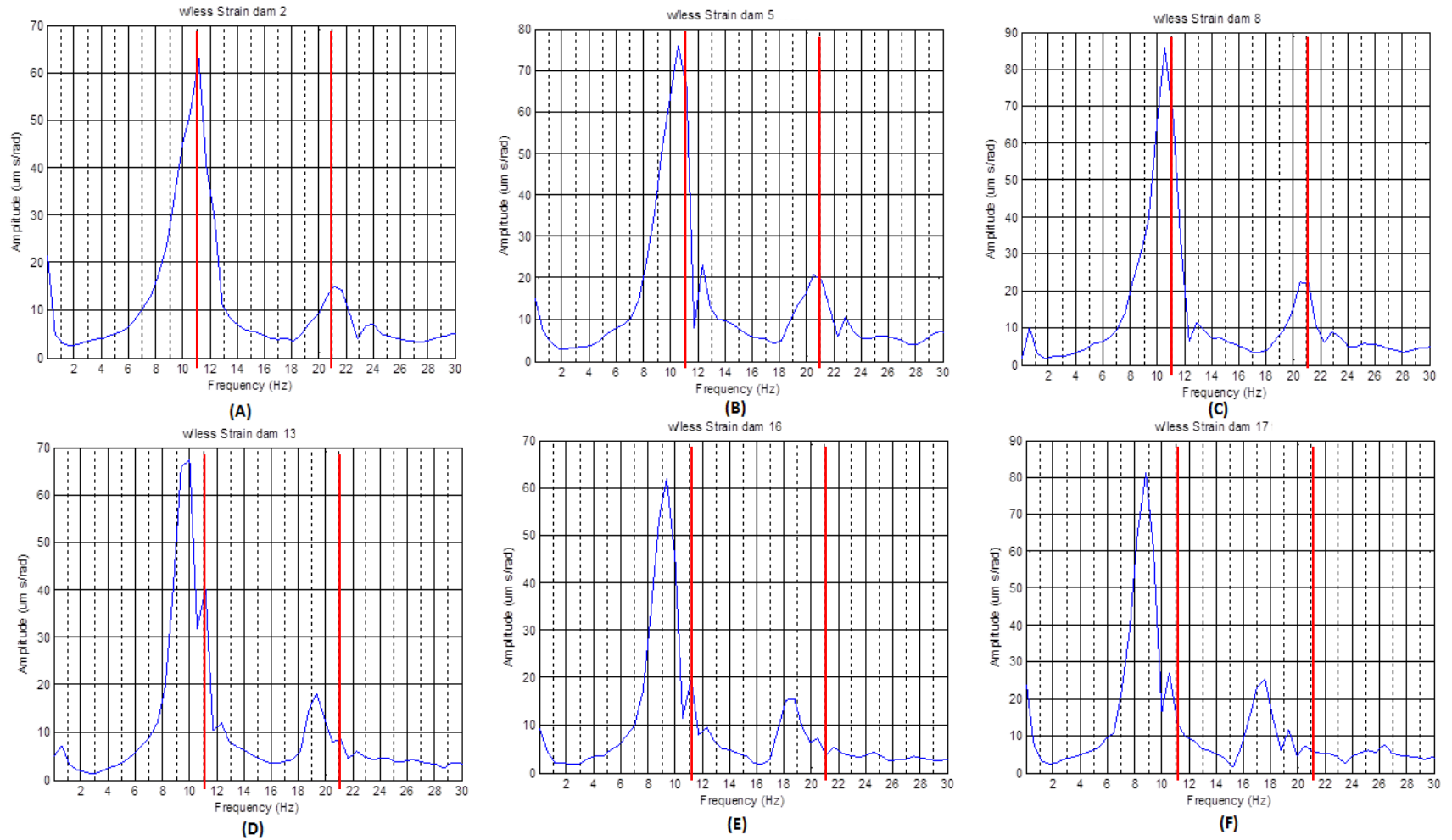


Figure 5-11: SG_2-2 frequency (A) Damage Stage 2, (B) Damage Stage 5, (C) Damage Stage 8, (D) Damage Stage 13, (E) Damage Stage 16, (F) Damage Stage 17.

The initial frequencies, identified at the first damage stage are indicated by vertical red lines on all graphs shown in

Figure 5-11. Damage Stage 5, shown in

Figure 5-11 (B), maintains a similar shape to that of Damage Stage 2. The frequency associated with the first mode of response has shifted left, lowering to nearly 10.5 Hz; a noticeable change in this graph. It can also be observed that the second frequency response has also shifted slightly to the left and the amplitude has increased.

Figure 5-11 (C) maintains a similar shape and has slightly shifted to the left, where the only significant change is an increase in amplitude. This minor change could be expected, as the only significant damage between Damage Stages 5 and 8 has been made to the decking, and no flexural components have been damaged.

Once damage has been made to flexural support members, as in Damage Stages 12 and 13, there becomes a larger reduction in frequency. As can be seen in

Figure 5-11 (D), damage to middle flexural tubes causes a frequency reduction to 10.0 Hz, which is very similar to the calculated frequency of 9.9 Hz, determined from the time-domain data. As damage to critical flexural load carrying components increases, the frequency of the bridge continues to reduce. As more GFRP tubing; a significant component of the flexural resistance, is removed in Damage Stages 16 and 17, the frequency changes are easily visible. In

Figure 5-11 (E), it can be seen that the frequency is slightly over 9.2 Hz, reduced from the original 11.1 Hz, and the second peak has also reduced to 18.5 Hz from its original 21.1 Hz. It was the intent during the project to slowly cause damage to the bridge, because the effects of a single large damaging incident can always be inferred from the resultant of a series of smaller damage stages.

Figure 5-11(F) shows that even minor damage to a small but critical component can result in a noticeable change in frequency response. From Damage Stage 16 to Damage Stage 17, a shift of almost 0.5 Hz occurred on the first frequency; while a shift of almost an entire 1 Hz occurred in the smaller peak.

From both the time-domain and frequency-domain, it has been determined that frequency change of a GFRP box-beam bridge structure can be attributed to damage incurred by the bridge. While progressive damage caused small frequency changes from damage stage to damage stage, it was more apparent when critical flexural components of the bridge were damaged. It can also be determined that large damage, would cause a very noticeable change in the frequency response of the bridge. For example if the bridge was considered to be at an initial state at Damage Stage 13; when symmetrical damaging was no longer used, and was then compared to Damage Stage 17 assuming all the damage in Damage Stages 14 to 17 happened at one occurrence, like an IED explosion, a large change in the frequency response would be expected. We can see that, when comparing

Figure 5-11 (D) and (F) that the shift in frequency is easily noticeable and would be a strong warning that something drastic has changed in the bridge structure.

As damage causes the bridge to loose stiffness, the change in frequency response becomes more noticeable. When comparing the frequency response change from damage stages where the bridge's longitudinal stiffness was not affected, to damage where the stiffness was significantly affected, the frequency response is much more drastic. Figure 5-12 shows the change in frequency over the different damage stages and Figure 5-13 shows the change in bridge frequency compared to the relative bridge stiffness. It is apparent in Figure 5-12 that the largest change in frequency; except for the failure, happens between Damage Stage 12 and 13. Damage Stage 13 removes the middle tubes from the west end of the bridge; this basically nullifies any flexural support that was being provided by the two middle tubes running down the bottom of the middle web. By removing the sections of middle tubes, the tensile capacity on the bottom of the bridge has been reduced by approximately 30%, with only four of six tubes remaining and the bottom plate carrying an additional small portion of the tensile loads. This loss dramatically affected flexural strength and stiffness. Damage Stage 17 created another large change in frequency, where part of a bottom flexural tube was removed from the north side of the bridge and in Damage Stage 18, the corresponding section on the south side of the bridge was removed.

While generally the frequency declines as the stiffness of the structure decreases as is shown in Figure 5-13, there are exceptions to this trend.

These are apparent where frequencies increase with increasing damage as shown in Figure 5-12. These increases are most likely explained by the removal of components from the bridge that had significant mass but contributed very little to the stiffness of the bridge.

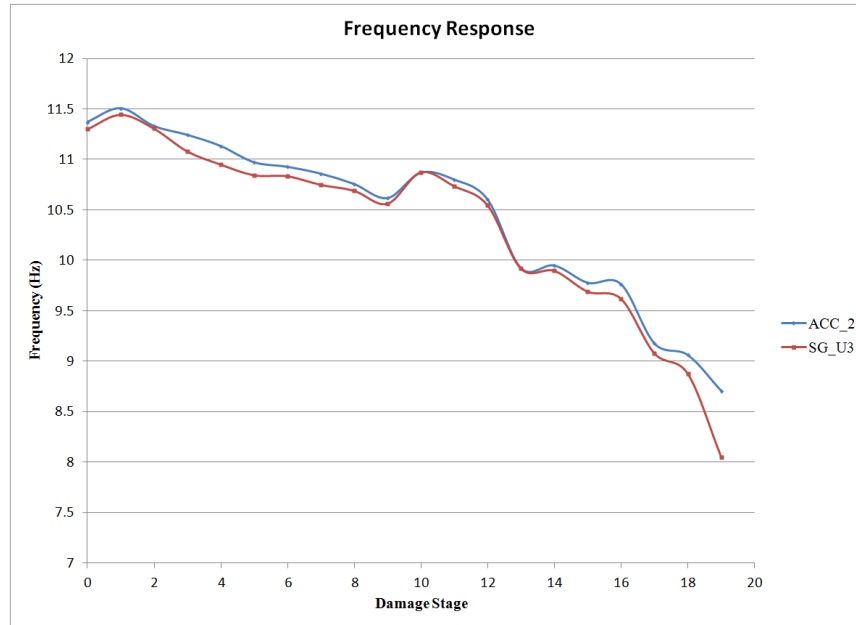


Figure 5-12: Bridge frequency for damage stages

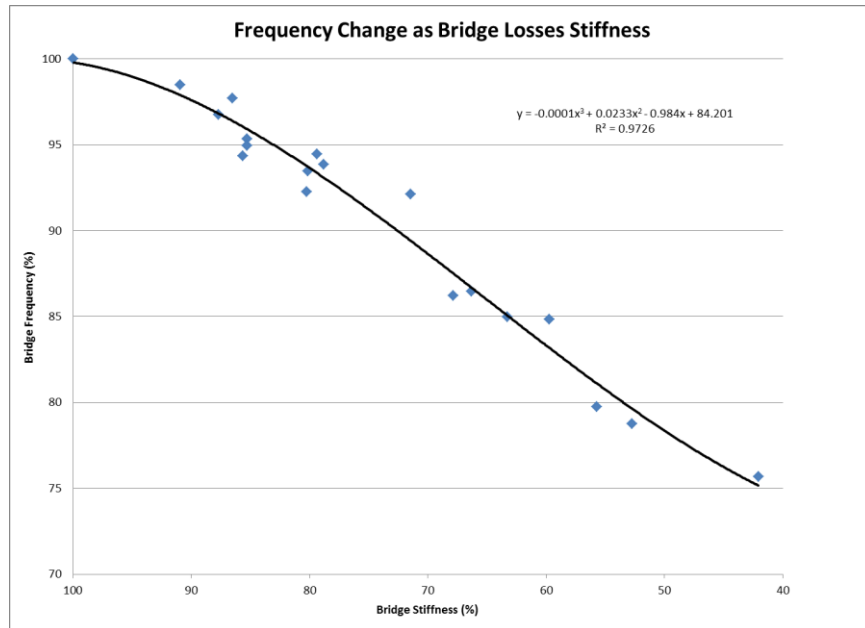


Figure 5-13: Frequency change of Bridge during change in stiffness

Another advantage to processing the data into the frequency-domain is that additional frequencies representing higher modes of response can be identified that were not readily visible in the time-domain. A second frequency that cannot be seen in the time-domain is very visible for this GFRP box-beam bridge and can also be used as a damage identifier in the frequency-domain. The second frequency is visible in all the FFT figures for different damage stages. Figure 5-14 shows that the 2nd frequency has a similar trend to the first frequency where it becomes lower as damage increases. The second frequency is influenced less by small levels of damage but it is influenced more than the first frequency by the entire damage process. While the first frequency is reduced by 23% from the initial state to failure, the second frequency is reduced by 32% over the same damage stages. The second frequency is easily visible and has been shown to act as a second damage indicator when data is viewed in the frequency-domain.

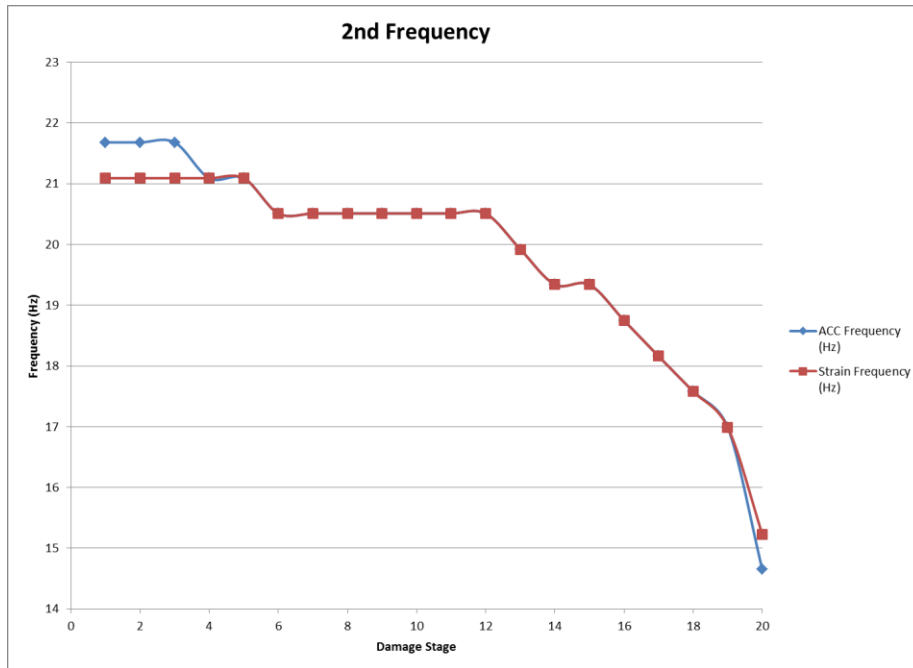


Figure 5-14: The 2nd frequency of bridge for damage stages

Testing conducted when the bridge was loaded and held at 100 kN showed similar results to the previous results of tests conducted with the release mechanism at a constant height. For Damage Stage 15 to Damage Stage 19, the additional tests to 100 kN load were completed and the frequency-domain results are shown in Figure 5-15. While the frequency response of the bridge is much lower with the heavy load that was applied, the change in frequency follows the same pattern for both testing regimes. When comparing Damage Stage 15 frequency-domain results between the two test methods (Figure 5-16), it was determined that the same fundamental shape occurred for both methods. While amplitude was different, similar frequencies are present in both methods' results. Figure 5-17 shows that the shape of frequency is very similar with little change caused by Damage Stage 16, a large change from Damage Stage 17, little change from Damage Stage 18 and a large change from the failure of Damage Stage 19. In both testing methods the change of frequency from Damage Stage 16 to 17 is 0.59 Hz and the change from Damage Stage 15 to Damage Stage 18 was

7.3 % and 6.7% for the standard height test and the 100 kN load test respectively. While the changes in frequencies are similar between the tests, the lower frequencies that result from hold down tests with a 100 kN load is logical because higher load causes larger deflection which increases the time required for the bridge to oscillate.

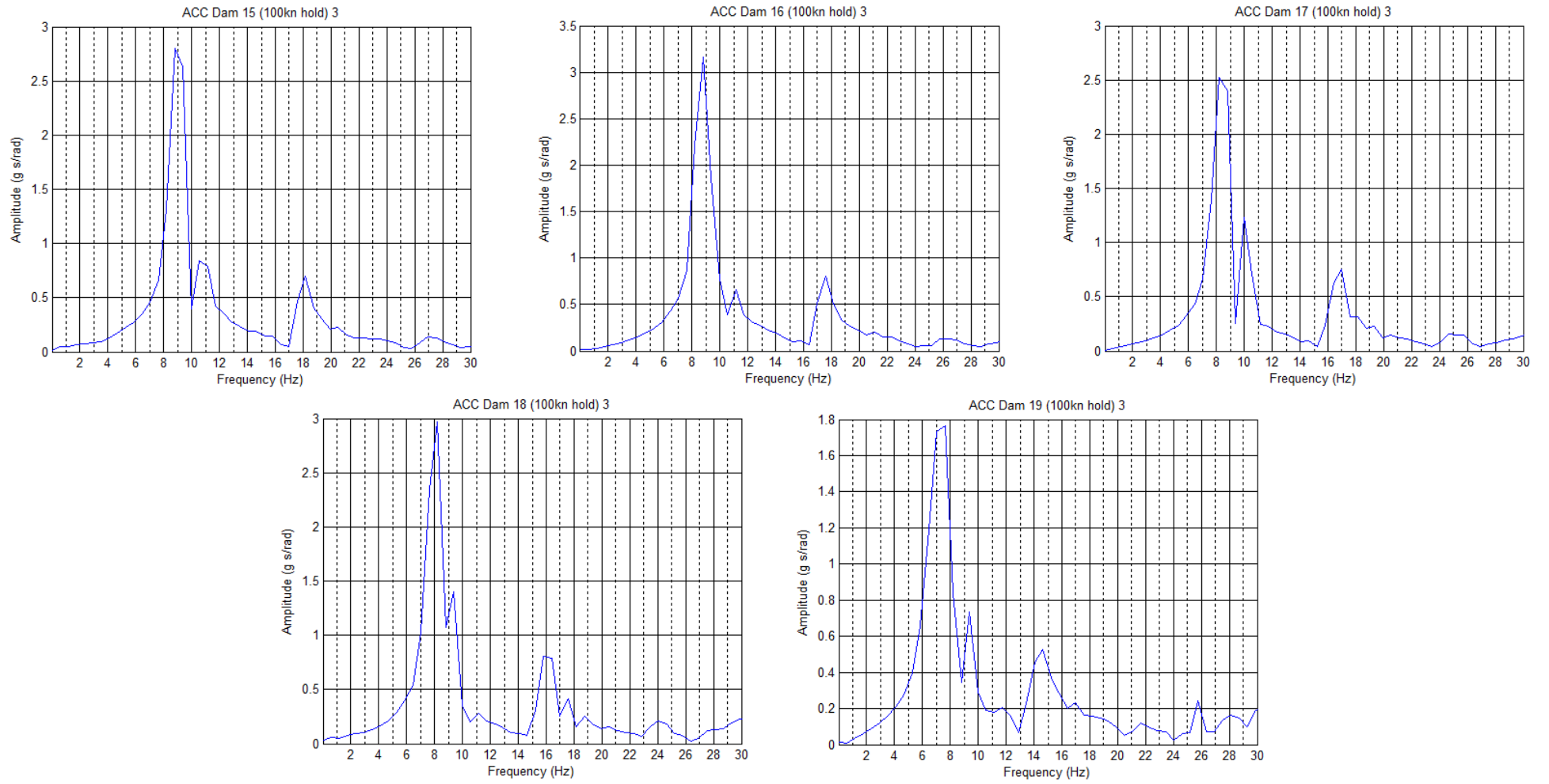


Figure 5-15: 100 kN load dynamic test FFT figures for Damage Stage 15-19

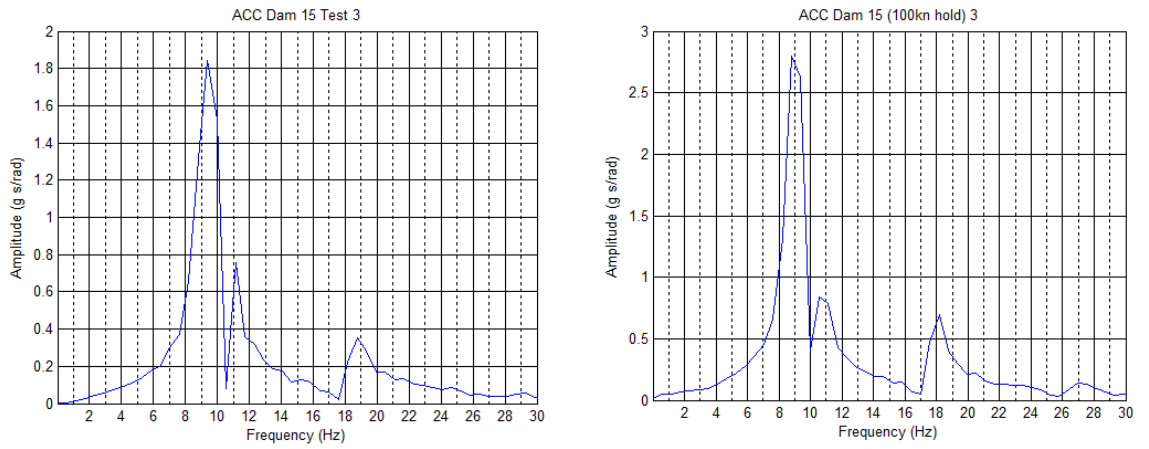


Figure 5-16: Standard height test compared to 100 kN load test for Damage Stage 15

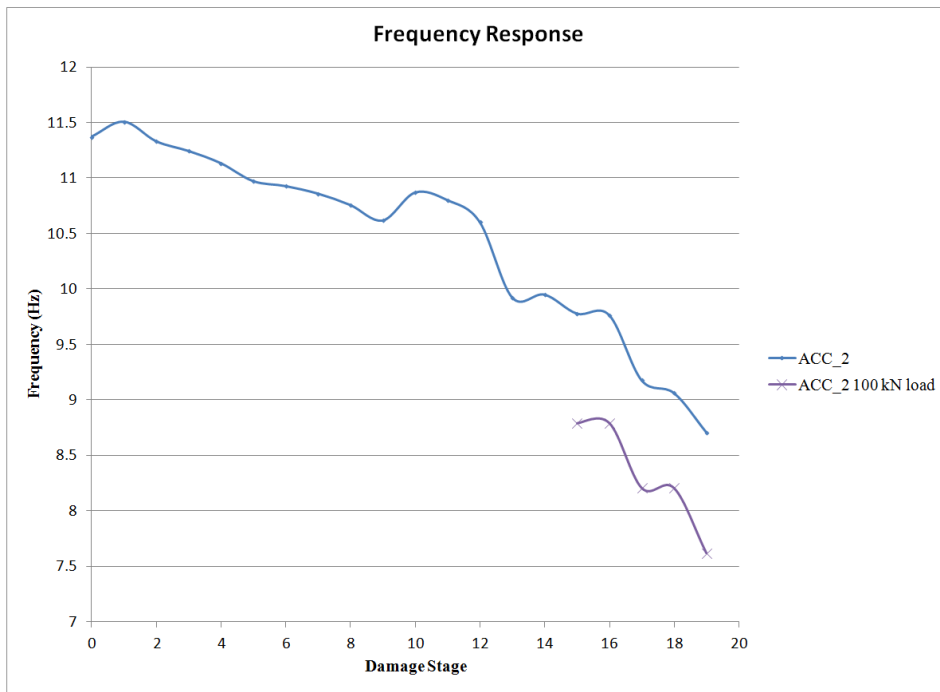


Figure 5-17: Frequency changes for both dynamic tests over incremental damage stages

Similar to the standard height tests, the second frequency of the 100 kN tests acts as a second indicator of damage. In Figure 5-18 it can be seen that the second frequency is very similar between the two test methods. There was a 21% change in frequency from Damage Stage 15 to 19 for the standard height tests while the 100 kN load tests had a 19% change over the same damage stages, very similar results for both methods.

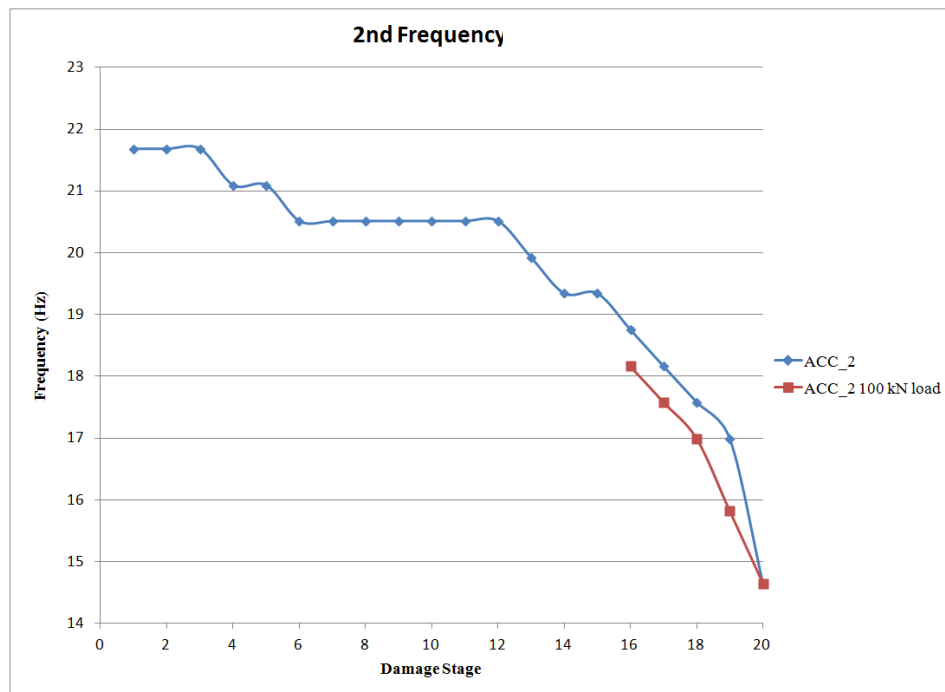


Figure 5-18: 2nd Frequency r for standard height tests and 100 kN load tests

5.4 SUMMARY

This chapter examined the results obtained from both the quasi-static and dynamic tests performed on the GFRP bridge. Load-deflection and Load-strain curves were created from the quasi-static testing. It was determined that the load-deflection and load-strain remained in the elastic region during quasi-static testing. Frequency shifts in both the time-domain and frequency-domain were examined to relate the type and amount of damage to the frequency shift in the bridge. It was apparent that large-scale damage to the bridge caused significant shifts to the frequency response of the bridge; making frequency shifts a viable option for large-scale damage detection.

A large number of sensors were placed throughout the bridge. The results from all sensors provided a consistent representation of the overall bridge response when loaded. Sensors located near the critical section at mid-span were able to provide the best overall representation of the structure. Furthermore, the wired and wireless systems were placed adjacent to one another for redundancy. The results of these sensors were consistent with each other

CHAPTER 6: MODELING

6.1 GENERAL

Generally the finite element method (FEM) is a numerical technique used to obtain approximate solutions of boundary value problems in engineering. The finite element analysis has become an integral part of the engineering design process to predict the response of a system and to evaluate the effects of changes to the system complementing and expanding the results of costly experimental testing. A finite element analysis was conducted to predict the response of the bridge structure due to damage and this model was validated by the experimental results.

Extensive modeling was previously conducted on the 10m GFRP bridge by both Xie (2007) and Landherr (2008). Xie (2007) used LUSAS to model the bridge for both her quasi-static and dynamic testing, while Landherr (2008) used Matlab for her modeling of the bridge. In both cases similar results were found from their models when compared to their experimental results.

For the current study, ANSYS and SAP2000 were used as two different programs for modeling. ANSYS was used for quasi-static modeling while SAP2000 was used for both quasi-static and dynamic modeling.

6.2 ANSYS MODELS

ANSYS is a suite of simulation-driven computer software. Within the suite, the different programs are used on the ANSYS Workbench Platform, where all data, information and results can be stored and accessed from different ANSYS programs. It provides a complete set of elements, material models and equation solvers for a wide range of engineering problems (ANSYS, 2013).

The GFRP bridge was imported into ANSYS after it was created as a 3D bridge in Solidworks. Within Solidworks, the bridge was created and assembled from drawings originally prepared by Xie (2007). The material properties of the bridge parts were created in ANSYS from Xie's (2007)

ancillary material testing results, as shown in Table 6-1. The bridge model's material and geometric behaviour was assumed to remain elastic, allowing a linear-elastic analysis to be completed. It was also assumed that joints were perfectly bonded and that the steel hinge present on the bridge added no significant structural support to the bridge. The bridge was modeled as simply supported, with the east end being a pin support and the West end being a roller support and the force was applied over the area of the dispersion block by a force in the direction of gravity.

The bridge was meshed with SOLID186 elements. The SOLID186 elements are higher order 3-D 20-node solid elements that exhibit quadratic displacement behaviour (ANSYS, 2010). All 20 nodes have 3 degrees of freedom: translations in the nodal x, y and z directions.

Table 6-1: Material Properties (Xie, 2007)

GFRP Profile	Property	Units	Values
Tube	Modulus of Elasticity	GPa	28.6
	Poisson's Ratio		0.35
	Density	Mg/m ³	1.90
Plate	Modulus (LW)	GPa	17.2
	Modulus (CW)	GPa	12.2
	Poisson's Ratio		0.32
	Density	Mg/m ³	1.90
Decking	Modulus (LW)	GPa	20.7
	Modulus (CW)	GPa	20.7
	Poisson's Ratio		0.32
	Density	kg/m ²	14.7

Note: LW = lengthwise; CW = crosswise

*The values of modulus were calculated from material tests, except for the Decking, which was supplied by manufacturer

The ANSYS model predicted deformations very well and were similar to results from laboratory testing. For brevity, models for Damage Stage 1 and Damage Stage 18 will be shown. In Figure 6-1 the directional deformation in the vertical axis is shown for the Damage Stage 1 model. In this model, a load of 150 kN resulted in a downward vertical deflection of approximately -24.2 mm at the position that LVDT_3 is located in the laboratory testing. The experimental results for LVDT_3 found a displacement of -23.5 mm when the bridge was loaded with 150 kN at Damage Stage 1 as seen in the

bridge profile depicted Figure 6-2. The bridge profile is composed of the data from the four LVDTs used on mid-plane and outer tubes respectively. The noticeable change of deflection at mid-span is actually the difference of deflection from the North and South side LVDTs caused by initial warp in the unloaded bridge that was straightened under the effects of an applied load.

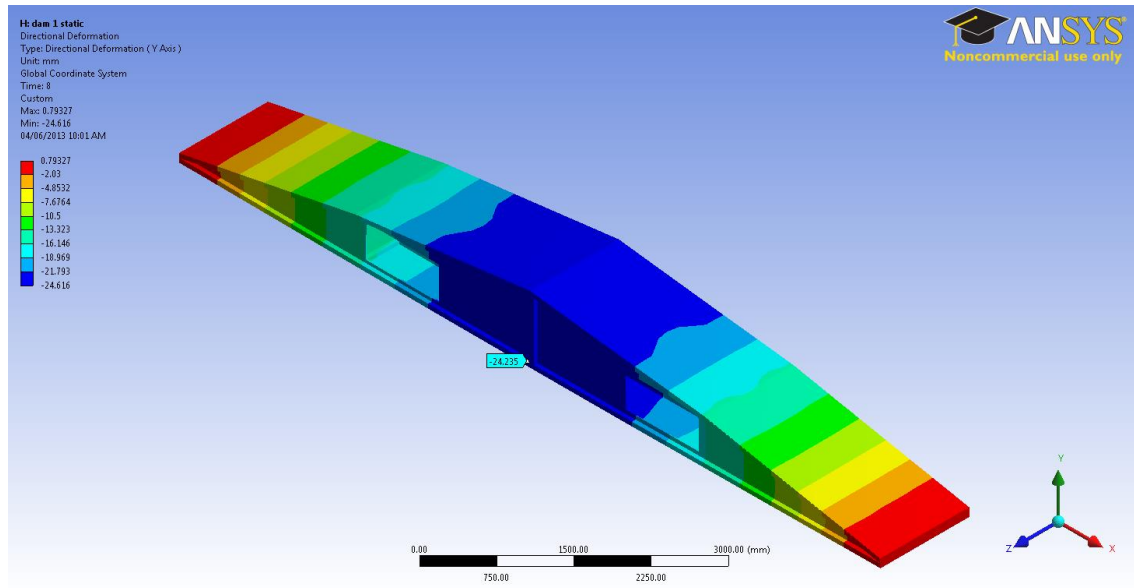


Figure 6-1: Vertical displacement result of quasi-static Damage Stage 1 ANSYS model (mm)

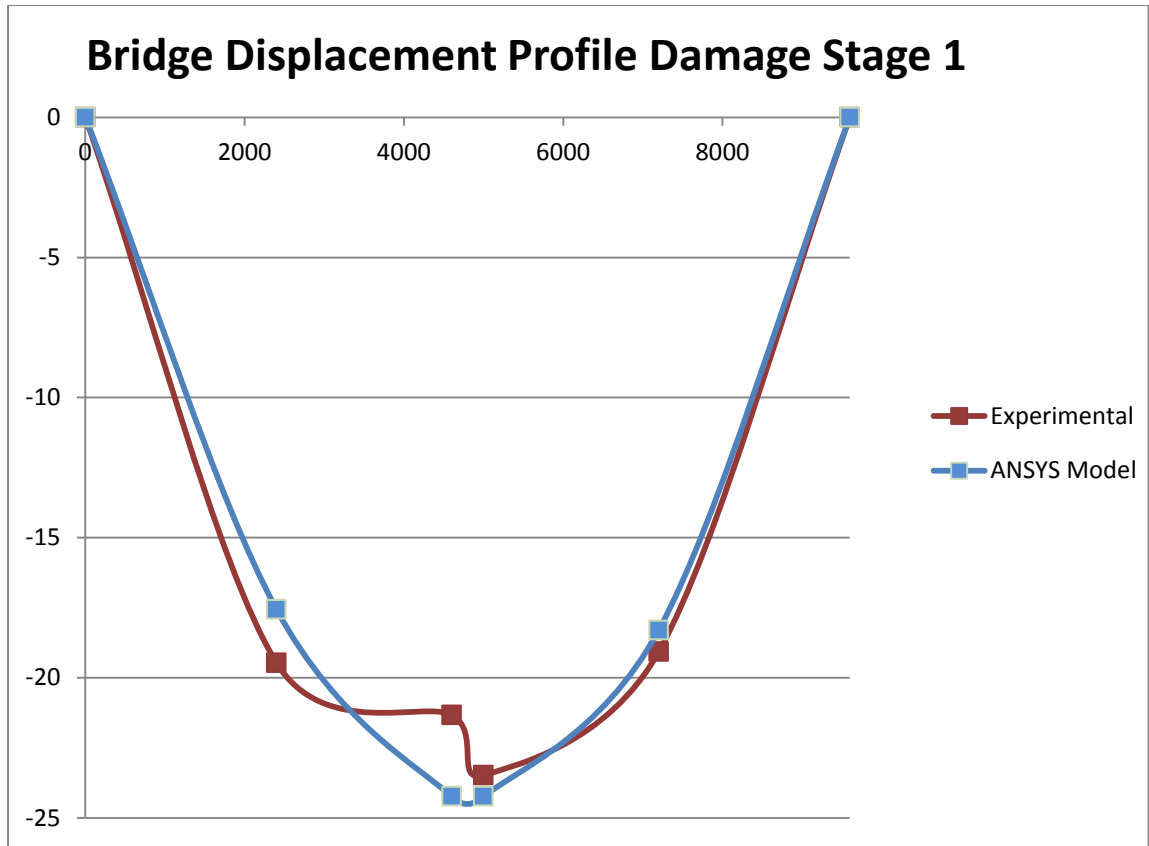


Figure 6-2: Bridge profile of Damage Stage 1 with 150 kN load

To model different damage stages, the damage was sketched onto the 3D model in ANSYS and an extrude material cut was performed. This was done for all 18 damage stages before the bridge failed. The laboratory tests for Damage Stage 18 produced a vertical displacement of -40.961 mm at LVDT_3. As shown in the bridge profile in Figure 6-3 the ANSYS model for Damage Stage 18 produces a similar displacement of -37.4 mm. The models in ANSYS have been determined to be acceptable quasi-static deformation models for the different damage stages applied to the GFRP bridge.

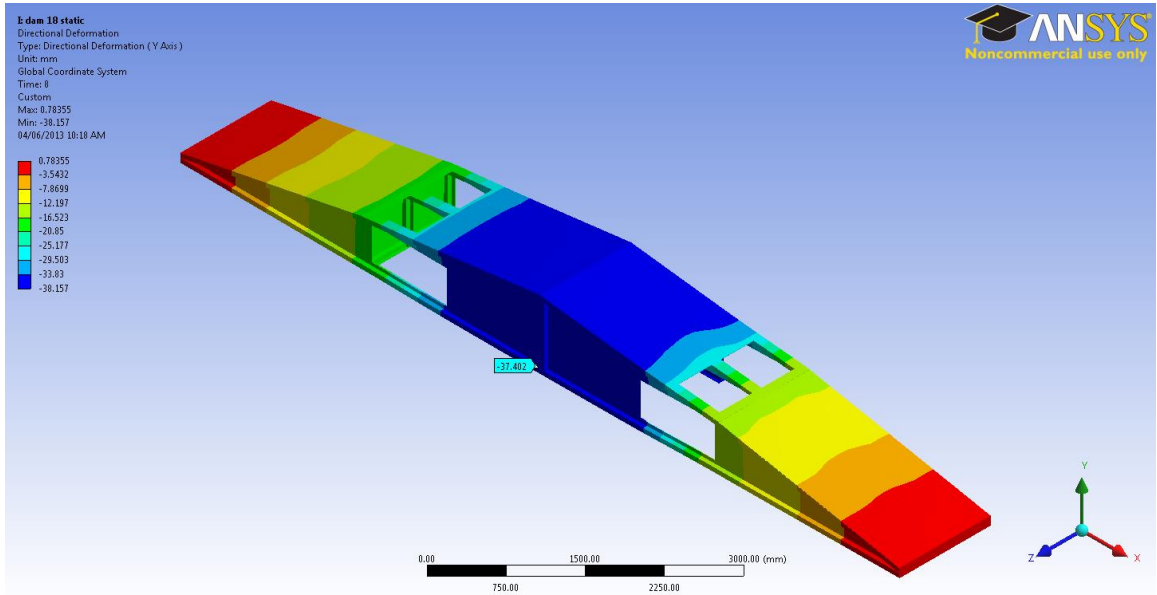


Figure 6-3: Vertical displacement result of quasi-static Damage Stage 18 ANSYS model

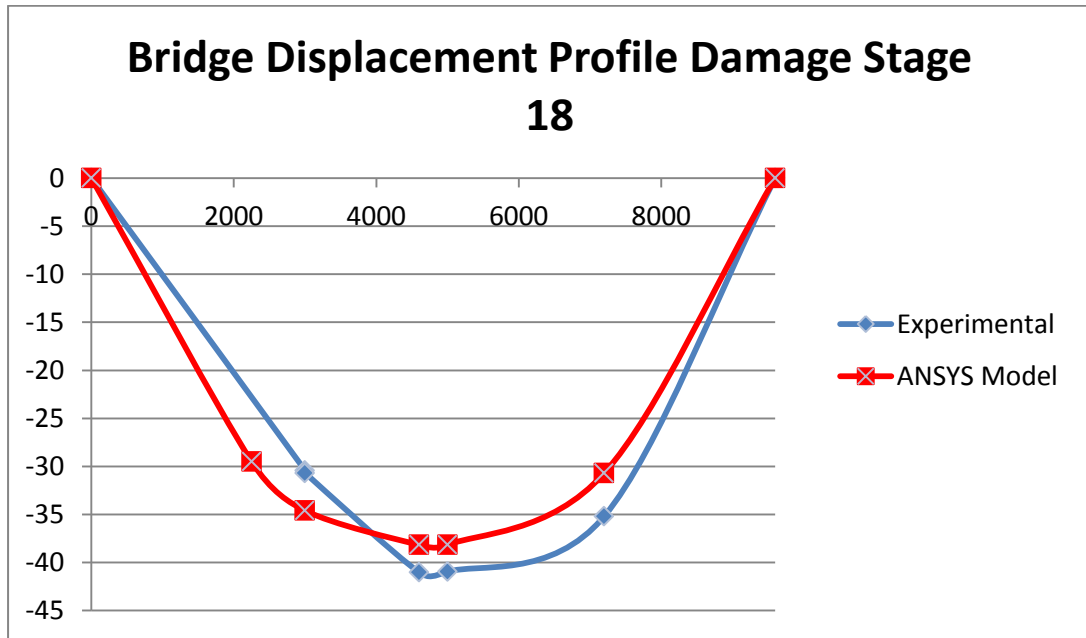


Figure 6-4: Bridge profile of Damage Stage 18 with 150 kN load

6.3 SAP2000 MODELS

SAP2000 is a structural analysis program for analysis and design tasks. It is a fully integrated structural analysis system for modeling, analyzing, designing and optimizing general structures, such as stadiums, towers, industrial plants, offshore structures, piping systems, buildings and dams. (CSi, 2011).

Within SAP2000, a 3D finite element representation of the GFRP bridge was constructed. The model bridge was constructed from frame elements that represented the structural tubing and shell elements for the GFRP plates and decking. Structural tubing members, one to four tubes depending on location, were represented by single frame elements that were assigned the material and geometric properties of one, two or four tubes depending on the location of the tubes and number of tubes that the frame element represented. The 3D model is shown in Figure 6-5 where the blue members are frame elements and the pink and red areas are the shell elements.

The shell elements are homogeneous elements with six degrees of freedom at each of its connected joints and are capable of supporting forces and moments. The shells are four node elements and use 2-by-2 Gauss integration points and extrapolate the results to the joints of the elements (CSi, 2011). The shell elements' material and geometric properties as listed in Table 6-1 describe the cross-section of the GFRP plates. The frame element is modeled as a straight line connecting two points and it activates all six degrees of freedom. Again the frame section is defined by the set of material and geometric properties that describe the GFRP tube.

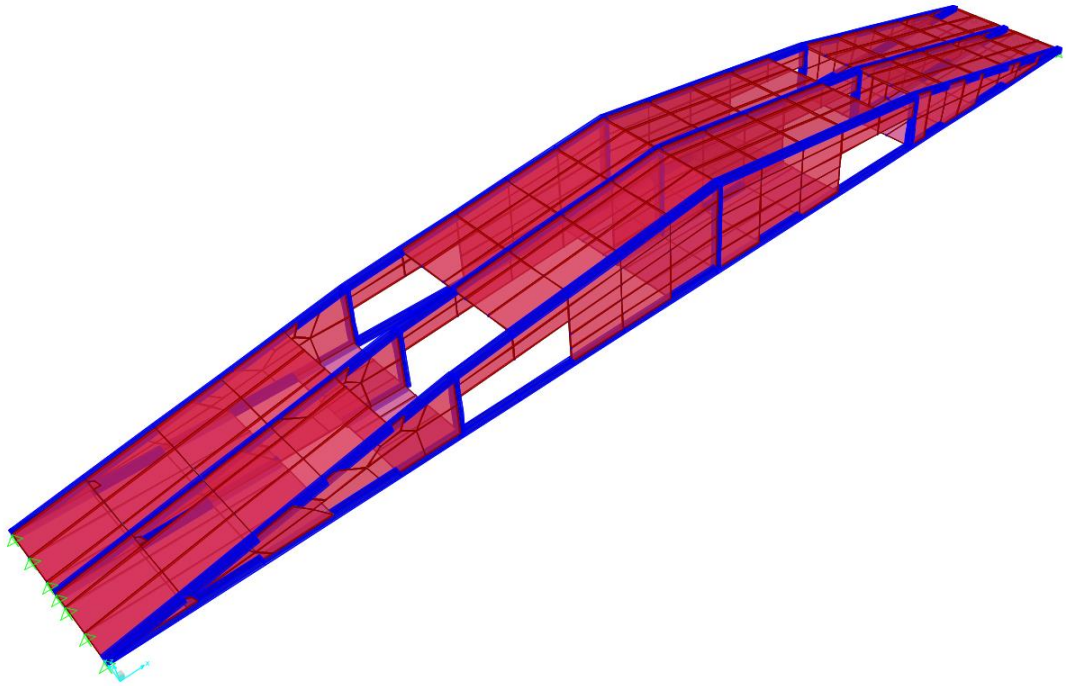


Figure 6-5: SAP2000 Model at Damage Stage 18

SAP Models produced similar quasi-static results to ANSYS models, so for brevity only SAP dynamic models will be discussed. When SAP2000 models were used for dynamic responses, the initial loading of the bridge was less important than the release of the bridge under loading. Because of this, the model was loaded at two nodes at the mid-span of the bridge with the appropriate load required to achieve similar deflections that were observed in laboratory testing. The load was applied in a time history function which allowed for a replication of the hold and release mechanism in the laboratory. The load was applied over three seconds, then it was removed in one one-thousandth of a second, recreating the action of the hold and release mechanism. The timings of the loading were varied initially, and it was determined it did not have any significant effects on the model. The rapid removal of the load from the bridge caused free vibration

of the bridge. To provide realistic response, a damping value estimated from laboratory testing was applied to the models; these values are shown in Table 5-1. Similarly to the ANSYS models, it was assumed that the bridge was simply supported, with a pinned connection on the East end and a roller support on the West end. It was also assumed that the bridge members were perfectly bonded, which was represented by the sharing of nodes between elements.

The results from the SAP2000 models include directional displacement, as seen in Figure 6-6, modal response, including frequency, as well as specific deflection and accelerations due to the time history loading. For brevity, the results from Damage Stage 1 and 18 will be discussed.

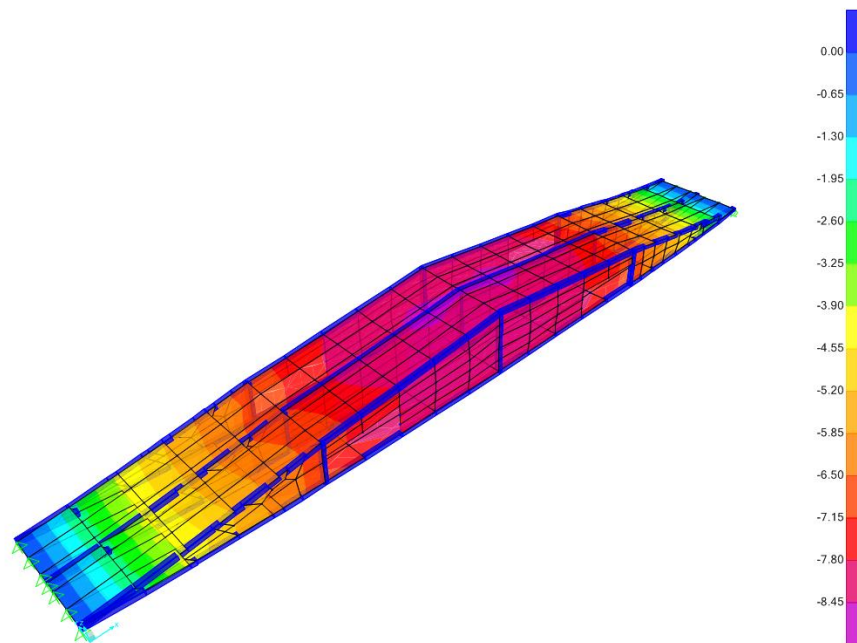


Figure 6-6: SAP2000 vertical displacement envelope of Damage Stage 1

Results from the model of Damage Stage 1 were similar to the expected results from laboratory testing. The frequency of the bridge at Damage

Stage 1 was 11.64 Hz in the SAP2000 model while during the laboratory testing it was found that the frequency was 11.5 Hz. Figure 6-7 shows the time-domain displacement response of the model bridge compared to the displacement response of LVD_2. Even though the displacement values are different, the frequency response is very similar; visually there are 11 peaks that can be counted in both figures during one-second time period.

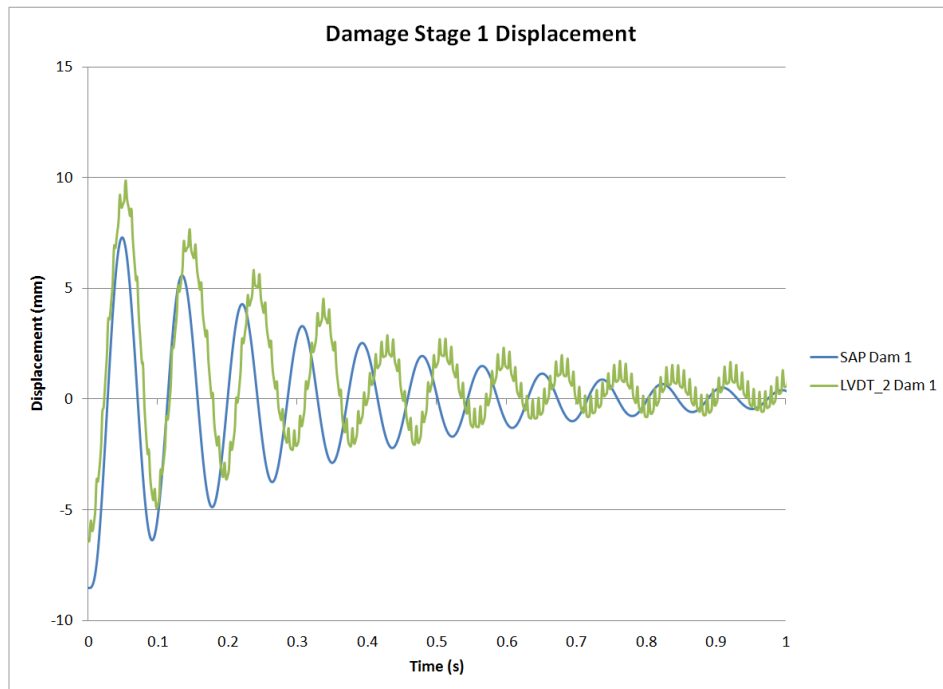


Figure 6-7: Time-domain Damage Stage 1 displacement response

Much like the displacement results, the acceleration results from the modeling of Damage Stage 1 are very similar to the results from experimental testing. Figure 6-8 shows the time-domain acceleration responses from both the model and laboratory testing respectively. It can be seen again that the frequency of the two results is very close. It can also be concluded that the accelerations obtained from the model are similar to the experimental results. While results from the model are similar to the experimental results, it is understood that the model bridge does not account

for slack in the system created from the deformation of components from the harness and the release mechanism. It is likely that this slack, the mass and elastic response of the harness components causes larger rebound displacements and slower periods. It is likely because of this effect that the time-domain data from the SAP2000 models are not exactly overlaid with experimental data.

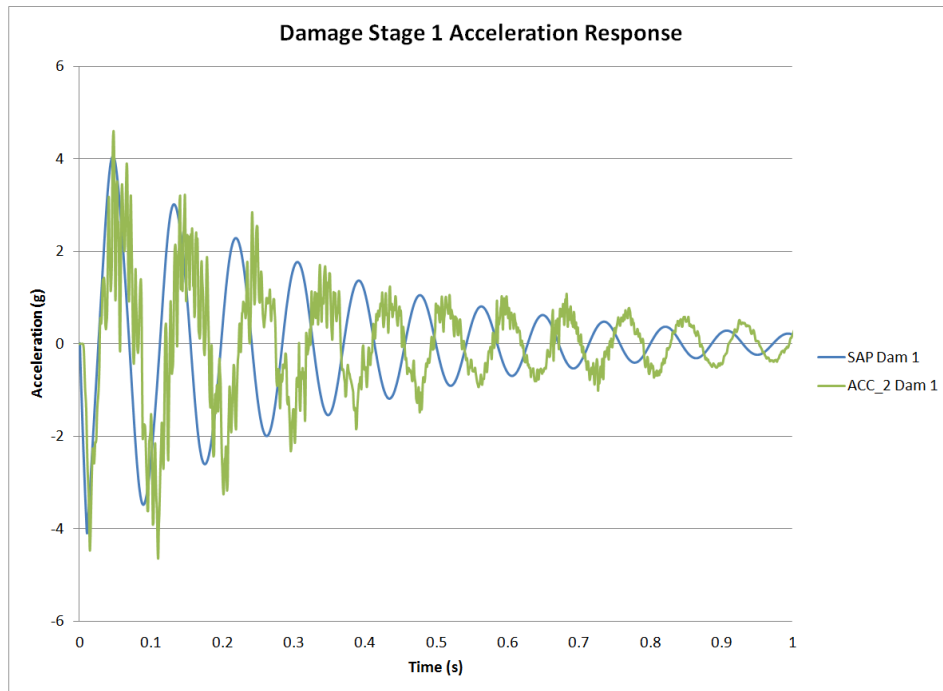


Figure 6-8: Time-domain Damage Stage 1 acceleration response

To represent damage to the models, mesh elements were deleted or in the case of some frame elements, the property modifiers were changed to represent the appropriate reduced cross-sectional area of tubes represented by the frame element. The modal results from the Damage Stage 18 model showed a frequency of 9.21 Hz, very similar to the calculated frequency of 9.06 Hz from laboratory testing. The frequency of the model at Damage Stage 18 is a 20.9% reduction in from the frequency of 11.64 Hz in Damage Stage 1. The 20.9% reduction is very close to the 21.2% reduction over the

same damage stages from the laboratory tests. The vibration response of displacement and acceleration of the model are also both similar to the results from experimentation.

Figure 6-9 shows the vibration response of the SAP2000 model and laboratory testing of displacement for Damage Stage 18. The displacement values and periods are similar for both the model and experimental results in the time-domain. The same trend can be observed in Figure 6-10 which shows the accelerations due to vibration of the model and experiment respectively.

Similarly to the experimental results, time-domain results can be informative however frequency-domain results will typically offer more information for the frequency response of a structure.

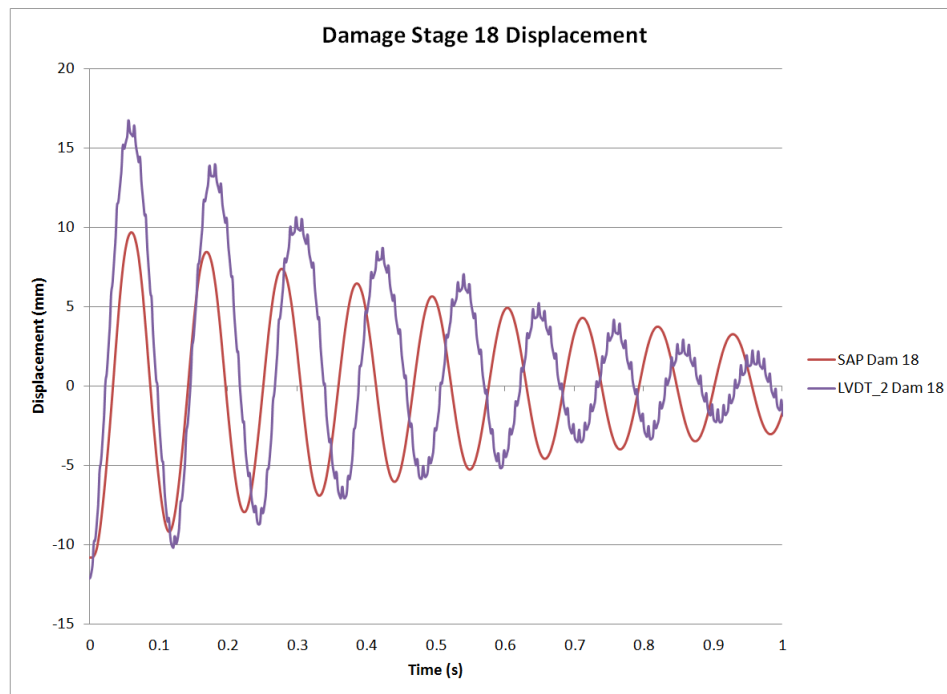


Figure 6-9: Time-domain Damage Stage 18 displacement response

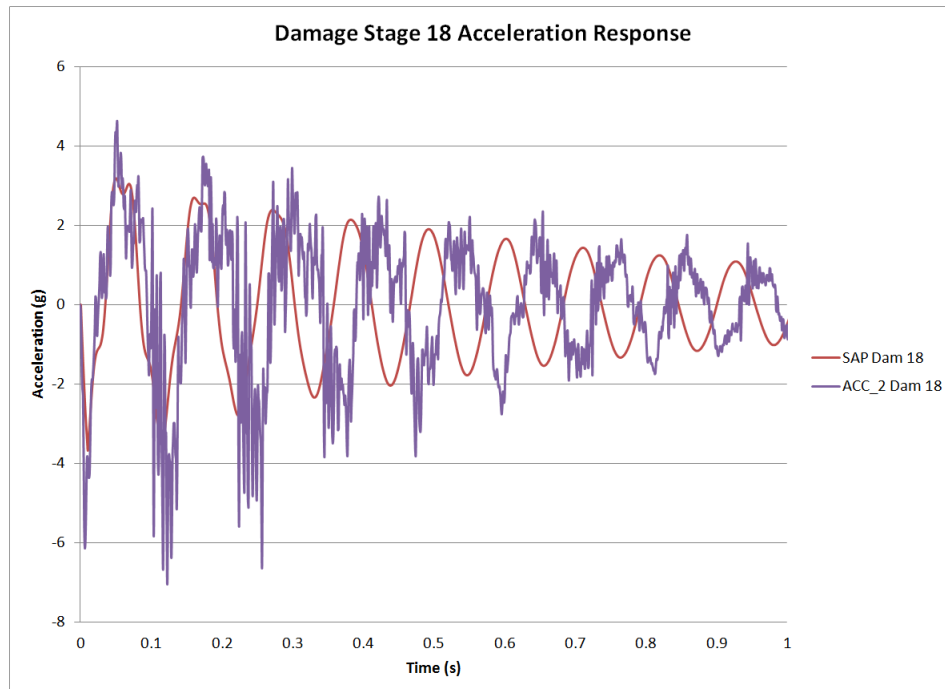


Figure 6-10: Time-domain Damage Stage 18 acceleration response

In addition to the time-domain results, SAP2000 does have a basic FFT output for model response. However, for continuity, the data from the SAP models was exported to excel where Matlab was used to create FFT figures. Figure 6-11 shows the FFT for the Damage Stage 18 model in SAP2000. The frequency from the figure is approximately 8.80Hz which is very similar to the 8.90 Hz determined from Figure 6-12, an FFT figure of Damage Stage 18 from laboratory testing. Both at Damage Stage 1 and 18, the experimental results are similar to the results from the models in both the time and frequency domains. It may be noted that the second frequency vibration at approximately 17 Hz in the experimental data was not detectable in the model. There are several possible explanations for this difference. The extra mass, slack and vibration of the harness may have created a dynamic sub-system that may be a source of this second mode in the experiments but was not represented in the finite element model.

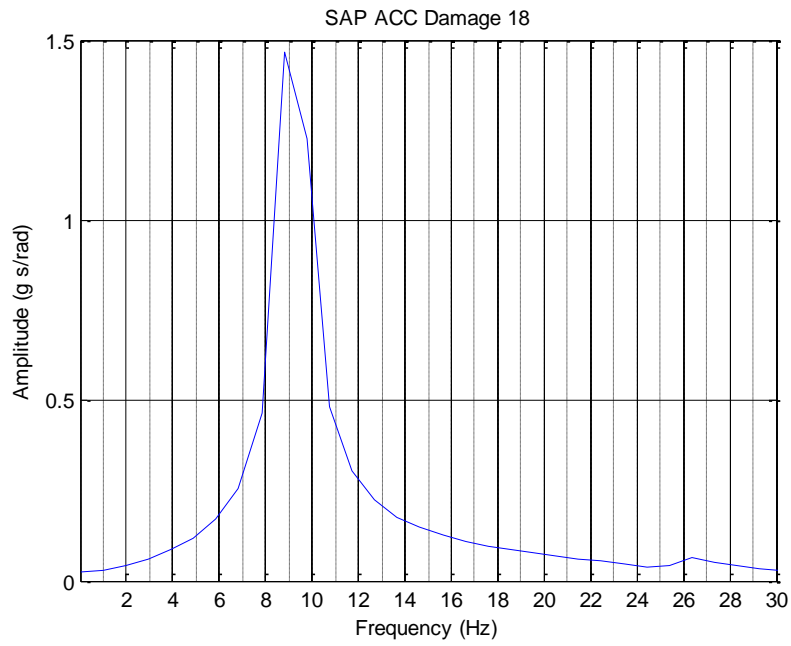


Figure 6-11: SAP2000 Damage Stage 18 model FFT

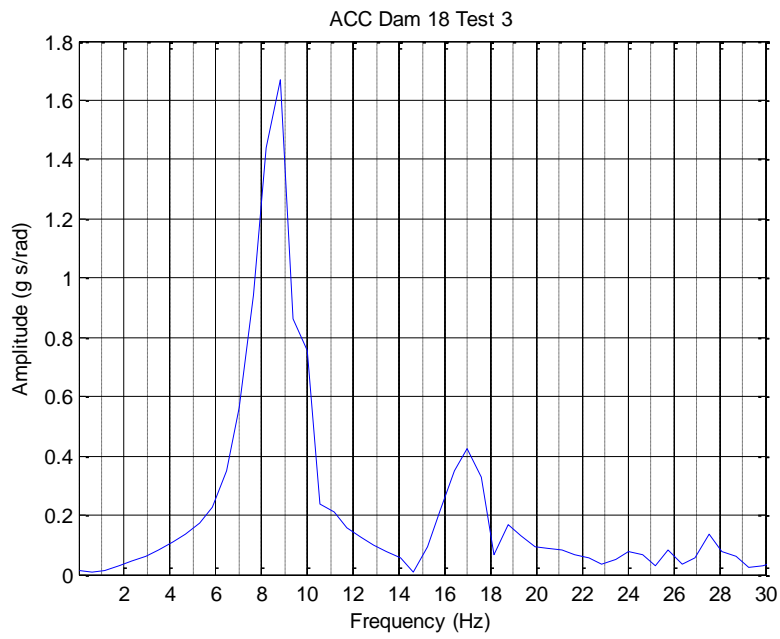


Figure 6-12: Experimental Damage stage 18 FFT

In addition to individual damage stage models being similar, it can be seen in Figure 6-13 that a similar trend is shown between the SAP2000 models and the experimental results. While not all nineteen (19) damage stages were modeled in SAP2000, nine (9) damage stages were modeled to capture the most significant damage stages and to show any trends that occurred. The models show a large frequency change similar to experimental results around Damage Stage 13 and 16, both which involved damage to structural tubing.

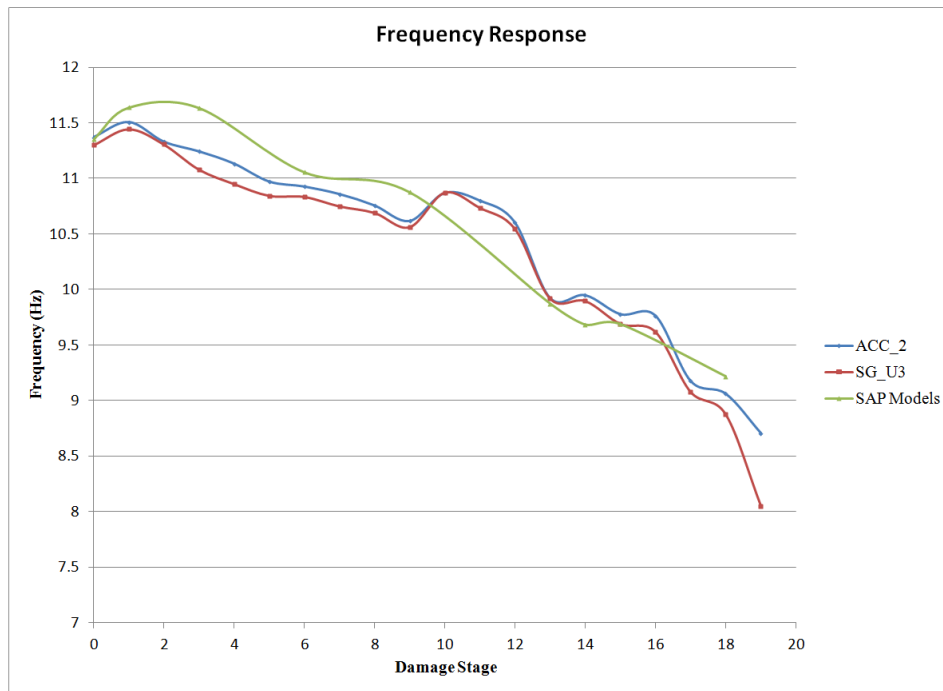


Figure 6-13: Frequency of SAP models and instruments

6.4 FAILURE PREDICTION

In addition to predicting the frequency change and the displacement of the bridge as it becomes damaged, the models were also able to make a conservative estimation of the failure strength of the bridge structure. From manufacturer's data sheets, the ultimate strength of the fibre reinforced tubes is 258 MPa. At Damage Stage 16, with an applied load of 150 kN, the model computes an axial force of approximately 190 kN in the double tube area in the heavily damaged region. Taking into account the area of two tubes ($1129 \text{ mm}^2/\text{tube}$), one base plate (682.24 mm^2), and a plate between the tubes (322.6 mm^2), for the side with undamaged tubes, the stress is predicted to be approximately 58 MPa, well under the ultimate strength of the tubes. The load and force distribution in the components of the bridge remains similar for the damage stages until failure. As further damage occurs in Damage Stage 17 and 19 the axial force remains at approximately 190 kN in the tubes while the cross-sectional area becomes smaller and the stress increases. When the inner tube and part of the bottom plate of the cross-sectional area is reduced by approximately half to 1815 mm^2 , the stress is increased to 105 MPa which is still under the predicted ultimate strength of a single tube. In the final damage stage, the tube is cut further, reducing the cross-sectional area by over 50% to approximately 746 mm^2 . The externally applied 150 kN load creates a 190 kN axial force which results in a calculated stress of 255 MPa in the tube and a calculated strain of approximately 8906 microstrain, which would be a prediction that failure is imminent.

At failure, strain gauges in the area of the failure from the experiment read 5455 microstrain. The difference between the strain gauge readings and the predicted failure strain can be attributed to the relatively short length of the concentrated damage of Damage Stage 19 which was the width of a saw blade. Tension in the area of this cut would have created a complex field of stress and strain at the tip of the crack. It is expected with the complex strain distribution, the gauges being longer than the crack length and slightly offset from the crack location, that the gauges could not provide a thorough and accurate estimate of peak strains.

From the model's prediction, one would expect a failure at approximately a 150 kN externally applied load at Damage Stage 19. From experimental data, failure occurs at a load of 190 kN. It should be noted however, that as the tube begins to fail, the web is still intact at the top of the beam. It is

likely that as the lower tubes began to fail and shed load, that the tension in the lower region of the undamaged web increased. This was confirmed in further modelling, where the failing tubes were modeled with a dramatically decreased stiffness. The load in the tubes dropped to 180kN but the predicted tension in the bottom of the web increased from 13 to 40 MPa. This additional tension capacity in the web may be primarily responsible for the additional capacity that was observed in the experiment. In any case, the predicted ultimate capacity of the bridge to sustain a 150 kN external load is conservative and provides a reasonable estimate of the experimental failure load.

In the case of an operational military application, as the model showed loads creating corresponding stress that approached the ultimate strength of the bridge, the bridge would be shut down and would have to be manually inspected and be subjected to a detailed assessment.

6.5 SUMMARY

This chapter on modeling examined the different predictive models that were created and used to predict the behaviour of the GFRP bridge. Finite element method software ANSYS and SAP2000 were used to create 3D models and perform both static and dynamic loading analysis. The quasi-static and dynamic tests in both ANSYS and SAP2000 produced results that were similar to experimental laboratory results.

CHAPTER 7: CONCLUSION

7.1 GENERAL

The requirement to monitor structures such as bridges has become apparent over the last few decades and it is for that reason that significant research is being carried out for the detection of damage in bridges. While studies have been completed elsewhere on frequency shifts as a damage detector, they have generally all been applied to structures with minor damage. There is however, a dearth of information for the use of this technique for detecting major damages that might be apparent on military deployments. There has also been very little research conducted on full scale FRP bridges and even less on damage detection of FRP bridges. The laboratory testing conducted was meant to determine if large damage to a GFRP bridge structure could be detected using frequency shifts and if a wireless monitoring system could be used to yield accurate results. Predictive modelling was also conducted. The following sections outline the conclusions and recommendations of this project.

7.2 CONCLUSIONS

The following conclusions are made based on the laboratory testing and finite element analysis conducted on a 10 m span GFRP box-beam bridge outfitted with an SHM system suitable for military engineering applications and subjected to quasi-static and dynamic loading. Quasi-static loading determined that the strain and deflection response due to progressive damage to the bridge were detectable and could be modeled and appropriately predicted using FEM software. Specific quasi-static testing conclusions included the following:

- The load-deflection of the bridge remained linear and elastic until complete bridge failure occurred.
- Strains observed from the 150 kN loading, indicated that the GFRP materials of the bridge remained well under their predicted ultimate strengths for all Damage Stages 1-18.

Conclusions associated with the dynamic static testing include the following:

- Large-scale damage to the 10 m span GFRP Bridge could be detected by monitoring the change in dynamic response. Damage detection using frequency change is plausible. A 21% reduction in frequency was detected before the final damage stage where failure occurred.
- Damage to non-redundant structural support members shows more noticeable frequency shifts than damage to other members.
- Using a commercially available wireless monitoring system in redundancy with a similar wired system proved the feasibility and reliability of using a wireless system. Strains varied by less than 10% between the wireless and wired system throughout all 18 damage stages of testing. Frequency calculations between the two systems were within 1.0% on average over all damage stages.

Conclusions associated with the predictive finite element analysis modeling include the following:

- The static and dynamic response of the increasingly damaged GFRP box beam structure could be appropriately predicted by finite element software. Displacement values predicted by the model were within 14% of the experimental results. Frequency of the bridge was found to be within 2.0% on average throughout the different damage stages.
- The failure of the bridge at Damage Stage 19 could be adequately predicted using commercial finite element analysis software.

7.3 RECOMMENDATIONS FOR FUTURE WORK

The following recommendations are made for further research in the Structural Health Monitoring (SHM) of bridges subjected to extreme damage:

- Conduct tests on a large-scale concrete or steel bridge structures subjected to several levels of severe damage that may be representative of the damage that would occur to infrastructure in a theatre of military operations.
- Investigate the response of structures subjected to severe damage when subjected to military and civilian traffic suitable for a theatre of military operations. This may be done experimentally and with predictive finite element analysis.
- Conduct tests in field conditions including different temperatures to confirm the robustness of the SHM system and to determine if frequency shifts from large damage are detectable outside shifts caused by temperature change
- Conduct dynamic testing using different methods of excitation, such as an impact hammer, dropped mass, moving loads such as vehicle loading.
- Investigate the usage of different SHM technologies that may be suitable for monitoring of GFRP bridges or bridges in a military environment such as Particle Image Velocimetry (PIV) using high speed cameras or Fibre Optic Sensors (FOS).

REFERENCES

- Anderjasic, M. (2008). *MEMS ACCELEROMETERS*. University of Ljubljana Faculty for mathematics and physics.
- ANSYS. (2010). *SOLID186*. ANSYS Inc.
- ANSYS. (2013, 05). *About ANSYS*. Retrieved from ANSYS: <http://www.ansys.com/>
- ASCE. (2013). *2013 Report Card for America's infrastructure*. ASCE.
- Canadian Standards Association. (2014). *Canadian Highway Bridge Design Code*. Canadian Standards Association.
- Chase, S. B., & Washer, G. (1997, July/August). *Nondestructive Evaluation for Bridge Management in the Next Century*. Retrieved Feb 2013, from US Department of Transportation: Public Roads: <http://www.fhwa.dot.gov/publications/publicroads/97july/ndeJuly.cfm>
- Cochran, W. T., Cooley, J. W., Favin, D. L., Helms, H. D., Kaenel, R. A., Lang, W. W., . . . Welch, P. D. (1967, March 10). What is the Fast Fourier Transform. *IEEE Trans. Audio Electroacoustics* (pp. 45-55). Institute of Electrical and Electronics Engineers Inc.
- Commission of Inquiry. (2006-2007). *Commission of Inquiry into the Collapse of a Portion of the de la Concorde Overpass*. Montreal.
- Commission of Inquiry. (2006-2007). *Commission of Inquiry into the Collapse of a Portion of the de la Concorde Overpass*. Montreal.
- Cooley, J. W., & Tukey, J. W. (1965). An Algorithm for the Machine Calculation of Complex Fourier Series. *Mathematics of Computation*, 297-301.
- CSI. (2011). *Computers and Structures Inc, CSI Analysis Reference Manual: for SAP2000, ETABS, SAFE and CSiBridge*. Berkeley.

- De Roeck, G., Peeters, B., & Maeck, J. (2000). Dynamic Monitoring of Civil Engineering Structures. *Computational Methods for Shell and Spatial Structures*.
- DND. (2002). *FM 3-34.343 (FM5-446) Military Nonstandard Fixed Bridging - Draft*.
- Doebling, S. W., Farrar, C. R., Prime, M. B., & Shevitz, D. W. (1996). *Damage Identification and Health Monitoring of Structural and Mechanical Systems from Changes in Their Vibration Characteristics: A Literature Review*. Los Alamos: Los Alamos National Laboratory.
- Farrar, R. C., Doebling, S. W., Cornwell, P. J., & Straser, E. G. (1997). Variability of Modal Parameters Measured on the Alamosa Canyon Bridge. *1997 IMAC XV - 15th International Modal Analysis Conference*. Orlando.
- FHWA. (2001). *Reliability of Visual Inspection for Highway Bridges, Volume 1: Final Report*. US Department of Transportation. McLean: Federal Highway Administration.
- Gastineau, A., Johnson, T., & Schultz, A. (2009). *Bridge Health Monitoring and Inspections - A Survey of Methods*. Minneapolis: Department of Civil Engineering, University of Minnesota.
- Green, M. F. (1995). Modal Test Methods for Bridges: A Review. *Proceedings of the 13th International Modal Analysis Conference*, (pp. 552-558). Nashville.
- HBM. (2013). *MGCplus - Laboratory & Test Stand DAQ*. Retrieved from HBM Canada: <http://www.hbm.com/en/menu/products/measurement-electronics-software/laboratory-test-stand/>
- Honorio, U., Wight, G., Erki, M.-A., & Heffernan, P. (2003). *Assessing and Strengthening Severely Damaged Large-Scale Concrete Bridges*. Royal Military College, Civil Engineering. Kingston: Military Engineering Research Group.

- Hsieh, K. H., Halling, M. W., & Barr, P. J. (2006). Overview of Vibrational Structural Health Monitoring with Representative Case Studies. *Journal of Bridge Engineering*, 707-715.
- Huston, D. (2011). *Structural Sensing, Health Monitoring, and Performance Evaluation*. Boca Raton, FL: Taylor and Francis Group.
- ISIS Canada. (2001). Guidelines for Structural Health Monitoring Design Manual No.2. Winnipeg, MB: ISIS Canada Corporation.
- ISIS Canada. (2011). An Introduction to Structural Health Monitoring. *ISIS Educational Module 5*. ISIS Canada.
- Kato, M., & Shimada, S. (1986). Vibration of PC Bridge During Failure Process. *Journal of Structural Engineering*, 1692-1703.
- Landherr, J. C. (2008). *Dynamic Analysis of A FRP Deployable Box Beam*. Kingston: Queen's University.
- Landherr, J. C., Wight, G., Green, M. F., & Erki, M.-A. (2009). Vibration Characteristics of a damaged FRP vehicle bridge. *4th International Conference on Structural Health Monitoring on Intelligent Infrastructure (SHMI-4)*. Zurich.
- Lynch, J. P., & Loh, J. K. (2006). A summary Review of Wireless Sensors and Sensor Networks for Structural Health Monitoring. *The Shock and Vibration Digest*, 38(2), 91-128.
- Macro Sensors. (2003). *LVDT Basics: Technical Bulletin 0103*. Pennsauken.
- MathWorks. (2012). *MATLAB The Language of Technical Computing*. Retrieved from MathWorks: <http://www.mathworks.com/products/datasheets/pdf/matlab.pdf>
- Mazurek, D., & DeWolf, J. (1990). Experimental Study of Bridge Monitoring Technique. *Journal of Structural Engineering*, 2532-2549.
- Ministry of Transportation (Ontario). (2008). *Ontario Structure Inspection Manual*. St. Catharines: Policy, Planning & Standards Division; Engineering Standards Branch; Bridge Office.

- MIT OCW. (2010). *13. Natural Frequency and Damping Ratio*. Retrieved from MIT OpenCourseWare: http://ocw.mit.edu/courses/mathematics/18-03-differential-equations-spring-2010/readings/supp_notes/MIT18_03S10_chapter_13.pdf
- Mosavi, A. (2010). *Vibration-based Damage Detection and Health Monitoring of Bridges*. Dissertation, North Carolina State University, Civil Engineering, Raleigh.
- Mosavi, A., Seracino, R., & Rizkalla, S. (2012). Effect of Temperature on Daily Modal Variability of a Steel-Concrete Composite Bridge. *Journal of Bridge Engineering*.
- NARADA. (2013). Operating Instructions (Windows): Wireless Sensing System (Version 3.0). Ann Arbor, USA: Civionics.
- National Instruments. (2013). *Strain Gauge Measurements - A Tutorial*. National Instruments.
- National Instruments. (2013). *What is Data Acquisition?* Retrieved from National Instruments: <http://www.ni.com/data-acquisition/what-is/>
- NATO. (2011). *STANAG 2021 MILENG (Edition 7) - Military Load Classification of Bridges, Ferries, Rafts and Vehicles*. NATO Standardization Agency.
- Ramirez, R. W. (1985). *The FFT Fundamentals and Concepts*. Englewood Cliffs: Tektronix inc.
- Rao, K. R., Kim, D. N., & Hwang, J. J. (2010). *Fast Fourier Transform: Algorithms and Applications*. London, NY: Springer.
- Salawu, O. S., & Williams, C. (1995). Review of full-scale dynamic testing of bridge structures. *Engineering Structures*, 113-121.
- Smith, S. W. (1997). *The Scientist and Engineer's Guide to Digital Signal Processing*. California Technical Publishing.
- Wang, Y. (2011). *Vibration-Based Damage Detection on a Multi-Girder Bridge Superstructure*. Saskatoon: University of Saskatchewan.

- Wight, R. G., Erki, M. A., Shyu, C. T., Tanovic, R., & Heffernan, P. J. (2006). Development of FRP Short-Span Deployable Bridge - Experimental Results. *Journal of Bridge Engineering*, 489-498.
- Wight, R. G., Erki, M. A., Shyu, C. T., Tanovic, R., & Xie, A. (2006). Design and Analysis a 10-m FRP Deployable Bridges. *Third International Conference on FRP Composites in Civil Engineering (CICE 2006)*, (pp. 131-134). Miami .
- Wowk, D. (2012). Advanced Finite Element Methods (MEE547 Course Notes). Kingston, Ontario.
- Xie, A. (2007). *Development of an FRP Deployable Bridge*. Kingston: Royal Military College of Canada.
- Xie, A., Wight, R. G., & Erki, M. A. (2008). Development of an FRP Deployable Bridge. *Advanced Composite Materials in Bridges and Structures*. Winnipeg.
- Yantha, P. (1995). *Static and Dynamic Behaviour of a GFRP Prototype Vehicle Bridge*. Kingston: Department of Civil Engineering, Royal Military College of Canada.
- Zhang, Y., Cai, C. S., Shi, X., & Wang, C. (2006). Vehicle-Induced Dynamic Performance of FRP versus Concrete Slab Bridge. *Journal of Bridge Engineering*, 410-419.
- Zhou, Z. (2006, Dec). Vibration-Based Damage Detection of Simple Bridge Superstructures. Saskatoon, SK, Canada: University of Saskatchewan.
- Zhou, Z., Wegner, L. D., & Sparling, B. F. (2007). Vibration-Based Detection of Small-Scale Damage on a Bridge Deck. *Journal of Structural engineering* , 1257-1267.

APPENDIX A:

Calculation of Single Point load for MLC 30 design Bridge

The following curves were derived using Standard NATO vehicles as defined by STANAG 2021. The unit bending moments for each vehicle were derived from the effects of a convoy of vehicles of a similar class at a spacing of 30.5m between vehicles over simply support spans varying from 1 to 100 m.

The unit bending moment at a 10 m span for a MLC 30 wheeled vehicle can be estimated from these curves as 50 kNm/m as shown in the Figure

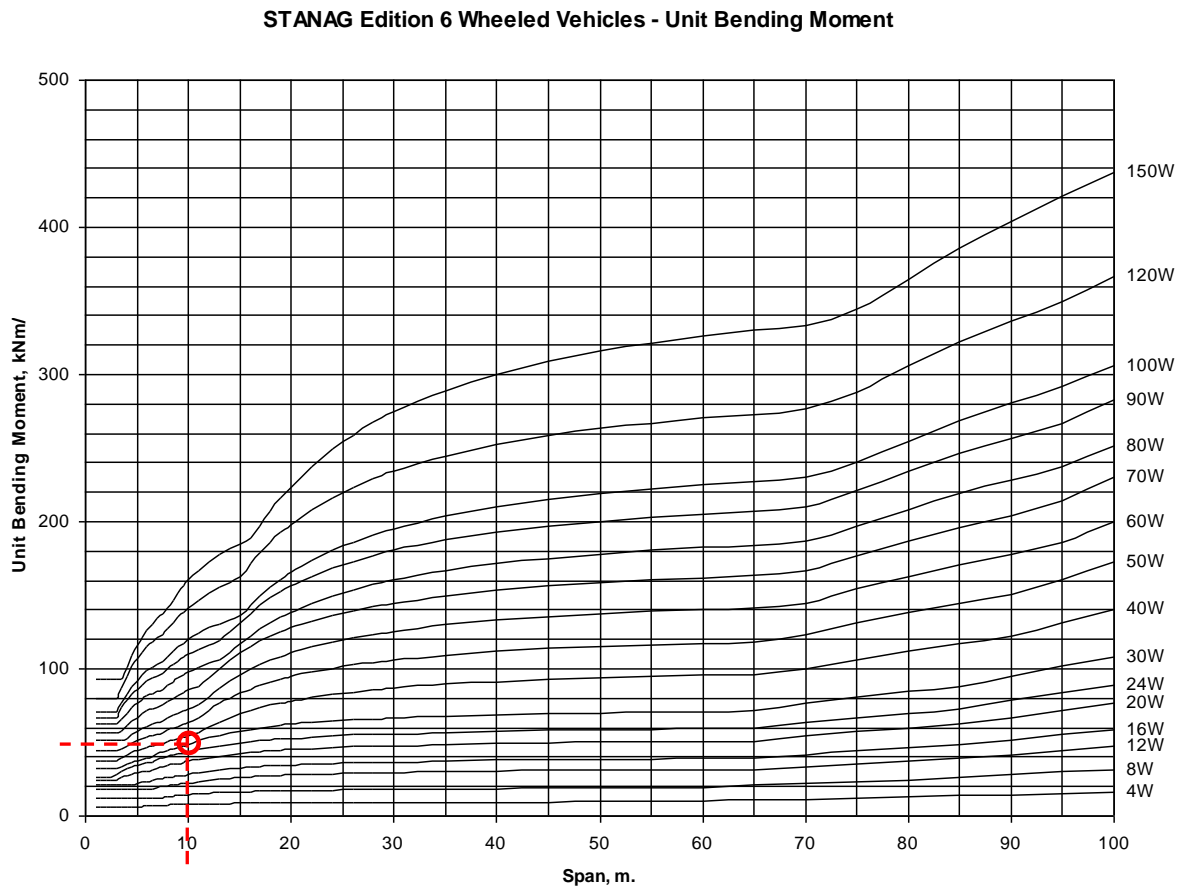


Figure A-1: Bending Moments of Wheeled Vehicles as per STANAG 2021. The selected span and MLC has been noted.

Using Fig A-1:

Unit Bending moment		$50 \frac{kNm}{m}$
10 m Bridge span	$50 \frac{kNm}{m} \times 10m$	500kNm
Bending Moment for half vehicle	$\frac{500kNm}{2}$	250kNm
Factored ¹ Bending moment or Mmax	$250kNm \times 1.3 \times 1.15$	373.75 kNm
$M_{max} = \frac{PL}{4}$		
P= Point load	$4 \times \frac{373.75kNm}{L} = P$	$P = 149.5 kN$
L = Span length		

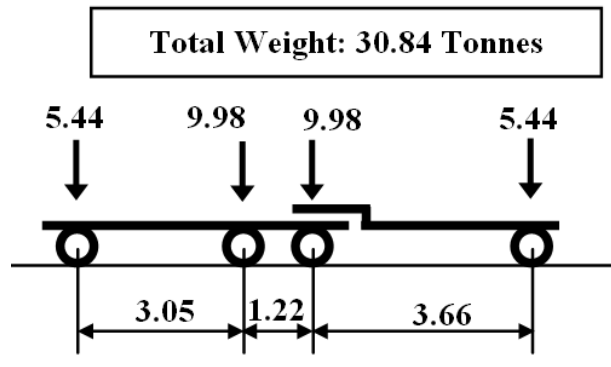
Pmax = 149.5 kN (or 150 kN)

Note: 1. A military live load factor of 1.3 and a military dynamic load allowance were used in the calculations above.

MLC 30 Vehicle:

(Axle weights in tonnes)

(Axle spacing in metres)



APPENDIX B:

WIRED RAW DATA (EXAMPLE)

Table B 1: Damage 10 Test 2 (1.75-1.775 sec)

Time	SG_B2	SG_B3	SG_B4	SG_B5	SG_B6	SG_B7
1200	μm/m	μm/m	μm/m	μm/m	μm/m	μm/m
1.75	417.3	23.79167	42.66667	45.45834	17.90833	529.2917
1.750833	421.0584	32.96667	43.725	44.65	25.06667	532.7834
1.751667	416.725	42.24167	41.475	41.075	34.09167	524.5834
1.7525	402.6084	56.90834	37.51667	37.35834	49.85	504.2584
1.753333	368.3667	69.03334	30.65	31.33333	64.65834	459.8084
1.754167	339.6084	96.80834	40.03334	39.23334	91.15834	401.725
1.755	282.8167	107.625	31.85833	31.73333	103.8583	324.925
1.755833	224.825	116.4833	22.9	23.85833	116.0083	253.0833
1.756667	167.0833	123.85	19.03333	21.41667	127.2917	187.925
1.7575	116.5833	124.6917	18	21.11667	129.1	132.2333
1.758333	61.81667	105.675	2.583333	7.991667	106.4667	84.58334
1.759167	22.925	80.61667	-0.06667	6.583334	73.03334	43.24167
1.76	-10.075	42.08334	-1.65833	5.258334	34.15	4.825
1.760833	-25.6167	7.216667	-6.14167	1.158333	-0.50833	-17.9167
1.761667	-27.75	-24.9917	-12.2167	-5.30833	-37.1	-37.4083
1.7625	-21.4917	-52.3917	-1.89167	1.916667	-62.4417	-58.2
1.763333	-31.8	-94.6083	-4.74167	-1.85833	-92.4333	-80.0833
1.764167	-26.3917	-120.675	-6.575	-3.15	-101.425	-71.8083
1.765	1.625	-130.467	-4.575	-0.025	-105.5	-56.3083
1.765833	13.775	-147.492	-15.2083	-9.53333	-124.458	-78.3917
1.766667	-41.2833	-186.975	-39.2667	-31.7083	-157.425	-167.692
1.7675	-80.2167	-169.892	-30.3417	-21.875	-130.967	-238.342
1.768333	-107.992	-132.775	-26.0917	-20.15	-85.55	-272.675
1.769167	-108.058	-90.7167	-32.1083	-25.2583	-39.6667	-243.183
1.77	-131.842	-71.875	-35.1583	-24.1083	-22.3167	-228.742
1.770833	-162.325	-32.8	-18.6667	-10.4083	1.658333	-252.483
1.771667	-198.9	11.50833	-26.7333	-15.9833	22.975	-283.683
1.7725	-237.333	29.575	-31.275	-20.225	2.125	-322.383
1.773333	-289.842	4.591667	-25.1917	-14.9417	-42.7333	-373.575
1.774167	-303.05	-5.53333	-19.8667	-10.275	-28.675	-353.917
1.775	-276.583	-5.325	-34.3167	-22.575	-11.075	-284.025

APPENDIX C:

WIRELESS RAW DATA (EXAMPLE)

Table C-1: Damage 10 Test 2 (2.35 – 2.375 sec)

Time	1-2	1-3	2-2	2-3
s	Um	Um	Um	um
2.35	292.2484	231.693	222.9038	291.5656
2.350833	270.1228	220.0961	212.3751	266.1593
2.351667	247.2343	206.7445	200.3204	237.8538
2.3525	224.1932	190.7225	183.8407	215.3468
2.353333	203.7461	170.1991	163.1647	195.2049
2.354167	178.645	143.8773	130.4341	176.9703
2.355	169.8711	132.4331	130.7393	162.8557
2.355833	148.9662	119.1577	116.3195	141.1116
2.356667	124.8569	101.1521	100.7553	117.8416
2.3575	100.4425	83.60418	82.97856	94.26642
2.358333	78.7747	61.4786	63.44701	74.04822
2.359167	61.45571	40.11597	44.22065	59.70474
2.36	47.95148	20.66072	24.00244	46.12421
2.360833	35.59167	2.65507	2.716106	36.35843
2.361667	27.19921	-12.6802	-13.9162	25.21935
2.3625	16.21271	-28.2444	-28.4886	13.92767
2.363333	5.30251	-45.4108	-43.061	-0.79728
2.364167	-7.0573	-60.2884	-59.3881	-19.2607
2.365	-14.6105	-76.463	-75.2575	-34.1382
2.365833	-22.0111	-90.6538	-88.9143	-46.6506
2.366667	-27.3518	-102.861	-99.8245	-54.7379
2.3675	-31.548	-112.322	-109.438	-60.3075
2.368333	-36.4309	-115.984	-113.405	-60.9941
2.369167	-43.2975	-119.341	-115.312	-59.163
2.37	-48.1804	-123.156	-115.846	-57.9423
2.370833	-47.9515	-126.36	-116.304	-55.6535
2.371667	-47.4174	-125.75	-117.22	-54.3565
2.3725	-46.273	-126.665	-117.525	-54.2039
2.373333	-48.333	-159.472	-144.457	-63.0541
2.374167	-59.8535	-194.644	-180.24	-79.9153
2.375	-90.4479	-218.372	-201.602	-109.365

APPENDIX D:

MATLAB CODE

```
k=1; % test placeholder
q=figure; % place holder for saveas
[num.txt,row] = xlsread('compare damage test 3s matlab.xlsx', 7, 'B3:AD3');% get test headings
Fs=1200; % Sample frequency
T=1/Fs;
L=1200; % length of sample (1s)
t=(0:L)*T;
NFFT = 2^nextpow2(L);
f=Fs/2*linspace(0,1,NFFT/2+1);

while k<=5 % number of tests

MatrixB= ['B'; 'C'; 'D'; 'E'; 'F'; 'G';'H'; 'I'; 'J'; 'K'; 'L'; 'M'; 'N'; 'O'; 'P'; 'Q'; 'R'; 'S'; 'T'; 'U'; 'V'; 'W';
'X'; 'Y'];
%range of numerical data x8:x1208
range = sprintf('%s%d:%s%d', MatrixB(k,1),8,MatrixB(k,1),7008);
% time axis
time = xlsread('compare damage test 3s matlab.xlsx', 7, 'A8:A7008');
% numerical data for test
MatrixA = xlsread('compare damage test 3s matlab', 7, range);
% fft function of data
Y=fft(MatrixA,NFFT)/L;
% plot fft
plot(f,2*abs(Y(1:NFFT/2+1)));
xlim([0 30]); % x axis limit
set(gca,'XGrid','on'); % x grid lines
set(gca,'YGrid', 'on'); % y grid lines
set(gca,'XTick', 2:2:30); % x scale
set(gca,'GridLineStyle', '-'); % grid line style
set(gca,'XminorGrid', 'on'); % minor grid lines on
xlabel('Frequency (Hz)'); % x axis label
ylabel ('Amplitude (g s/rad)'); % y axis label
title(raw(1,k)); % chart title

filename=sprintf('ACC_100knfigure%d',k); % create changing file name number
```